In presenting this dissertation as a partial fulfillment of the requirements for an advanced degree from Emory University, I agree that the Library of the University shall make it available for inspection and circulation in accordance with its regulations governing materials of this type. I agree that permission to copy from, or to publish, this thesis/dissertation may be granted by the professor under whose direction it was written when such copying or publication is solely for scholarly purposes and does not involve potential financial gain. In the absence of the professor, the dean of the Graduate School may grant permission. It is understood that any copying from, or publication of, this thesis/dissertation which involves potential financial gain will not be allowed without written permission.

_____

Andrew G. Palmer

Semagenesis & Xenognosis: Translating the Molecular Dialogues of Host-Parasite Interactions

By

Andrew G. Palmer
Doctor of Philosophy

Department of Chemistry

_____
Professor David G. Lynn, Ph. D.
Adviser

_____
Professor Vince Conticello, Ph. D.
Committee Member

_____
Associate Professor Justin Gallivan
Committee Member

Accepted:

_____
Lisa A. Tedesco, Ph.D.
Dean of the Graduate School

_____
Date

Semagenesis & Xenognosis
Translating the Molecular Dialogues of Host-Parasite Interactions

By

Andrew G. Palmer
B.S., Florida State University, 2001

Advisor: David G. Lynn, Ph. D.

An Abstract of a dissertation submitted
to the Faculty of the Graduate School of Emory University
in partial fulfillment of the requirements for the degree of
Doctor of Philosophy

Department of Chemistry

2008

Abstract

The sessile nature of plants has resulted in the coupling of basic developmental programs to a variety of external signals, as well as the evolution of an arsenal of small molecules with which to influence other organisms. These seemingly divergent concepts converge in the parasitic plants where host derived signals direct multiple stages of development. In the parasitic angiosperm *Striga asiatica*, the signals that regulate germination, host attachment, and shoot apical meristem development have been identified making this an ideal system for studying both the interface which defines interorganismal signaling events, as well as small molecule regulated development.

Host attachment and the subsequent siphoning of nutrients is marked by the development of a specialized organ, unique to the parasitic plants, the haustorium. The signals which regulate this developmental transition are *p*-benzoquinones generated by the oxidation of host derived monolignols via reactive oxygen species (ROS) released by the parasite in a process known as *semagenesis*. This active process sharply contrasts with more traditional passive signaling events and raises several questions as to its origins and regulation. The studies herein have confirmed the localization, regulation, and source of semagenic ROS. Furthermore, they suggest a mechanism for the perception of the haustorial inducing quinones is conserved among non-parasites. These results confirm the critical importance of tight regulation over the signaling events at the host-parasite interface, further defines this new role for reactive oxygen, potentially provides new targets for limiting successful parasitism, and insights into the molecular origins of host detection and parasitism.

Semagenesis & Xenognosis
Translating the Molecular Dialogues of Host-Parasite Interactions

By

Andrew G. Palmer
B.S., Florida State University, 2001

Advisor: David G. Lynn, Ph. D.

A dissertation submitted
to the Faculty of the Graduate School of Emory University
in partial fulfillment of the requirements for the degree of
Doctor of Philosophy

Department of Chemistry

2008

Acknowledgements

The PhD process, while personal, is not a solitary pursuit. My accomplishments, as well as my growth and maturation into a scientist, has been facilitated by the hard work and emotional support of so many that a few words of thanks seem inadequate but I will do my best. My deepest thanks to my mentor Professor David Lynn whose guidance, wit, and passion has made it so hard to leave. You gave me the freedom to make my own mistakes, which is quite possibly the greatest gift an advisor can offer their students. Thanks also to my other committee members, Justin Gallivan and Vince Conticello, whose constructive comments and sense of humor have been greatly appreciated. Special thanks to John Keyes, Lizhi Liang, Michael Chen, Nikhar Kinger, and Yue Liu whose work with me on the Striga project both empowered and enabled me. Such truly excellent collaborations are rare and should be cherished. Indeed collaboration and support is at the very heart of the Lynn lab and I thank all its members for their support over the past 6 years. In particular, Melissa Bobeck, Seth Childers, and Anil Mehta who have always brought a critical eye, constructive criticism, and a good laugh to our interactions. You all helped me to keep pushing forward even when I wanted to quit. To Justin Maresh, Rong Gao, and Jijun Dong whose passion and enthusiasm for research, while setting the bar high for an incoming graduate student, was infectious.

In addition to the support of the Lynn Lab and my committee I have been blessed with truly amazing friends both within the department and in the ‘real’ world whose love and support have made the last few years even more amazing. To Brian, Russ, Kelly, Anil, and so many others, I can’t say thank you enough. You are amazing people and I

am proud to call you my friends. Though the distance between us may grow I hope we will always remain close. In addition to spectacular friends I have been doubly blessed with a wonderful family who have always supported and believed in me, even when I did not believe in myself. Most especially my parents, whose drive, hard-work, love, and sacrifices have been a great support through the years. A special thanks to my grandfather whose childhood enthusiasm and curiosity stayed with him until the end of his days. You showed me that a scientist could be a poet and that there was a place for a poet in science.

Finally to my wife Heather, you have been my best friend, my biggest cheerleader, and my partner in crime. You always know when I need to turn off the laptop or come home from the lab and take a break. I appreciate all you have done and put up with for me to achieve this. I love you and look forward to all the times, good and bad, ahead.

Table of Contents

Table of Figures & Tables

CHAPTER 1 – Introduction

"In the beginning, the universe was created. This has made a lot of people very angry, and has been widely regarded as a bad idea." -Douglas Noel Adams

1.1 Small molecule perception – The Universal Sense

The perception of and response to external stimuli are fundamental to the survival of all living organisms, and represent one of the unifying themes across all kingdoms of life. Audio/visual cues, while common signaling schemes among higher order multicellular organisms such as *Homo sapiens*, are not the principal mechanisms by which environmental signals are encoded and/or transmitted. Indeed, the bulk of the information about an organism's surroundings, both biotic and abiotic, are encoded in small molecules and transmitted via diffusion through the environment. This is as true for olfaction in the higher organisms as it is for chemotaxis among bacteria. In many cases, the exchange of biotic signals between organisms, or interorganismal signaling, plays critical roles in regulating population dynamics and ecosystem viability. For example, chemical cues known as pheromones direct foraging behavior, hive construction, and sexual reproduction among insects, while in bacteria, a variety of small molecules can alter behavior upon reaching sufficient concentrations via the population dependent phenomenon known as quorum sensing [1-3].

1.2 Plants – Nature's chemical linguist

Due to their sessile nature, plants are critically dependent on, as well as susceptible to, a variety of other organisms and have, not surprisingly, developed a wide array of signals to regulate such encounters. One might say that plants have learned to 'speak the chemical languages' of a variety of organisms. The biosynthesis of such a wide array of signals, while an energetically expensive strategy, is tenable due to the ability of plants to 'fix' carbon directly out of the atmosphere from CO_2 during photosynthesis. This capability provides a vast carbon reservoir for the biosynthesis of a wide array of natural products with diverse structures and functions. From pigments and antibiotics to other small molecules that diffuse through air or soil to regulate behavior and/or development, this library of compounds enable plants to kill, coerce, and otherwise manipulate the behavior of organisms they encounter within their environment.

Airborne signals (Figure 1.1) such as ethylene accelerate the ripening of fruit and have been proposed as a growth regulator in dense plant populations [4, 5]. Such broad purpose signals are frequently inadequate to meet the demands of unique situations and as a result more refined signaling processes have evolved. For example, infestation of *Glycine max* (soybeans) with *Aphis glycines* (Soybean aphid) results in the release of the airborne signal methyl salicylate which specifically attracts *Coccinella septempunctata* (ladybugs) a known predator of the insect [6]. This production is specific to herbivory as manual wounding of the plant shows no increase in the release of methyl salicylate. However, such signaling processes need not be an on-off switch or in direct response to a potential threat. For instance, herbivory of *Artemisia tridentate* (sagebrush) alters the cis-

to trans- ratio of methyl jasmonate released into the air, inhibiting both germination and herbivory of *Nicotiana attenuate* (coyote tobacco), a common neighboring plant species [7-9]. In this example, *N. attenuate* "eavesdrops" on a different species and responds to a more subtle change than the presence or absence of a signal.

Soil-borne, or rhizosphere, based signaling processes show similar diversity in both structure and function (Figure 1.1). Members of the strigolactone family of compounds, originally isolated from cotton, regulate the activity of symbiotic fungal associations to roots [10, 11]. Exudate components capable of regulating bacterial quorum sensing processes such as biofilm formation have been observed in *Glycine max* (soybean), *Pisum sativum* (pea), *Medicago trunculata* (alfalfa), and others; although their structure(s) remain undefined [12-15]. Numerous compounds have been isolated from root exudates which serve to reduce the growth and development of neighboring plants in a broad, often non-specific process known as allelopathy. 5-hydroxy-1,4-naphthoquinone (Juglone) exuded from the roots of members of the *Juglandaceae,* or walnut family, and 6-methoxy-2-benzoxazolinone (MBOA) released by *Zea mays* (corn) are both compounds able to effect the germination, growth, and development of neighboring plants [16, 17].

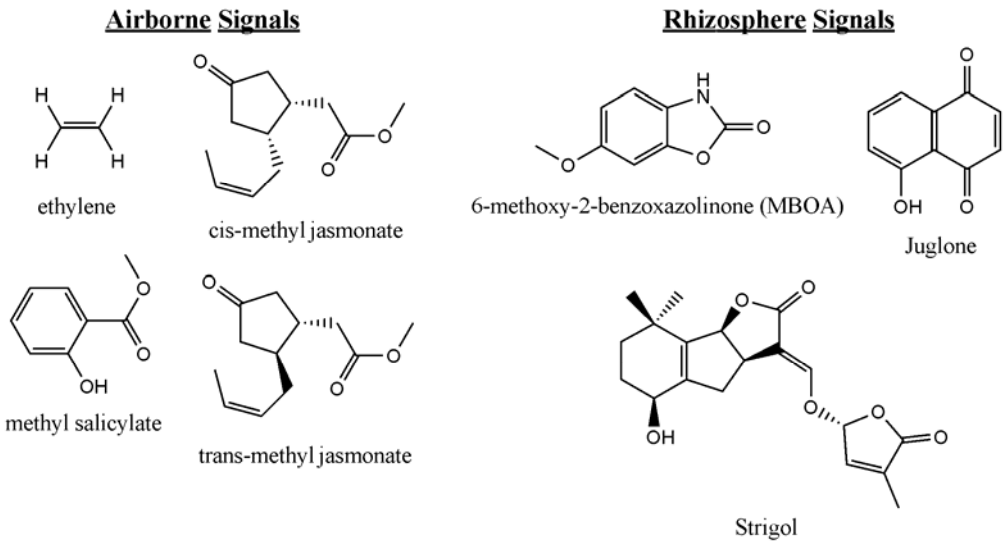

Figure 1.1 – *Structures of known plant derived interorganismal signaling molecules.*

1.3 The Parasitic Plants – An ideal system for the study of signaling

Another allelopathic growth regulator is the *p*-benzoquinone Sorgoleone, the major component of the organic-soluble fraction of *Sorghum bicolor* (Sorghum) root exudate (Figure 1.2) [18]. Originally discovered by Chang *et al.,* it was isolated along with its reduced form, dihydrosorgoleone, while attempting to identify a stimulant for the germination of the parasitic angiosperm *Striga asiatica* (Figure 1.2) [19]. These studies established that the reduced hydroquinone is exuded into the rhizosphere where it initiates germination of the parasite. Rapid oxidation yields the allelopathic quinone (sorgoleone) which lacks germination activity, effectively restricting its use as a signal for the parasite to distances proximal to the host root [19-21]. Dihydrosoroleone, was the first host derived signal, or *xenognosin,* for germination discovered and was originally dubbed SXSg, the **S**orghum **X**enognosin for **S**triga **g**ermination. Interestingly, the strigolactones are also potent germination stimulants of Striga seeds, however both the

biosynthetic origins and even the presence of such compounds in the root exudates of hosts for these parasites remains unclear [5, 22].

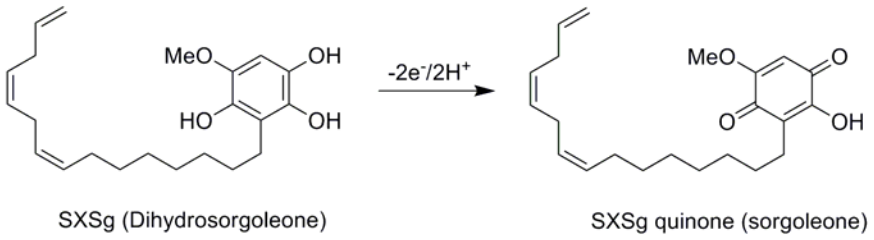

Figure 1.2 - *Reduced (dihydrosorgoleone) and oxidized (sorgoleone) states of SXSg*

The detection of such host derived signals, or *xenognosis*, is common among the parasitic plants where such processes regulate the transitions between multiple developmental stages including germination, host attachment, shoot apical meristem development, and even reproduction [20, 22-25]. Parasitism is not uncommon in the Plantae Kingdom with over 3000 species documented among the angiosperms, an estimated 1% of the total population of flowering plants (Figure 1.3) [23, 26, 27]. Successful parasitism, made possible by the integration of and response to appropriate xenognosins, is responsible for billions of dollars in lost agricultural products worldwide, and contributes significantly to human malnutrition and poverty throughout the developing world [23, 28]. In Africa and Asia, members of the Striga and Orobanche families parasitize crops such as corn, sorghum, millet, cowpea (black eye pea), sugar cane, and potatoes resulting in reduced agricultural yields, with an estimated loss of up to $7 billion annually [29].

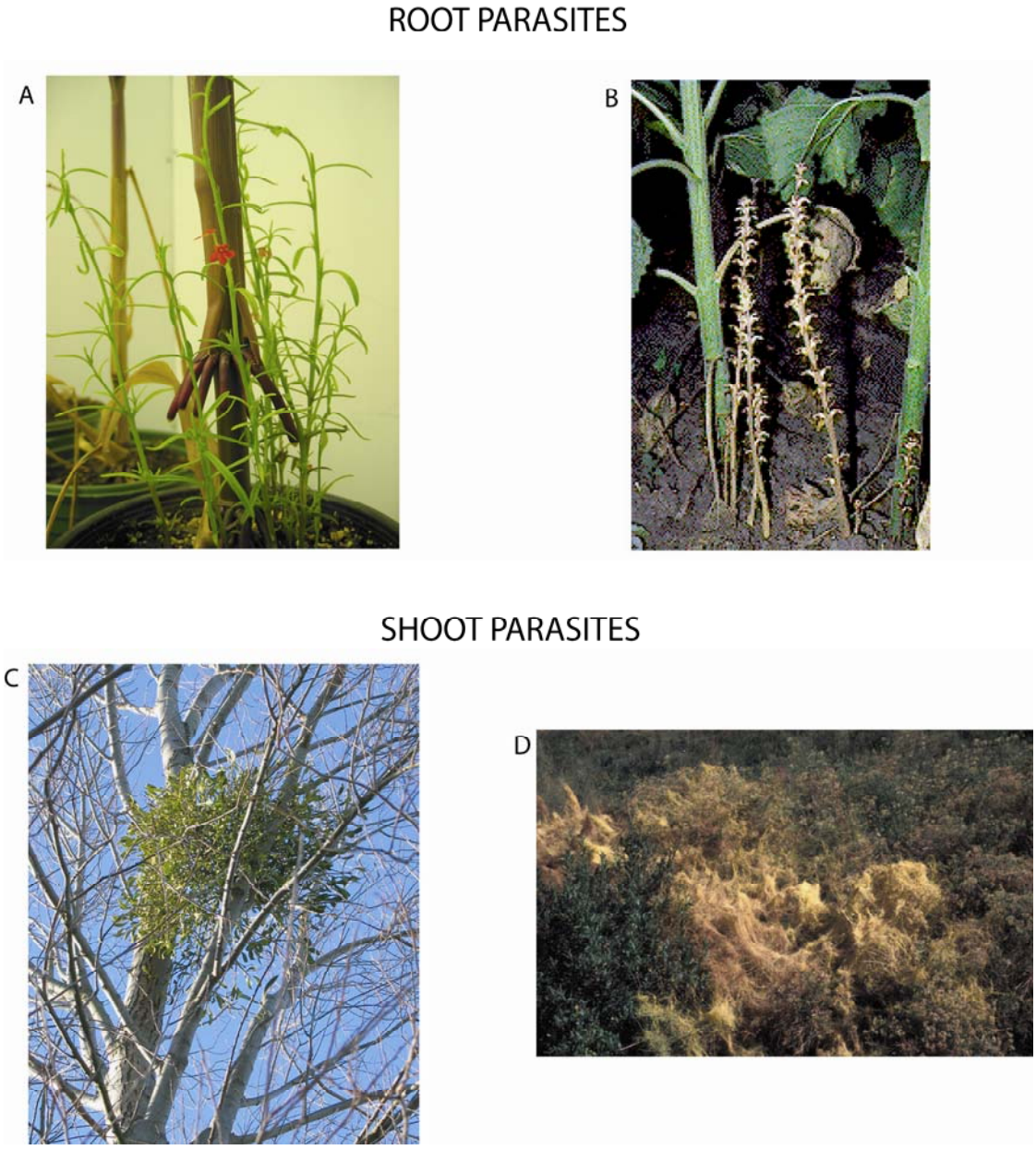

Figure 1.3 – *Root and shoot (aerial) parasitic angiosperms*

(A) *Striga asiatica* parasitizing *Zea mays* (image courtesy of Yue Liu). (B) *Orobanche* on sunflowers. (C) *Viscum* (Mistletoe) parasitizing a poplar. (D) *Dodder* covering a group of Asters (daisy).

Given both the humanitarian and economic impacts posed by such parasites there is, not surprisingly, considerable interest in the development of new strategies to disrupt xenognosis at the host-parasite interface. In addition, the absolute dependence on xenognosins for initiating critical developmental transitions in the parasites makes them an ideal system for the study of interorganismal, more specifically, plant-plant signaling. Furthermore, such xenognosin-dependent transitions suggest fundamental aspects of plant development such as organogenesis can be explored under controlled settings. As distinct signals for germination as well as host attachment have been identified, the Striga spp. present an opportunity to evaluate both xenognosin-mediated development and interorganismal signaling [20, 22-25].

1.4 Striga asiatica – Regulation of Development at the Host-Parasite Interface

The Striga species, e.g., *S. asiatica*, *S. hermonthica*, and *S. gesneroides*, commonly known as 'witchweed' because of their bewitching effect on their host, currently infest approximately 22-40 million hectares of arable land in sub-Saharan Africa [30]. The impact on maize (corn) yields alone is staggering, with over 2.5 million hectares (25,000 km^2) of land infested, reducing crop yields 30-80%, with over $1 billion in lost agricultural yields annually [29, 30]. The fine dust-like seeds of these species can remain dormant in the soil for up to 20 years awaiting a prospective host [23]. However upon germination, the seed's resources are sufficient for only five days of growth in the absence of a host, hence the dependence on xenognosins such as SXSg to ensure host proximity.

Host attachment, occurs via a specialized organ unique to the parasitic plants known as the haustorium [23]. In Striga, the transition from vegetative growth to haustorium development is initiated upon contact with a host root at which point cell division and root elongation abruptly halt, followed by radial swelling of the root tip and the formation of haustorial hairs over the next 24 hours. The simplest model, that haustorium development is a mechanosensitive (touch) event, proves not to be the case, as contact with the glass or plastic surfaces which house the germinated seedlings fail to initiate organogenesis. The necessity for host proximity along with the apparent absence of haustorial inducing signals in the root exudate of prospective host plants suggested the presence of an additional xenognosin, one potentially restricted to the cell wall, which regulated this transition [31, 32].

Indeed, cell wall fragments isolated from the surface of sorghum roots possess haustorial inducing activity, confirming the presence of xenognosins in this tissue. Fractionation of these fragments confirmed that this activity was exclusively associated with the phenylpropanoid, or monolignol, constituents of the cell wall [24]. Furthermore the commitment to haustorium development is both concentration and time dependent (Figure 1.4). Such sustained exposures ensure host proximity, a critical requirement given that premature commitment to haustorium development results in the arrest of root elongation. Removal of these signals prior to commitment results in a return to vegetative growth. Interestingly, haustorium development was initiated more rapidly and at lower concentrations in response to *p*-benzoquinones, the products of phenylpropanoid oxidation at the aryl-Cα bond (Figure 1.4).

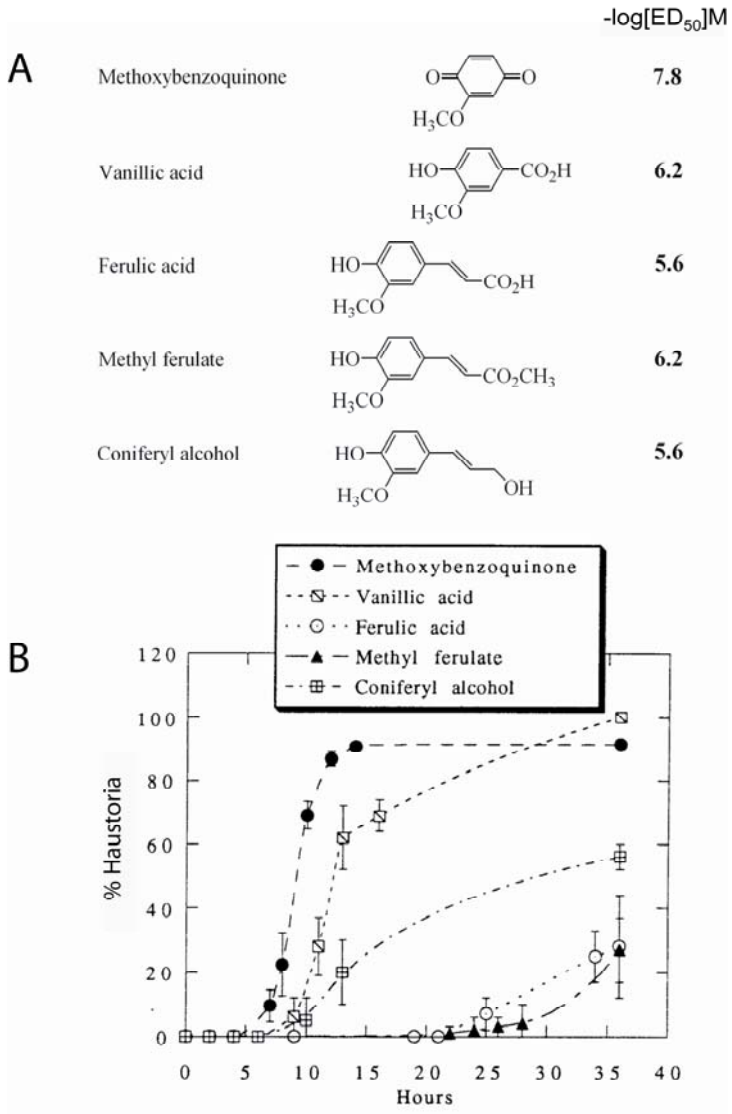

Figure 1.4 - *Induction of haustorial development in S. asiatica*

(A) Structure, and effective dose required for 50% of the seedlings to develop haustoria (ED_{50}). One day-old seedlings are incubated with the indicated compound at set concentrations, (0.1-100 μM) and scored for haustorium formation after 36 hours. (B) One day-old seedlings are incubated in a 10μM solution of the indicated inducer. At the indicated time points, seedlings are washed to remove inducer and scored for haustorium formation after 24 hours. Results expressed in terms of % Haustoria. All assays performed in triplicate with standard deviation expressed as +/- SD. Figure reproduced from [31].

1.5 A mechanism for the production of xenognostic quinones

The evidence above suggested that host cell wall phenylpropanoids may function as haustorial-inducing xenognosins upon oxidation to their corresponding quinones [32-34]. This oxidation is easily catalyzed by co-incubation of phenols, like syringic acid, with reactive oxygen species (ROS) and peroxidases, common enzymatic constituents of plant cell walls (Figure 1.5) [32, 34]. The time elapsed development of the haustorium in a 10μM solution of 2,6-dimethoxybenzoquinone (DMBQ), the product of syringic acid oxidation, is shown in Figure 1.6.

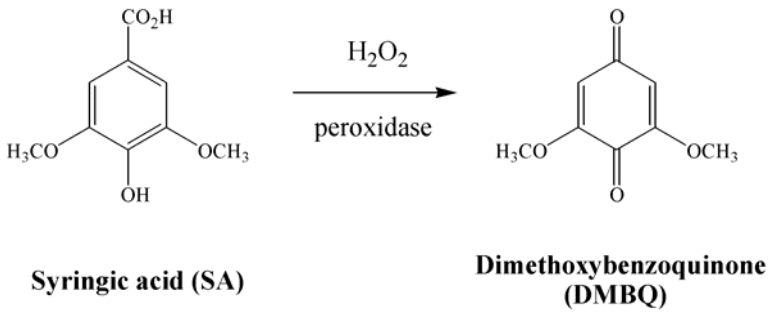

Figure 1.5 – *Reaction scheme for the oxidation of phenols to p-benzoquinones*
Syringic acid (SA) incubated with commercially available horseradish peroxidase in the presence of reactive oxygen species (ROS) such as hydrogen peroxide (H_2O_2) are oxidized at the aryl-Cα bond to generate *p-benzoquinone*s.

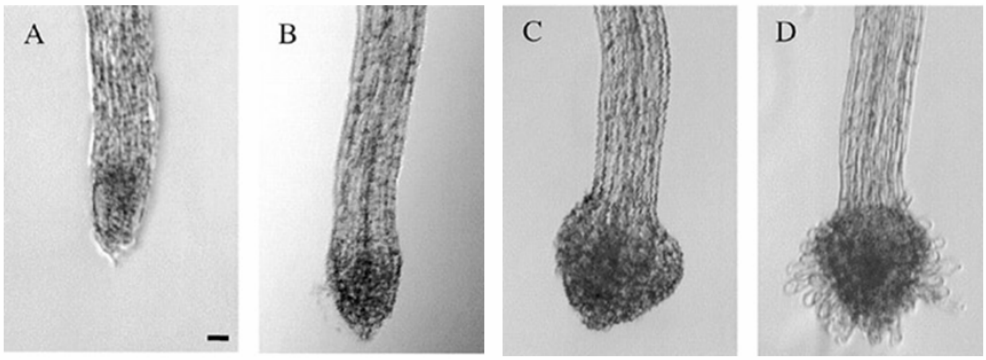

Figure 1.6 – *S. asiatica seedling response to 10μM DMBQ*

Magnification (x20) of 2-day-old *S. asiatica* seedlings exposed to 10 μM DMBQ for 0hr **(A)**, 8 hr **(B)**, 16 hr **(C)**, and 22 hr **(D)**. Bar in **(A)** = 50 μm for **(A)** to **(D)**. Figure reproduced from: [22]

1.6 Activity of xenognostic quinones

A structure-activity relationship (SAR) study of *p*-benzoquinones restricted the haustorial inducing activity to compounds within a redox window from -250 mV to 0 mV relative to the saturated calomel electrode (SCE) [35]. This correlation to the electromotive potential (Em), the energy required for a single electron reduction of the quinone, suggests the generation of a semiquinone intermediate during xenognosis. Additionally, these redox limits suggests both a reduction as well as an oxidation event may be involved in this process. The resulting model facilitated the design of redox sensitive inhibitors of haustorium development [35].

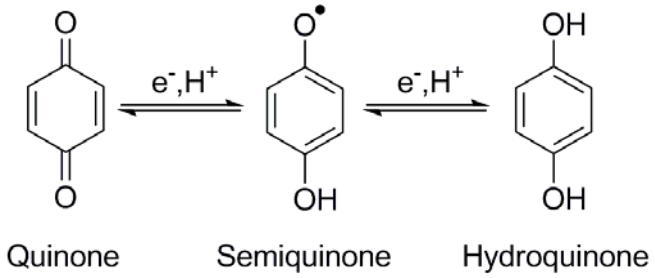

Figure 1.7 – *REDOX states of p-benzoquinones*

The reversible oxidation/reduction steps for quinone/hydroquinone interconversion. Reduction of the quinone to the semiquinone radical anion occurs by the addition of one electron/proton pair. An additional electron/proton reduction converts the semiquinone into the hydroquinone.

In addition to electrochemical constraints, steric limitations to the quinone were found to play an important role in triggering haustorium development [35]. Quinones with bulky substituents, such as *t*-butyl or benzyl, are unable to induce haustorium development as are tri-substituted quinones. However, mono-substituted quinones with smaller functional groups (-OMe, -OH, etc.) are active inducers. Similarly substituted ortho- and meta- di-substituted quinones were also active while substitutions in the para orientation generally rendered the quinone inactive. Such steric limitations further support the existence of a structured binding site.

1.7 Evaluating and justifying a model for phenol oxidation to xenognostic quinones

While a model in which the *p*-benzoquinone xenognosins for haustorium development are derived from the oxidation of host monolignols is reasonable, no direct evidence had been presented. As a result, a search for parasite peroxidases and ROS was initiated. Pyrogallol forms red insoluble deposits upon oxidation via peroxidases and ROS and can be used to detect either enzyme or oxidant by adding the other in excess [31]. Peroxidase activity was assayed by staining one, two, and three day-old seedlings of *Striga asiatica* with pyrogallol in the presence of excess hydrogen peroxide (H_2O_2). As seen in Figure 1.8, stains accumulated largely at the root tip, the site of haustorium development, and the seed coat of the parasite while significant peroxidase activity was observed throughout the root of the model non-parasite *Arabidopsis thaliana* [31, 36]. In addition to peroxidases, the oxidation of the monolignols to the proposed haustorial inducing quinones is ROS dependent suggesting the parasite must produce sufficient oxidant to drive this reaction. Indeed, increasing concentrations of the H_2O_2 scavenging enzyme catalase inhibited haustorium development from syringic acid, but had no effect on DMBQ induction (Figure 1.9) [31, 36].

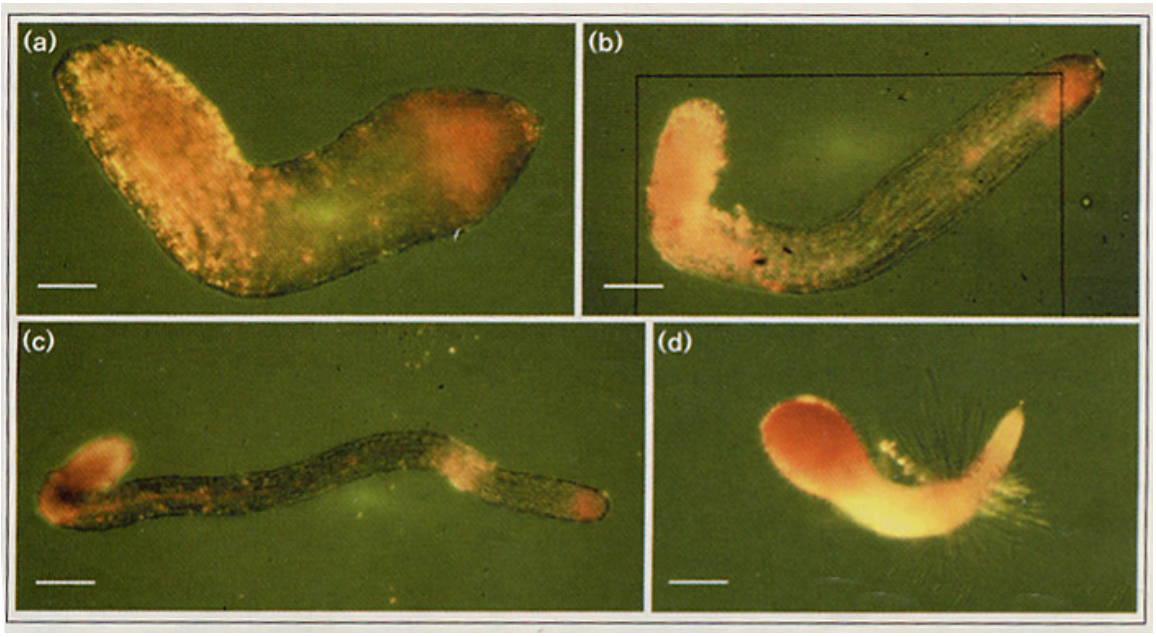

Figure 1.8 - *Histochemical staining of S. asiatica and Arabidopsis thaliana.*

(a) One day-old *S. asiatica* seedling. **(b)** Two day-old *S. asiatica* seedlings. **(c)** Three day-old *S. asiatica* seedling. **(d)** Two day-old *Arabidopsis thaliana* seedling. Scale bars: (a) 40 µm; (b)80 µm; (c)150 µm; (d)250 µm. Figure reprinted from: [31].

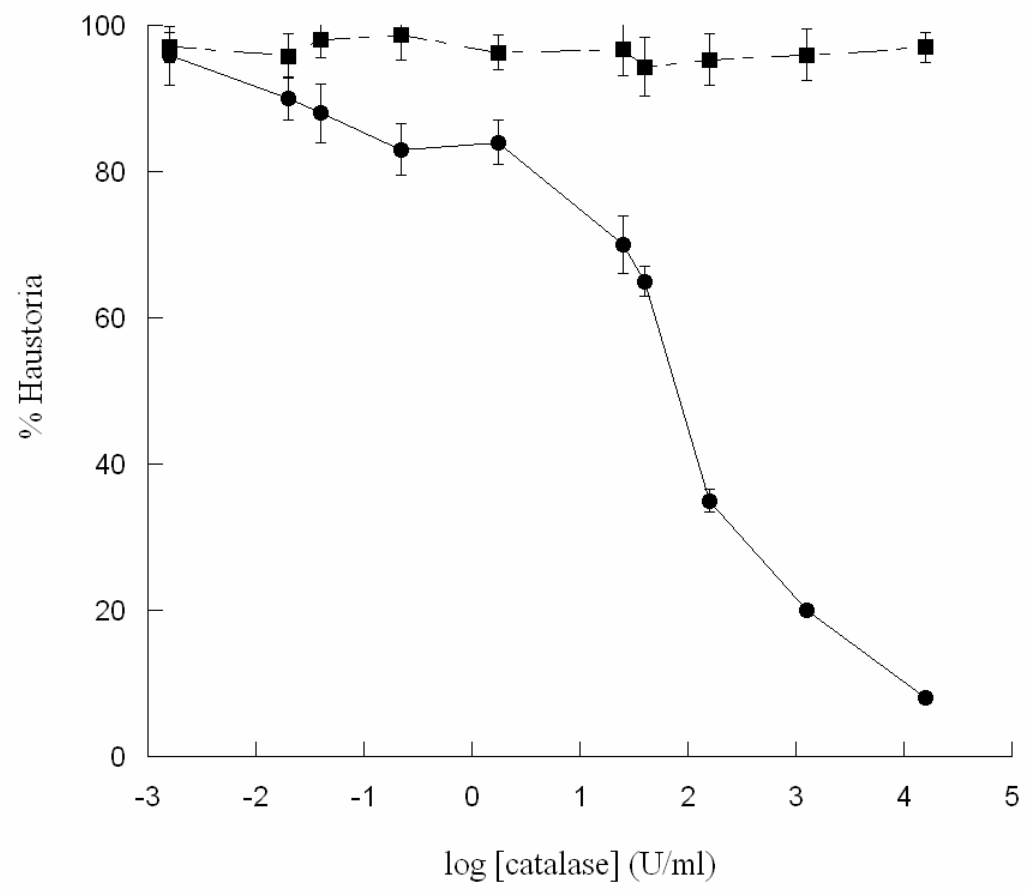

Figure 1.9 - *Catalase treatments inhibit haustorial induction.*

Two-day-old *S. asiatica* seedlings were incubated at 30 °C for 24 hr with (●)100 µM SA or (■)10 µM DMBQ at the indicated catalase concentrations before scoring for haustoria. The induction percentage was determined in triplicate and expressed as ±SD. Figure reprinted from: [36, 37]

If phenylpropanoids are common components of plant cell walls, how then does Striga avoid premature commitment to haustorium development via oxidation of its own phenolics? Monolignols, the major source of autofluorescence in plant roots, are easily observable under UV light allowing phenol content to be qualitatively assessed. Interestingly, while roots of *A. thaliana* and host plants like *Z. mays* show significant autofluorescence, the germinated seedlings of *Striga asiatica* show none (Figure 1.10). The absence of these monolignols in the root of the parasite prevents premature commitment to haustorium development due to self-recognition, and also explains why Striga seedlings do not parasitize one another [26, 27].

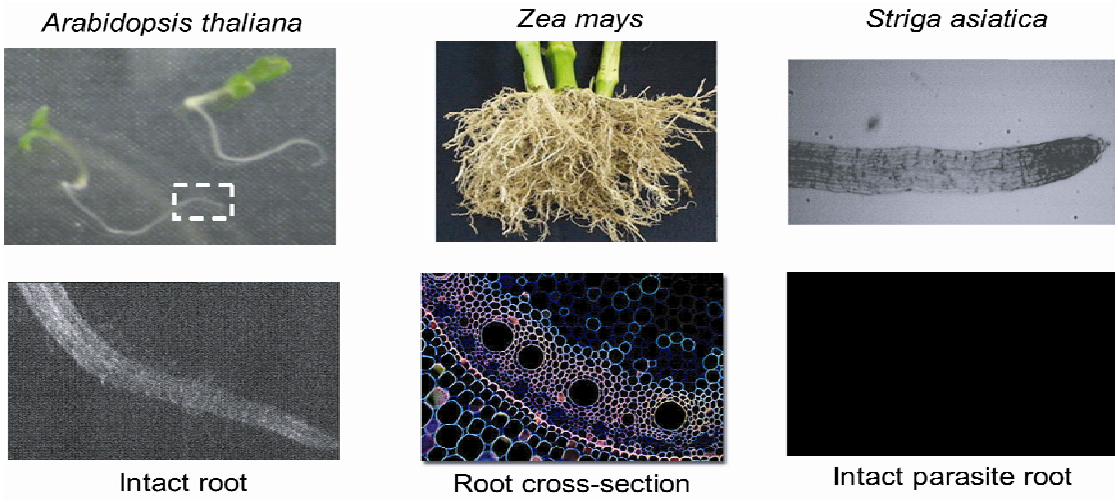

Figure 1.10 – *Monolignol autofluorescence in: A. thaliana, Z. mays, and S. asiatica*
(Top) optical micrographs of intact plant tissue. (Bottom) Autofluorescence images of the top plants collected by UV excitation. Images of *Arabidopsis thaliana* and *Striga asiatica* are courtesy of Lizhi Liang. Autofluorescence image of *Zea mays* from cross section of root fixed to a microscope slide and is from the Olympus image library: (http://www.olympusconfocal.com/gallery/plants/index.html).

1.8 Refining a model for the oxidation of host root surfaces

The results presented thus far are consistent with a model in which Striga exudes ROS and/or peroxidases into the rhizosphere to oxidize host cell wall monolignols. However, Striga root exudate showed little peroxidase activity arguing against the enzyme's release. The ability of non-cell permeable catalase to inhibit oxidation of the monolignols suggests H_2O_2 is present in the extracellular matrix, at the very least, and potentially available to react with host phenols at the host-parasite interface [31]. Such a reaction would exploit the high density of peroxidases and monolignols typically associated with the roots of non-parasites (Figures 1.8 & 1.10). This active process of signaling, in which the parasite participates chemically in the search for its host, stands in sharp contrast to the passive process of host detection seen in germination. This active process of signal generation was named: semagenesis from the Greek words *sema* (signal) and *genesis* (Figure 1.11) [22, 37, 38].

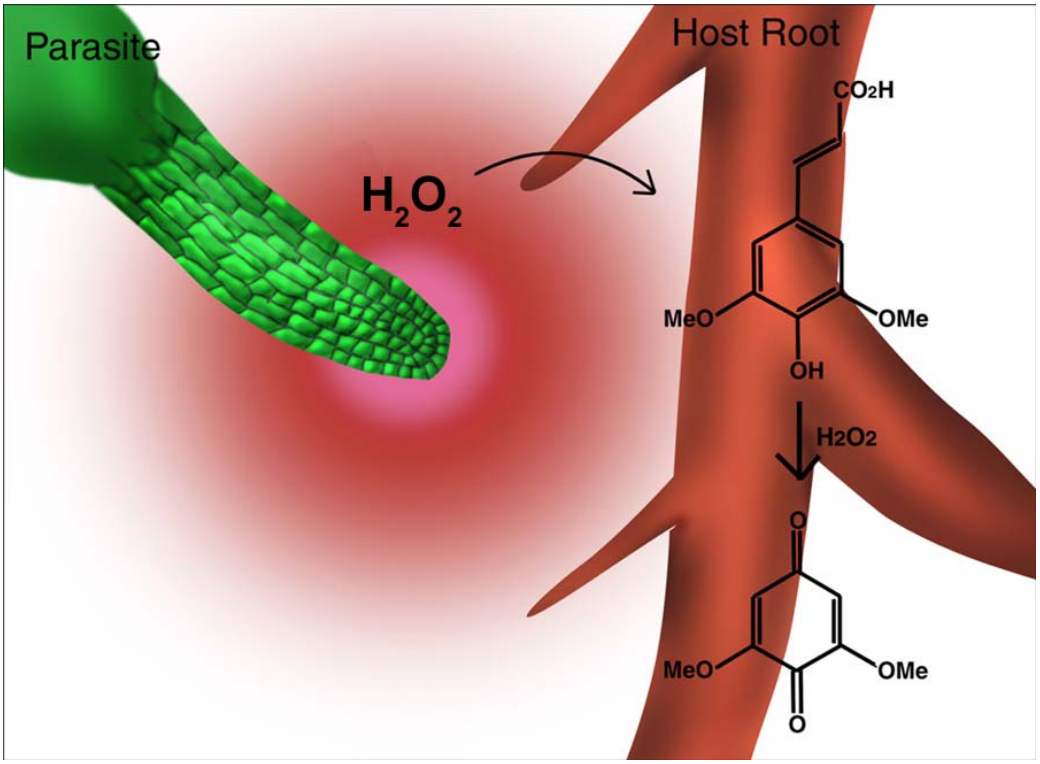

Figure 1.11- *A model for semagenesis.* Seedlings of Striga asiatica exude H_2O_2 (red) which diffuses away from the host root. Upon contact with the host root surface, the oxidant in conjunction with host derived peroxidases catalyzes the release of xenognosic quinones. Figure reprinted form: [37].

1.9 The many faces of ROS

As the production of reactive oxygen species is clearly critical to this novel and obligatory interorganismal signaling process, a close examination of the identity and roles of these common oxidants seems appropriate. Reactive oxygen species (ROS) is the general term used to describe the potent oxidants superoxide ($O_2^{\bullet-}$), hydrogen peroxide (H_2O_2), and hydroxyl radical ($^{\bullet}OH$). These reactive intermediates are capable of oxidizing a variety of biomolecules, including lipids and DNA; and have been implicated in both aging and disease [39-41]. The potential dangers of such oxidants, an obvious challenge for aerobic life, is made all the more interesting by the observation that eukaryotes actually generate $O_2^{\bullet-}$ during ATP biosynthesis [42]. In the cell, $O_2^{\bullet-}$ is disproportionated to the more stable O_2 and H_2O_2. As the latter accumulates, it can react with free metals in solution or peroxidases to generate $^{\bullet}OH$ through the Fenton reaction [43].

While ROS are an inevitable aspect of aerobic life, eukaryotes have evolved to exploit these potent oxidants in defense. Plants and animals both generate substantial amounts of ROS to defend against invading pathogens in a process known as the oxidative or respiratory burst response [44-46]. In plants, the oxidative burst is not limited to a specific cell type but rather can occur in any cell at the site of attack [44, 45]. Stimulation of the oxidative burst occurs in response to mechanical wounding, small molecule or peptide elicitors typically derived from plant pathogens, or even abiotic stressors such as metal accumulation [47-49]. Substantial analysis of the oxidative burst has led to the elucidation of multiple roles for ROS in this process including inducing incompatible interactions between plants and avirulent pathogens [48, 50-52], inhibiting

pathogen growth by cross-linking cell wall components [51, 53], killing invading pathogens by regulating defense gene expression [49, 51], and triggering programmed cell death [54].

In addition to its critical roles in defense, growing evidence now suggests additional roles for ROS in cell growth and eukaryotic development. For example, in the nematode *Caenorhabditis elegans*, ROS is required for cross-linking tyrosine residues. This reaction is critical to stabilization of the extracellular matrix, preventing severe epidermal abnormalities; its absence resulting in the 'leaky worm' phenotype [55]. In plants, ROS production is critical to root tip growth, root hair and pollen tube elongation, guard cell regulation, and other developmental events [56-60].

The use of ROS as an interorganismal signal has not previously been observed, broadening the roles for reactive oxygen. However, the use of such potent oxidants as probes for host proximity is contradictory to their roles in both defense and development suggesting they must be tightly regulated in order to function. This work employs a variety of microscopy techniques in conjunction with physiological and molecular biology assays to evaluate this hypothesis. The results reported herein reveal an interorganismal signaling process that is robust and tightly regulated at both the biochemical and genetic level, which appears to have evolved from physiological processes already present among non-parasites. These findings impact our understanding of the small molecule regulation of growth and development among plants, the roles ROS can play in interorganismal signaling as well as development, and the evolution of parasitism.

CHAPTER 2 – Defining Semagenesis

Localization and Regulation of ROS Production

"If you don't like their rules, whose would you use?" – Charlie Brown

2.1 Introduction

In addition to their commonly accepted role in the defense response of eukaryotes reactive oxygen species (ROS), such as hydrogen peroxide (H_2O_2), have more recently been associated with a number of developmental events including root hair growth [56], gravitropism [60], and stomatal closure [59]. These expanded roles for oxidant production make it increasingly clear that plants exploit these intermediates not only in acute responses to a changing physical and biotic environment, but also in long-term developmental programs. To this growing list of ROS-mediated events we can now add semagenesis, in which reactive oxygen species are employed to detect prospective host root surfaces. This discovery highlights a novel interorganismal signaling process which regulates development of the host attachment organ, the haustorium, among the parasitic plants.

However, the use of ROS for the purposes of signaling is almost certainly complicated by its roles in defense and development. Indeed the production of reactive oxygen appears to be both spatially localized and tightly regulated to prevent overlap and/or undesired cross-talk between these distinct pathways [56, 57, 60, 61]. For example, in the case of polar (directional) growth as in pollen tubes and root hairs, ROS accumulates exclusively at the growing tip directing elongation [56, 57]. Oxidant production at these sites is under the overlapping control of several regulatory components including kinases, GTPases, and cytoplasmic calcium [56, 62, 63]. Similar regulatory controls almost certainly underpin semagenesis to prevent the initiation of host defenses.

Dihydrodichlorofluorescein diacetate (H_2DCFDA)(Figure 2.1) and its derivatives has previously been used to visualize cytoplasmic ROS production and regulation in plant cell cultures experiencing mechanical stress [64], guard cells exposed to abscisic acid [59], and in parsley cells prior to death by fungal infection [65]. This reduced, acetylated, and non-fluorescent derivative of fluorescein is cell-permeable, and remains trapped in the cell following hydrolysis by cytoplasmic esterases. Subsequent oxidation of H_2DCF by cytoplasmic ROS yields the highly fluorescent dichlorofluorescein (DCF) (λ_{ex}=488 nm; λ_{em}=530 nm) [66]. In each previous case, oxidation, rather than hydrolysis, proved to be limiting, providing a marker for cytoplasmic ROS [54, 66].

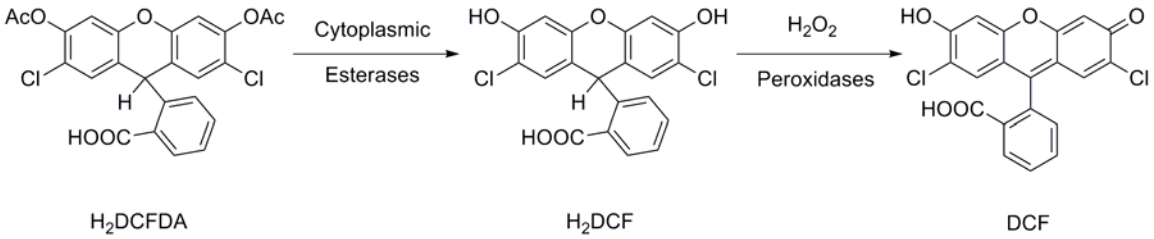

Figure 2.1: *H_2DCFDA Activation.*

Neutral dihydrodichlorofluorescein diacetate (H_2DCFDA) is cell permeable and cleaved by cytoplasmic esterases to yield H_2DCF which can be oxidized by cytoplasmic ROS such as H_2O_2 to yield fluorescent dichlorofluorescein (DCF) (λ_{ex}=488 nm; λ_{em}=530 nm).

Herein the small size and transparency of the Striga seedling has been exploited to evaluate the localization and regulation of ROS production during semagenesis by fluorescence microscopy. These studies employ H_2DCFDA as a probe for oxidant production in a robust assay which facilitates both spatial and temporal regulation of ROS to be evaluated in the parasite. Collectively, these studies further define the process of semagenesis, establish a robust assay for monitoring oxidant production in the parasite, and hint at the potential molecular origins of this novel interorganismal signaling process.

2.2 Results

2.2.1 Localization of ROS accumulation in S. asiatica seedlings.

Localization of oxidant production was accomplished by loading one day-old seedlings of *Striga asiatica* with 10 μM H_2DCFDA for three minutes, washing to remove excess dye, and imaging via laser scanning confocal microscopy (LSCM). Excitation of DCF via LSCM permits the three dimensional visualization of ROS localization *in vivo*. Imaging of a single two-dimensional cross-section midway through the vertical axis of the seedling established fluorescence accumulation was localized to the surface cells of the root tip (Figure 2.2A). This "surface only" accumulation was consistently observed in multiple seedlings as shown in Figure 2.2B in which the pixel intensity across the region (denoted by the white arrows) was reproduced in 5 separate samples.

Fluorescein diacetate (FDA), which upon esterase cleavage yields the fluorescent probe directly, was loaded into the seedlings to evaluate H_2DCFDA accessibility to the inner cells of the root tip. As seen in Fig. 2.2C&D, incubation with FDA for 3 minutes resulted in uniform fluorescence intensity throughout the root tip. This suggests that neither dye accessibility nor the loss of emission intensity with tissue depth accounts for the differential fluorescence accumulation seen in Fig. 2.2A&B. Furthermore, neither longer incubation times (15 min) nor increased H_2DCFDA concentrations (50 μM) alter the observed fluorescence localization. As ROS production appears limited to the root surface, LCSM is not necessary and further ROS assays were conducted on a standard fluorescence microscope.

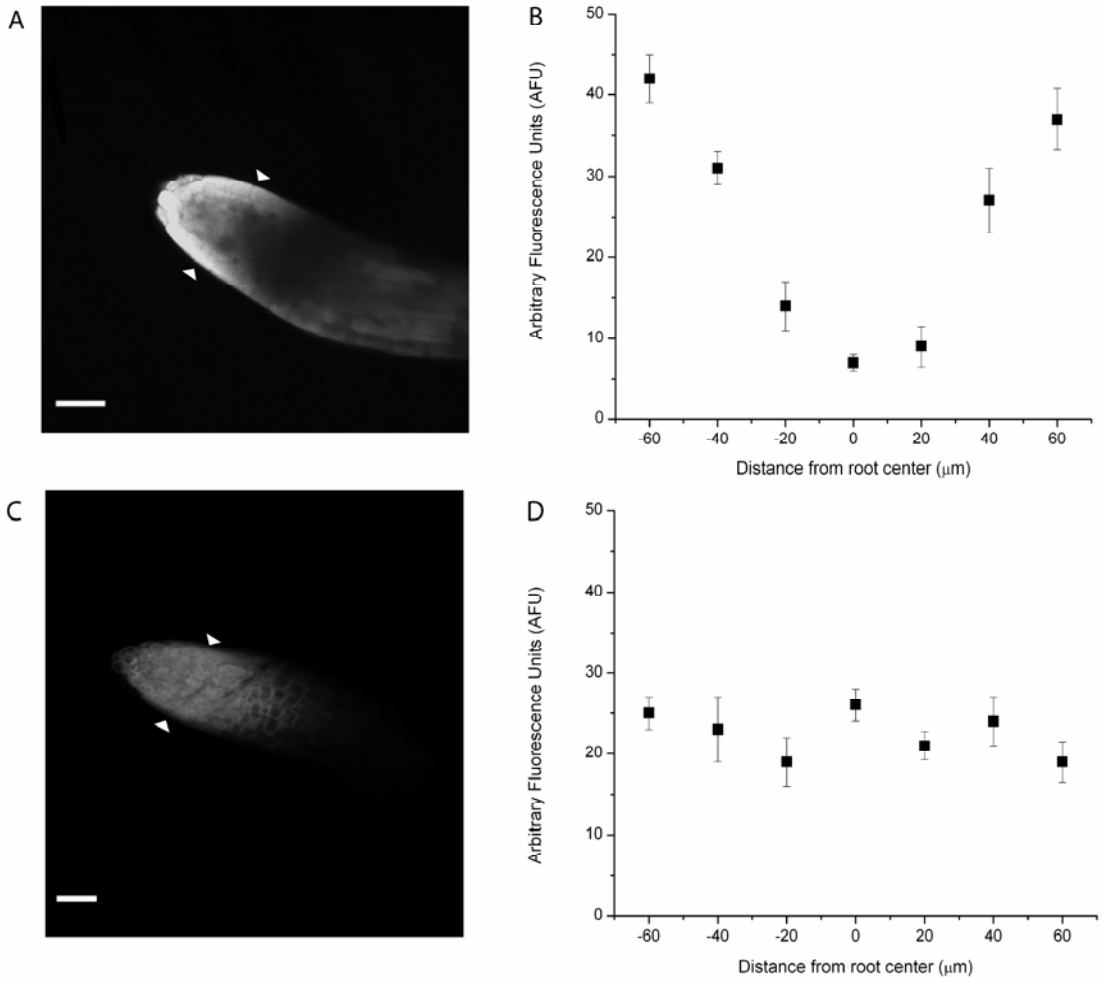

Figure 2.2: *Laser scanning confocal microscopy (LSCM) image of H_2O_2 localization in Striga asiatica seedlings.*

One day-old seedlings of *S. asiatica* were incubated in 10 μM H_2DCFDA or DCF for 3min, washed 3X, and scored for fluorescence. The relative fluorescence intensity (B and D) across the seedling root at the white arrows highlights the differential localization of the oxidation across the root tip. Plots are derived from the average fluorescence distribution across 5 different seedlings and expressed as ± SD. Bar= 50 μm**.** Image A taken by W.J. Keyes.

2.2.3 ROS accumulation is not due to wounding

Given their role in the oxidative burst, the production of ROS may simply be associated with generalized stress, such as radicle (seedling) emergence from the seed coat, which would be expected to decline over time. As seen in Figure 2.3A, H_2DCFDA florescence intensity remained constant and localized to the meristem over the five days the seedlings are capable of haustorial development. Alternatively, oxidant production could be an indicator of stress-induced apoptosis of the surface cells. To specifically evaluate cellular viability, seedlings were treated with propidium iodide (PI), a fluorescent dye previously used to observe aluminum (Al^{3+}) toxicity in seedlings of *Arabidopsis thaliana* [47, 67]. Increased PI fluorescence in response to $AlCl_3$ treatments of one day-old Arabidopsis seedlings served as a positive control for toxicity (Figure 2.3B). PI is excluded by Striga seedlings throughout the 5 days of their viability while prior treatment with toxic $AlCl_3$ resulted in significant root tip-localized PI staining (Figure 2.3B).

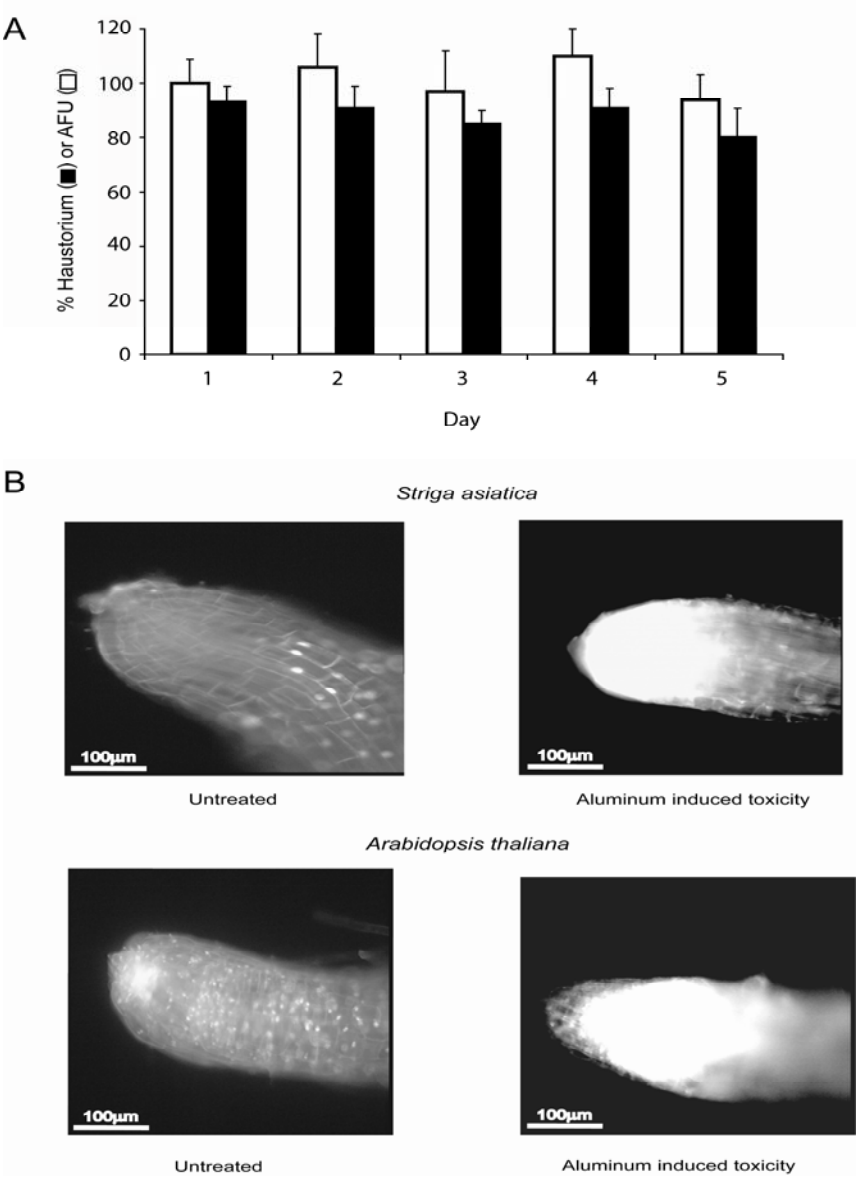

Figure 2.3: *H_2O_2 accumulation and viability.*

(A) Striga seedlings from one to five days post germination are treated with H_2DCFDA and scored for florescence. The average pixel intensity at the root tip of 3 seedlings is plotted as arbitrary fluorescence units (AFU) (□). The seedlings at each age group are treated with 10 µM 2,6 dimethoxy-*p*-benozquinone (DMBQ) and scored for haustorial development after 24 hours (■). (B) One day-old Striga and Arabidopsis seedlings are scored for florescence from 10 µM propidium iodide (PI) without (left) or with (right) treatment in 10 mM of $AlCl_3$ for 8 hr.

2.2.4 ROS accumulate in extracellular spaces

The histochemical analyses confirm the presence of H_2O_2 in the cytoplasm as well as its localization to the root tip, the site of haustorium development [31]. However, semagenesis requires ROS to be present in the extracellular, or apoplastic spaces, if it is to be available for the oxidation of host cell wall phenols. To characterize apoplastic localization of ROS, its specific reaction with cell-impermeable $CeCl_3$ was exploited. The resulting cerium hydroxide salts form insoluble, electron-dense perhydroxide deposits easily observable by transmission electron microscopy (TEM) [49, 68, 69]. *S. asiatica* seedlings were treated with $CeCl_3$, fixed, sectioned, and visualized by TEM. As shown in the montage of low-magnification electron micrographs (Fig. 2.4A), extracellular deposits of cerium perhydroxide localized to the interstitial spaces (Fig. 2.4B) along the surface of the meristem. The intensity of the deposits diminished distally along the root axis, always disappearing by at least 8-10 cell lengths past the tip. Multiple deposits within the cellular interstitial spaces, similar to that shown in Fig. 2.4C, were also apparent. This apoplastic deposition along the surface cells of the meristem correlates with the cells identified as accumulating H_2O_2 by LSCM in Figure 2.2.

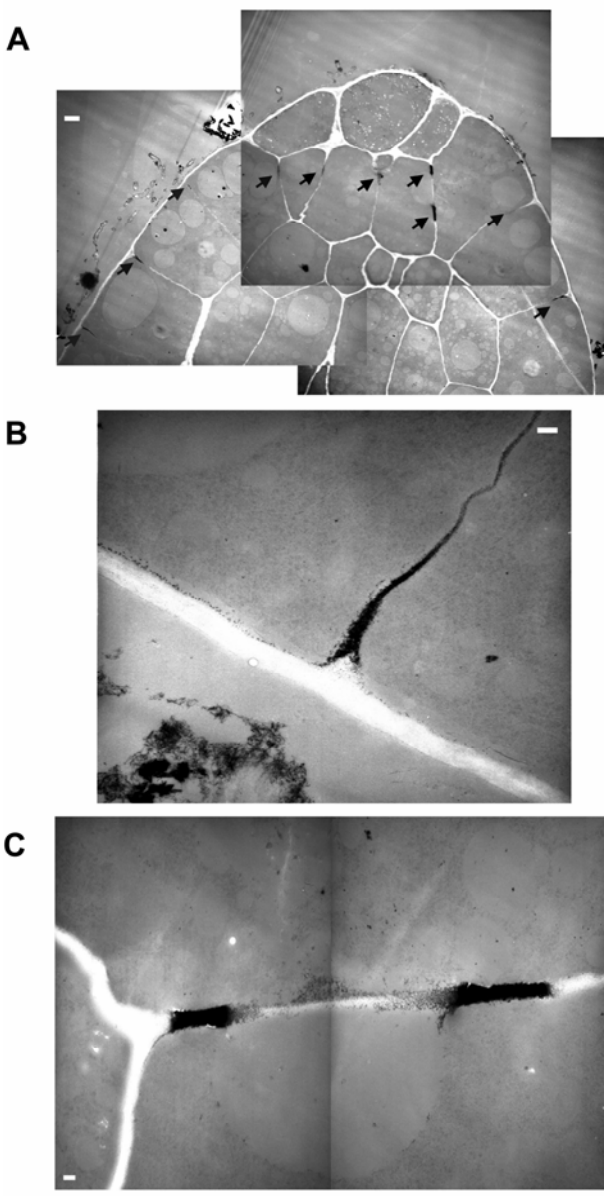

Figure 2.4: *Extracellular localization of H_2O_2.* Eighteen hours post germination, *S. asiatica* seedlings were incubated in freshly prepared solutions of $CeCl_3$ for 2 hr, fixed, sectioned, and analyzed via TEM. (A) electron dense deposits (arrows) are shown in low magnification TEMs of root tip sections, Bar = 2 µm. (B) Enlargement of the cellular junctions of the bottom left corner of Figure 3A, Bar = 200 nm. (C) Enlargement of cells at the root tip of Figure 3A, Bar = 200 nm. TEM images collected by W.J. Keyes [36, 37].

2.2.5 Regulation of ROS accumulation

In sharp contrast with the staining of the vegetative root meristem, Striga seedlings treated with 10 μM DMBQ for 12hrs were virtually devoid of cerium perhydroxide deposits (Fig. 2.5A&B). These results prompted further exploration of the effects of the xenognostic quinones on cytoplasmic H_2O_2, as measured by the rate at which DCF fluorescence accumulates. Due to the time for dye loading (3 minutes), successive washings to remove excess H_2DCFDA, and positioning onto the microscope, the earliest time points at which fluorescence could be accurately measured was 5 minutes. As seen in Figure 2.5C, the rate of fluorescence accumulation was significantly reduced in Striga seedlings pre-treated with 10 μM DMBQ, consistent with the TEM studies. Under these conditions the increase in fluorescence of untreated seedlings (NO DMBQ) plateaus after 15 minutes. The average fluorescence intensity at this maximum (15 min) was set at 100 and all other images were then referenced to this intensity to produce the relative fluorescence measurements. Longer dye loading times and higher dye concentrations both increased the rate of fluorescence accumulation and extended the plateau to longer times, consistent with assigning the plateau to internal dye depletion. Therefore, the linear range from 5 to 15 min allowed for a comparison of the relative cytoplasmic H_2O_2 concentrations per seedling in response to haustorial inducing quinones (Figure 2.6A).

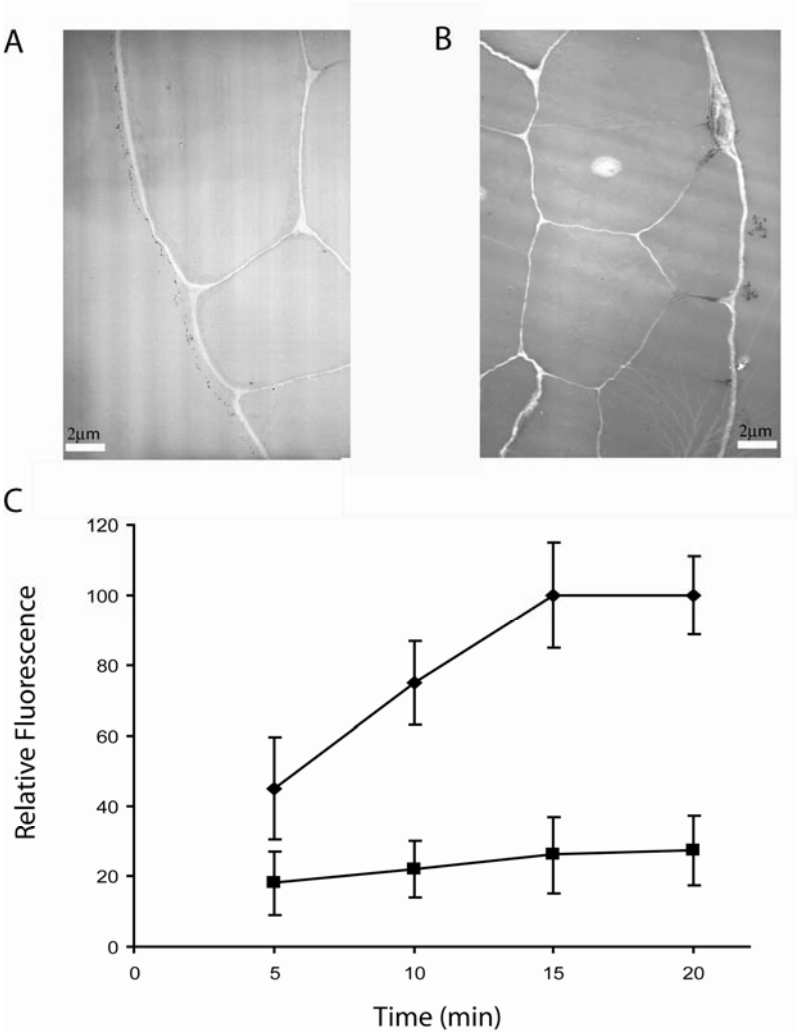

Figure 2.5: *DMBQ perception and H_2O_2 accumulation.* Day-old seedlings of *S. asiatica* were incubated with or without 10 µM DMBQ for 12 hrs (A&B respectively), transferred to $CeCl_3$ for staining, fixed, sectioned, and analyzed by TEM. (C) Five seedlings treated with (■) or without (♦) DMBQ were scored for fluorescence at the indicated time periods. Relative fluorescence is the ratio of the pixel intensity of the root tip at the given time and to the average intensity in untreated seedlings after 20 min expressed as ± SD. TEM images by Keyes [37].

Day-old Striga seedlings were exposed to DMBQ for 0 to 16 hours then washed and scored for ROS production at set time intervals. Images were collected at both 5 and 15 minutes after staining was completed and the ratio of fluorescence change (15 min/5 min) was normalized to control seedlings (NO DMBQ) set as 100 (See Methods). By making this measurement dependent on the rate at which ROS accumulates this expression normalizes for variations in seedling size and the initial levels of the oxidant. As seen in Figure 2.6B, 10 μM DMBQ depletes ~90% of the intracellular H_2O_2 within 2 hr. Following this initial down regulation, oxidant production remained at this new steady state for at least 16 hrs with DMBQ present in the media.

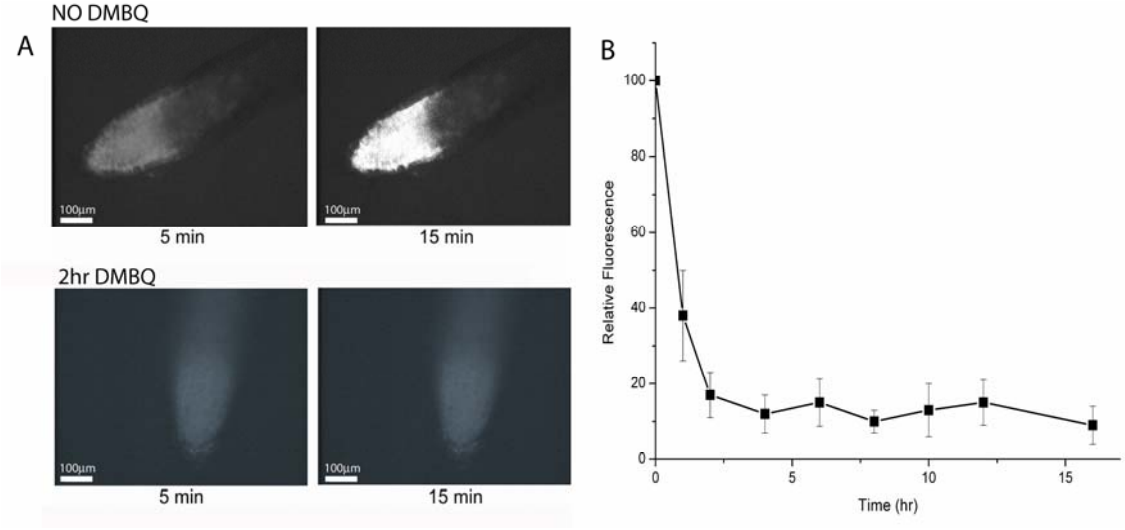

Figure 2.6: *Time dependence of H_2O_2 down-regulation.*

One day-old seedlings of *S. asiatica* were treated with 10 μM DMBQ for the indicated time, washed, incubated with 10 μM H_2DCFDA and scored for fluorescence. (A) Representative 2 hr images with and without DMBQ exposure. (B) The ratio of pixel intensity of each root tip (15 min/5 min) the relative fluorescence was scaled as a percentage and expressed for five replicate seedlings as the average ± SD.

2.2.6 Fluorescence loss is due to change in ROS production

The reduced accumulation of fluoresence in Striga seedlings treated with DMBQ suggests a decline in ROS production in response to the presence of haustorial inducing quinones. A 2 hr pretreatment with potassium iodide (KI), a known scavenger of ROS, reduced DCF fluorescence, while H_2O_2 showed a significant increase in relative fluorescence, consistent with changes in DCF accumulation reflecting changes in cellular oxidant levels (Figure 2.7). An alternative explanation for the reduced DCF fluorescence in response to DMBQ exposures is a reduction in esterase activity limiting the availability of H_2DCF for oxidation. As activation of FDA is only limited by esterase activity, it serves as an excellent positive control. As seen in Figure 2.8, seedlings incubated with FDA for three minutes accumulated fluorescence to similar levels, regardless of DMBQ exposure time, arguing against a simple loss of esterase activity as the source of reduced H_2DCF activation.

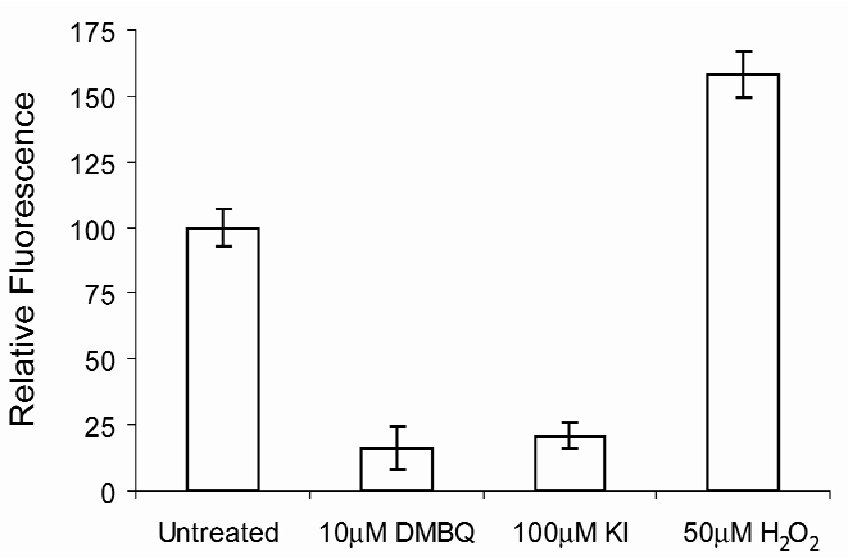

Figure 2.7*: Fluorescence accumulation reflects changes in cytoplasmic oxidant levels.*

Day-old seedlings of *S. asiatica* are incubated for 2 hours in the indicated compound, washed and scored for ROS production via H_2DCFDA staining as previously described.

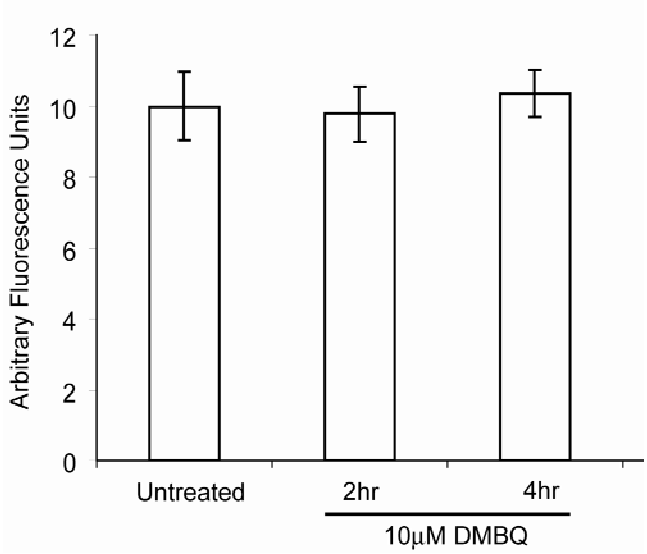

Figure 2.8: *Effects of haustorial inducers on esterase activity.*

Day-old seedlings of Striga are scored for fluorescence by incubation with 10μM fluorescein diacetate (FDA) with or without treatment with DMBQ.

2.2.7 H_2O_2 regulation correlates with haustorial induction

The DCF studies confirm that ROS production is indeed regulated by the presence of the haustorial inducer DMBQ. However the extent and sensitivity of this regulatory process remained in question and additional experiments were necessary. H_2O_2 depletion, like the commitment to haustorium development, proved concentration dependent with DCF accumulation inversely related to the DMBQ concentration between 1 and 10 μM (Fig. 2.9A) [34, 70]. This reduction in ROS production appeared specific for haustorial inducing quinones as the structurally similar inducer *p*-benzoquinone (BQ) down-regulated fluorescence accumulation at a similar rate, while the non-inducers tetrafluorobenzoquinone (TFBQ) and 2-methyl-naphthoquinone had no effect. (Figure 2.9B) [35]. Additional haustorial inducing quinones were evaluated for their effect on the initiation of organogenesis as well as reactive oxygen species down regulation. The $t_{1/2}$ for these processes are summarized in Table 2.1 and suggest the rates for these two events are similar, i.e. compounds which initiate developmental commitment more rapidly also down regulate oxidant production more quickly.

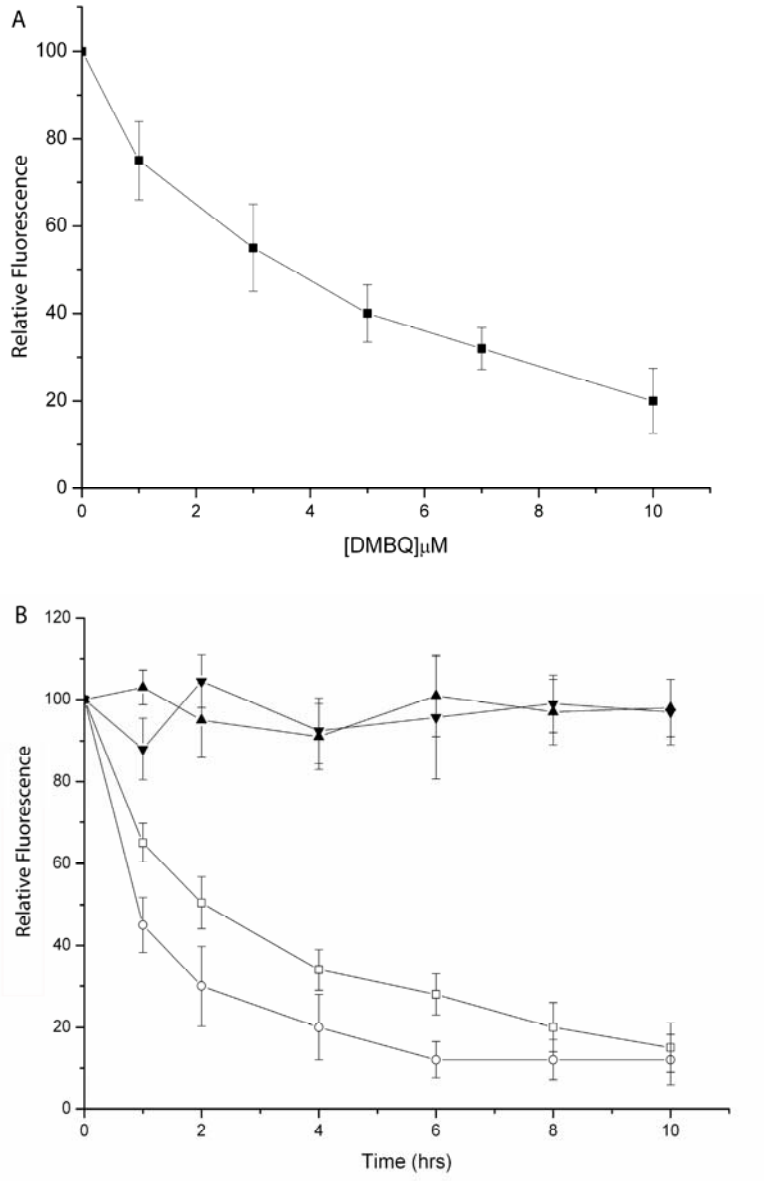

Figure 2.9: *Structural dependence of inducers on the rate of DCF accumulation.*

Day-old seedlings of *S. asiatica* seedlings were (A) incubated with the indicated DMBQ concentration for 2 hr, rinsed, loaded with 10 μM H_2DCFDA for 3 min, and scored for fluorescence. Results from five seedlings are averaged and presented as ± SD for each point. (B) Seedlings were incubated with 10 μM of: DMBQ (○), *p*-benzoquinone (□), 2-methyl-*p*-naphthoquinone (▼), or tetrafluoro-*p*-benzoquinone (▲) for the indicated times and scored for H_2DCFDA fluorescence as in (A).

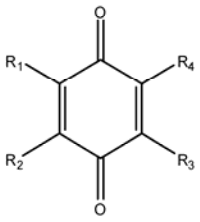

R1	R2	R3	R4	ID	REDOX (mV)	%Hau$_{MAX}$	$t_{1/2}$ Hau (hr)	$t_{1/2}$ ROS (hr)
OH	H	OH	H	1	25	41	9	2
C_6H_5	H	H	H	2	15	38	8	1.5
H	H	H	H	3	0	92	12	2.25
OMe	OMe	H	H	4	-60	91	1.6	0.5
Me	H	H	H	5	-80	93	8	1.5
OMe	H	H	H	6	-110	93	9	2
OMe	H	H	OMe	7	-225	92	6	1
OMe	H	OMe	H	8	-255	49	8	3

Table 2.1: *Effects of Haustorial Inducers of ROS down regulation.*

Day-old seedlings of Striga are placed in a 10 μM DMBQ solution, and scored for ROS at 30 min intervals over 3 hours. The point at which relative fluorescence reaches half maximal is expressed as $t_{1/2}$ROS (hr). After 24hr seedlings were scored for haustorial development expressed as %Hau$_{max}$. Redox potentials from [35]

Figure 2.10A further evaluates the inverse relationship between the commitment to haustorium development and the accumulation of ROS in response to timed exposures of 10μM DMBQ. At each time point, DMBQ is removed and portions of the Striga seedlings are either scored for fluorescence immediately, or for haustorium development 24 hours after inducer addition (t=0 hr). As previously observed, the half-maximal exposure times for these two events are different. A 1 hr DMBQ exposure, while insufficient to induce haustorium development in the seedlings, was sufficient to reduce DCF accumulation to half maximal levels. A 5 hr DMBQ exposure was required for 50% of the seedlings to commit to haustorial development at which time the reduction in ROS production (DCF accumulation) has reached its apparent minima.

2.2.8 ROS regulation is robust

By requiring sustained xenognosin exposure for commitment to haustorial development, the parasite ensures host proximity preventing the halt in root elongation and the resource intensive construction of the haustorium prematurely. Previous experiments have established that removal of the xenognostic quinones, prior to the commitment to haustorial development, results in the recommitment to vegetative growth [34, 70]. As ROS are crucial to xenognosin production, removal of these inducers should cause oxidant production to be restored. Indeed, when seedlings are treated for 1 hr with DMBQ and evaluated for dye oxidation following removal, H_2DCF oxidation rates recovered within 1-2 hr (Fig. 2.10B). Re-exposing the seedlings to DMBQ depleted the H_2O_2 levels a second time, and these rates recovered 1 hr after DMBQ removal. Such oscillations in oxidation potential continued for at least 6 hr (Fig. 2.10C), the critical exposure window necessary for haustorial commitment, establishing the ability of this system to integrate and respond to variable xenognosin exposures.

2.2.9 ROS production remains down regulated upon haustorium commitment

Once commitment to haustorial development is assured (>8 hr) the quinone is no longer required and haustorium development will continue in all seedlings even in its absence. As the xenognosin is no longer required, it seems reasonable that neither is the ROS which generates it. Indeed, in seedlings exposed to 10 μM DMBQ for 10 hours, washed in triplicate, and scored for ROS production (via H_2DCFDA) relative fluorescence levels remained low throughout the remainder of the 24 hr period required for haustorium development (Figure 2.10D). These results strongly support a model in

which ROS production, and therefore the process of semagenesis, is present during vegetative growth and not haustorial development. In the absence of a host, vegetative growth has been shown to resume in the absence of DMBQ providing a second opportunity for haustorium development and host attachment [34, 70]. Coincident with the recovery of vegetative growth, the oxidation of H_2DCF at the root tip is also re-established (Fig. 2.10D). The emerging root tip that develops from the haustorium shows equivalent oxidative potential (fluorescence) and DMBQ responsiveness as the initial germinated seedling.

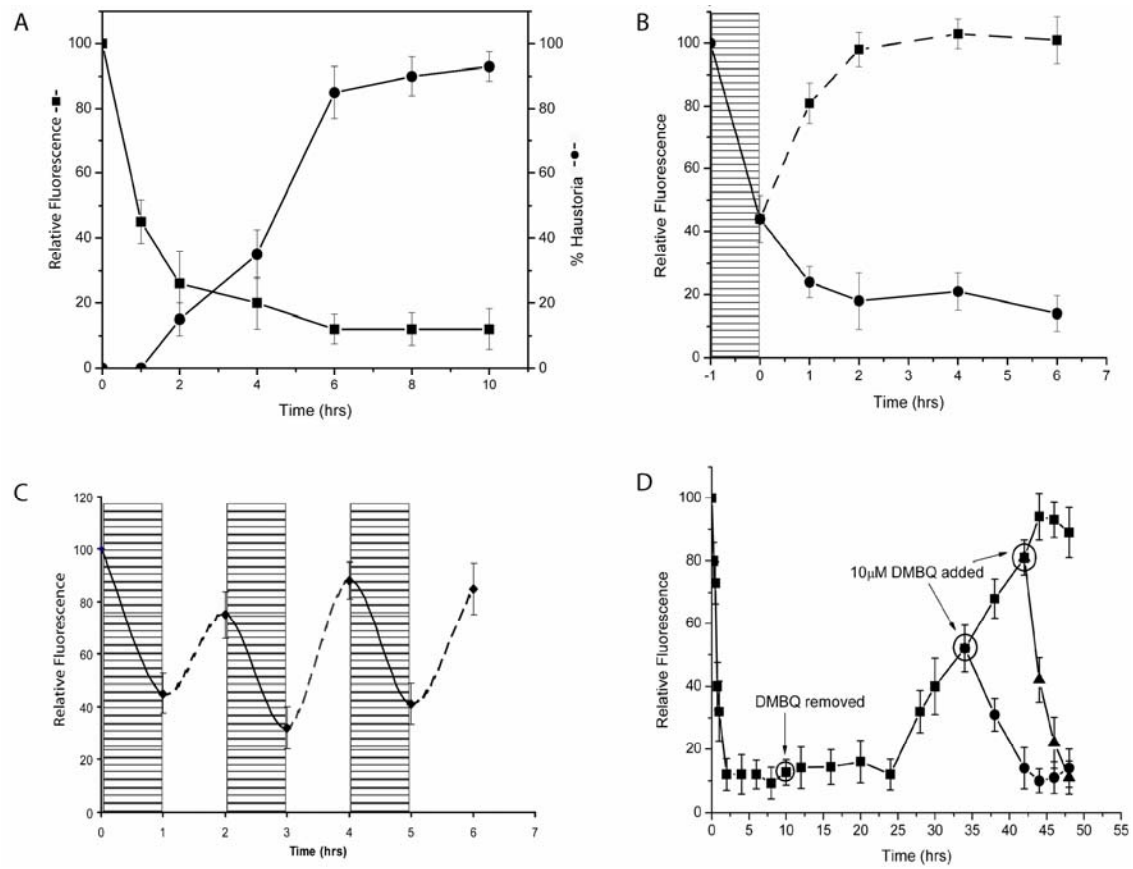

Figure 2.10: *H_2O_2 regulation and haustorial commitment.*

All experiments were conducted on day-old seedlings of *S. asiatica* with 10 μM DMBQ as the inducer. **(A)** Seedlings are induced for the indicated time periods and scored for fluorescence immediately (■) or for % haustoria development after 24 hr (●). **(B)** Seedlings are induced for 1hr (hatched area), separated into two fractions, and incubated with (●) or without (■) DMBQ for the indicated time, then scored for H_2O_2 production. **(C)** Seedlings were induced for 1 hr (solid line), washed and incubated in buffer for a second hour (dashed lines). This pattern was repeated two additional times. Equal portions of the seedlings were scored after each hour. **(D)** Seedlings were induced for 10 hr to ensure commitment to haustorial development, DMBQ was removed, and at the indicated time points, five seedlings were scored for fluorescence. At 34 hr (●) and 44 hr (▲), a fraction of the seedlings were again transferred to 10 μM DMBQ and fluorescence was scored at the indicated time points.

2.3 Discussion

2.3.1 Probing ROS production in semagenesis

Once considered the unfortunate by-products of aerobic life, growing evidence now suggests that ROS play roles in pathogen defense, cell growth, and eukaryotic development [71, 72]. In plant defense, these reactive intermediates function both to toxify the apoplast [73] and as substrates for the oxidative cross-linking of the outer cell wall barrier [53]. In the latter case, peroxidases utilize H_2O_2 to catalyze the oxidative cross-linking of cell wall phenols known as monolignols for both primary and secondary wall reinforcement. In *Striga asiatica*, the germinated parasite exploits this process by producing H_2O_2 proximal to the host root surface to oxidize monolignols into haustorial inducing quinones [37]. However this use of ROS at the host-parasite interface is in conflict with the roles of these oxidants in signaling and defense. Hypothesizing that this inherent conflict could be resolved by the specific localization and tight regulation of oxidant production, a series of microscopy experiments were undertaken to evaluate ROS in *Striga asiatica*. These studies produced several important results that impact our understanding of semagenesis.

First, H_2O_2 accumulates at the root tip, the tissue whose differentiation ultimately defines the transition to pathogenesis in these organisms. Both H_2DCFDA and $CeCl_3$ staining localize H_2O_2 accumulation to the surface cells of the primary root meristem (Figures 2.1 & 2.3). Previously, $CeCl_3$ staining in other plants have identified deposits in similar locations in the extracellular space between cells undergoing the oxidative burst, presumably directed at virulent bacteria lodged in the intercellular space or colonizing the

cell surfaces [74]. In constitutive ROS producing rice mutants, intended to mimic the oxidative burst, the sites of oxidant accumulation are also localized to similar intercellular spaces [75].

Second, the apparent insensitivity of the *S. asiatica* terminal root meristem to H_2O_2 accumulation is significant. Generally, the production of ROS is tightly regulated to avoid initiation of multiple responses, including programmed cell death [43, 51]. For example, the constitutive production of H_2O_2 in mutant rice plant cells results in spontaneous cell death in both transgenic cultures and regenerated plants [75]. Alternatively, oxidant production persists during polar growth of root hairs and pollen tubes but is aborted upon their completion [56, 57]. However ROS production is constant throughout the 5 days the seedling remains viable, and does not appear toxic based on the propidium iodide assays (Figure 2.2). Such insensitivity in *S. asiatica* may arise in part from the small size of the root meristem and the ready diffusion of the ROS from the producing cells. Certainly, tight regulation of both the production and degradation rates is critical to avoiding toxicity and regulation of the host-parasite interface.

Third, the structure/activity relationships previously characterized for haustorium development appears similarly effective in down regulating ROS. For example, the $t_{1/2}$ for haustorium development by 10 μM 2,6-DMBQ is 4 hours but only 1.5 hours for the 2,3-DMBQ ortho- substituted analog. Similarly, the $t_{1/2}$ for ROS down regulation is 1 hour for 2,6-DMBQ but only 30 minutes for a similar concentration of 2,3-DMBQ (Table 2.1).

Finally, and probably of greatest significance for pathogenesis, the xenognosin addition/removal experiments reveal a robust feedback circuit for H_2O_2 accumulation in Striga (Figure 2.10A-D). The haustorial inducing xenognosin down-regulates H_2O_2 accumulation in the parasite, and this suppression is rapidly reversed when DMBQ is removed prior to terminal commitment. As seen in Fig. 2.10, such phase-shifted oscillating concentrations of semagen (H_2O_2)/xenognosin (DMBQ) at the host-parasite interface may well maintain detectable signal concentrations, while minimizing the potential of activating host defensive responses. For example, the haustorial inducing xenognosins generated transiently during semagenesis will diffuse from the host root at a rate similar to that measured for the germination stimulants [20, 21]. As a result, any effective concentration of the signal could quickly drop to below the level detectable by the parasite. Should this signal depletion occur prior to commitment to haustorial development, H_2O_2 production would resume generating additional xenognosin.

2.3.2 Semagenesis functions as a chemostat

Such oscillatory, or chemostatic processes, are a common mechanism for regulating two inversely dependent components in a system such as sugar and insulin levels in mammals. Sugar consumption stimulates the release of an initially high burst of insulin to 'chelate' the free sugar. If the concentration of free sugar drops below a certain threshold, more sugar must be released to compensate. The levels of insulin and sugar oscillate in response to one another until an equilibrium is reached. The decreasing intensity of these oscillations mirror those suggested for the process of semagenesis in the damped sinusoidal graph shown in Figure 2.11.

The number and amplitudes of these oscillations during pathogenesis are expected to be modulated by the nature of the host/parasite interface, but some limits as to the expected range can be considered. Toxic concentrations of H_2O_2 and haustorial inducing quinones for Striga, estimated at 1 mM and 50 μM respectively, provide upper limits on the amplitudes ***A*** in Fig. 2.11. An effective lower limit on ***A*** would be the active concentration range of the xenognostic quinone. Remarkably, this active range spans 500-fold in concentration [34, 70, 76], but the lower concentrations do require longer exposure times, and accordingly, might change the number of 'beats' and/or the oscillation frequency. This oscillating frequency, ***B***, is expected to be largely defined by ROS accumulation and signal diffusion rates. These studies establish that the cytoplasmic H_2O_2 concentrations are reversed within 1-2 hr, making several damping oscillations possible within the 5 hr exposure required for terminal commitment to development by DMBQ. It is also well established that multiple xenognosin exposures are additive [34, 70], extending the window to times much longer than 5 hrs under oscillating exposures. These data underscore the extraordinary plasticity for both signal concentration and signal exposure time and the robustness of the semagenesis strategy for accurate temporal and spatial recognition at the host/parasite interface.

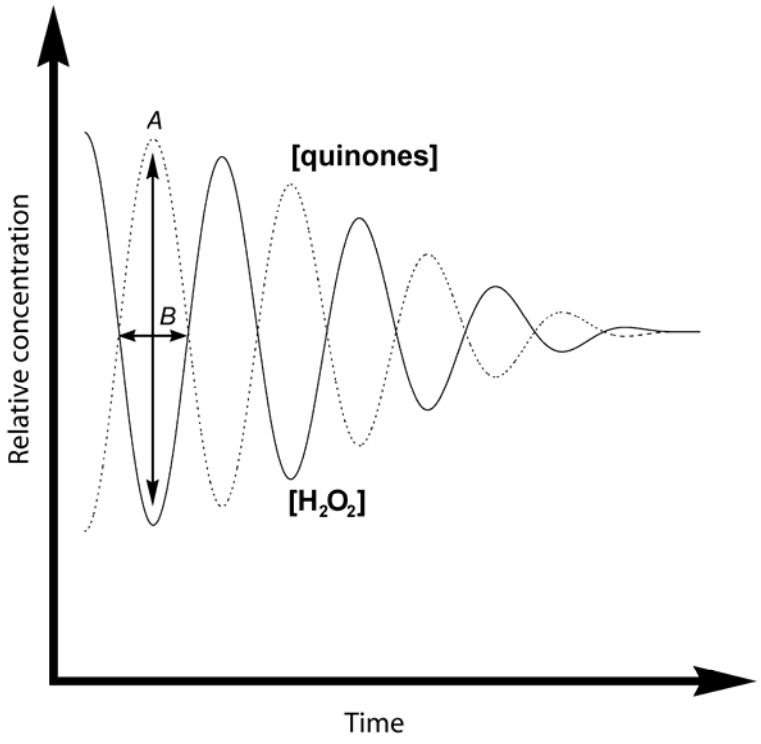

Figure 2.11: *Oscillation model for regulation of semagenic ROS production*

The reciprocal accumulation of semagenic H_2O_2 and xenognostic quinone is predicted to oscillate with amplitude ***A*** and a half-period ***B***. In this model, the accumulating H_2O_2 (solid line) increases the rate of production of the xenognostic quinones (dashed line). The presence of the xenognosin down-regulates H_2O_2, but as the xenognosin diffuses away, H_2O_2 accumulation increases. The oscillations are attenuated towards a final steady state necessary for haustorial commitment.

Further, these studies provide a more developed model of the process of semagenesis by identifying the localized site of ROS accumulation and correlating its regulation with the vegetative/parasitic transition in *Striga asiatica*. Given the general efficacy of the xenognostic benzoquinones in inducing haustorium formation in a number of parasites, the semagenesis strategy could prove to be a general feature of the evolution of parasitic angiosperms [25]. In this model, ROS accumulation by the parasite serves a role typically reserved for host-derived ROS during the hypersensitive burst response. H_2O_2, regardless of its origin, is capable of interacting with host derived phenols and peroxidases to liberate the benzoquinones that Striga uses as a cue for the initiation of haustorial development (Figure 2.12).

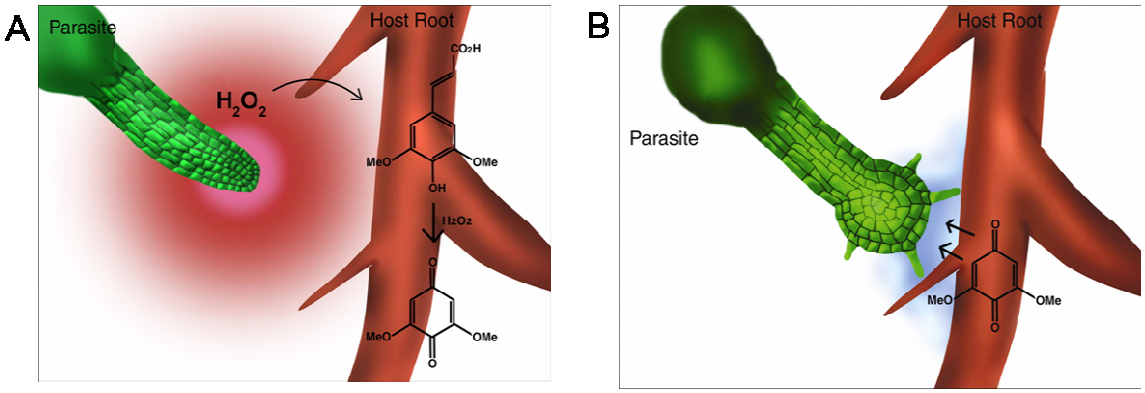

Figure 2.12 *Developmental phases in host commitment by Striga asiatica.*

(A) The growing seedling of *S. asiatica* produces H_2O_2 at the root meristem, giving rise to a localized oxidative gradient (*red*). This H_2O_2 and host peroxidases catalyze the oxidation of cell wall–localized phenolics, such as sinapic acid, into benzoquinones. (B) The accumulating quinones establish a similar chemical gradient (*blue*) necessary for the induction of haustorial development. Radial swelling and hair formation give rise to a functional attachment organ within 18 to 20hr.

2.3.3 What is the source of semagenic ROS?

The potential that both host defense and host recognition employ similar ROS sources might well highlight an evolutionary step towards parasitism, one in which the oxidative burst response is hijacked for the purposes of host detection. With the obligate parasites such as *Striga asiatica*, the ability to flexibly produce and integrate the xenognostic signal, both as a function of concentration and exposure time, becomes central to a semagenic strategy that allows parasitic angiosperms to broadly colonize and exploit their brethren. Most of all, this emerging model suggests that the intimate interplay between host recognition and pathogen defense, two distinct signaling events, may well be dependent on reactive oxygen species accumulation and utilization in higher plant cells. Given the importance of this process to our overall understanding of these events as well as the potential evolutionary divergence between them, identifying the source of the ROS is critical to further defining the regulation and origins of semagenesis. In Chapter 3 experiments to identify this source will be presented and discussed within the context of the evolution and regulation of semagenesis.

CHAPTER 3 – Defining a Molecular Source for ROS

Source and Evolutionary Origins of ROS production in Semagenesis

"The art and science of asking questions is the source of all knowledge."

- Thomas Berger

3.1 Introduction

The use of ROS as a critical component in haustorial xenognosis expands the roles for reactive oxygen in eukaryotes beyond defense and development [48, 50-53, 56, 57, 59, 60, 77-79]. Given the efficacy of such compounds as inducers of haustorium development in other parasitic angiosperms such as *Triphysaria versicolor*, semagenesis likely represents a general mechanism for host perception [38, 80]. While oxidant production may serve a different purpose in this system, the studies presented in Chapter 2 establish that like developmental or defensive ROS production, semagenesis is both spatially restricted and tightly regulated [45, 56, 57, 62, 81, 82]. The tightly regulated feedback between H_2O_2 levels and quinone production permits signal integration over the prolonged exposure time required for commitment to haustorial development (Chapter 2) [34, 38].

The striking similarities in ROS production and regulation between this interorganismal signaling process and both the oxidative burst response as well as programmed developmental events, raise questions as to the oxidant source as well as the evolutionary origins of semagenesis. Potential sources for ROS production during semagenesis include: xanthine oxidases [83], mitochondrial NADH dehydrogenases [42], peroxidases [84], lipoxygenases [85], polyamine oxidases [86], oxalate oxidases [87], and NADPH oxidases [82]. The importance of ROS in aging, disease, and development in eukaryotes has led to numerous studies to identify pharmacological inhibitors of these distinct enzymatic sources [46, 88-92].

While traditional molecular biology tools such as knockdowns/outs are not amenable to parasitic plants, genetic screens have previously correlated the halt of root growth and the initiation of radial swelling during haustorium development to the expression of specific expansins, enzymes that regulate cell wall extensibility [70]. Herein similar genetic screens, along with the small molecule inhibitors for oxidant production and the robust H_2DCFDA assay are employed to identify the source of semagenic ROS. In addition to further defining the regulation of semagenesis these studies provide further insight into the evolutionary origins of this novel signaling process.

3.2 Results

3.2.1 Pharmacological assays limit potential sources for ROS

In an attempt to restrict the number of potential oxidant sources, the effects of small molecule inhibitors on ROS production were evaluated by changes in DCF fluorescence. Table 3.1 summarizes the effects of the maximal non-toxic concentration assayed for each inhibitor on ROS production via the H_2DCFDA assay. Toxicity was evaluated by propidium iodide (PI) staining and longer exposure times, at these maximal inhibitor concentrations, failed to induce toxicity. Under these conditions only diphenylene iodonium (DPI) and phenylarsine oxide (PAO), inhibitors of NADPH oxidases (NOX), showed significantly reduced DCF fluorescence [46, 92].

H_2O_2 Source	Inhibitor (max. concentration (μM))	Relative Fluorescence
Xanthine Oxidase	Oxypurinol (300) [88]	100 +/-12
Xanthine Oxidase	Allopurinol (100) [88]	98 +/- 15
Mitochondrial NADH oxidase	Rotenone (50) [89]	94 +/- 9
Polyamine oxidase	MDL72527 (400) [86]	104 +/- 5
Peroxidase	Salicyhydroxamic acid (20mM)[90]	105 +/- 6
Lipoxygenases	Nordihydroguaiaretic acid (50)[91]	96 +/- 7
NADPH oxidase	Diphenylene iodonium (DPI) (10) [92]	12 +/-6
NADPH oxidase	Phenylarsine oxide (PAO) (1) [46]	18 +/- 6.5

Table 3.1: *Effects of ROS inhibitors on relative fluorescence*

One day-old seedlings of *Striga asiatica* are incubated in the indicated concentration of ROS inhibitor for 2 hours then scored for ROS production via H_2DCFDA. Experiments performed in triplicate and results expressed as average relative fluorescence +/- standard deviation as error.

These initial results suggested an NADPH oxidase as the ROS source, prompting further evaluation of both successful inhibitors. Inhibition by DPI, an irreversible inhibitor of flavin dependent oxidases, was concentration dependent between 1-10 μM while higher concentrations proved toxic (Figure 3.1). PAO or Lewisite, originally employed as a chemical weapon during World War I & II, has found application as a reversible molecular probe for disulfide bonds. As in human neutrophils, submicromolar concentrations of PAO inhibited ROS production (Figure 3.2A) [46]. Anti-lewisite, or 2,3-dimercaptopropanol, serves to chealte PAO and restores activity in neutrophil NADPH oxidases as well as ROS production in *S. asiatica* seedlings (Figure 3.2B)[46].

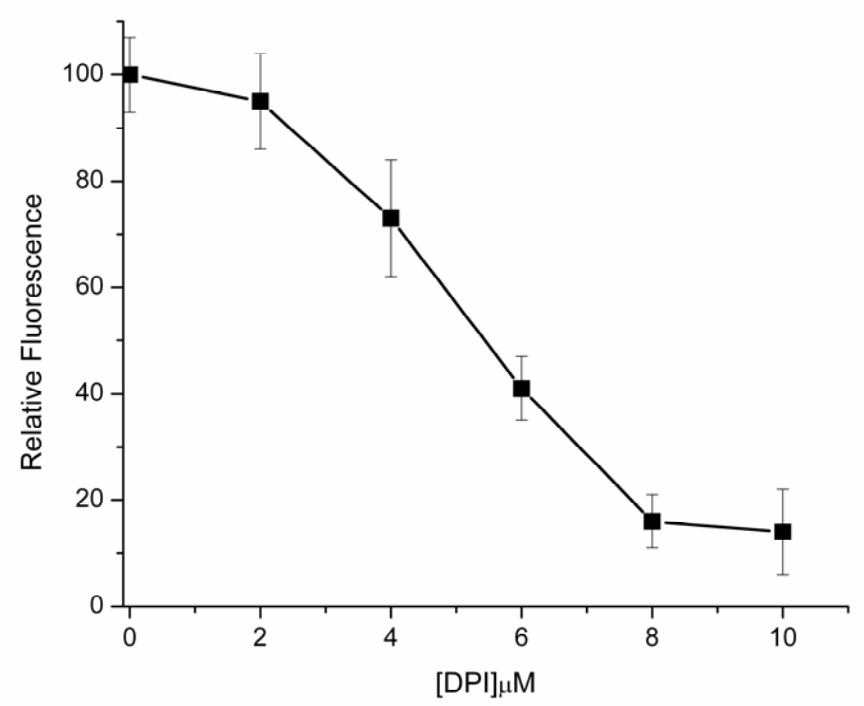

Figure 3.1: *Effects of DPI on ROS production*

Day-old seedlings of *S. asiatica* are incubated in the indicated concentration of DPI for 2 hours, washed, and scored for ROS production via H_2DCF-DA.

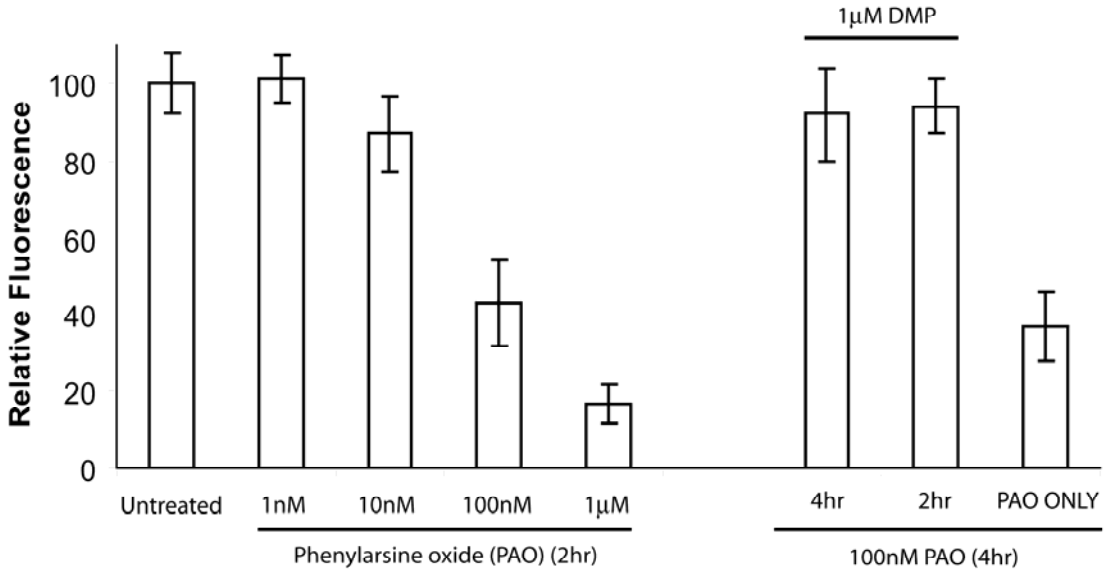

Figure 3.2: *PAO inhibition and reversibility of ROS production*

(Left) Day-old seedlings of *S. asiatica* are incubated with the indicated concentration of PAO for 2hr then scored for ROS production via H_2DCFDA. (Right) Seedlings are incubated with 100 nM PAO. 1 μM DMP is added either 2hr or 4hr after PAO addition. 4 hours after PAO addition the seedlings are scored for ROS production via H_2DCFDA.

3.2.2 Homology cloning of putative Striga NADPH oxidases (SaNOX)

In eukaryotes, NOX have several highly conserved regions which have facilitated homology cloning in a number of species [57, 62, 82, 93-95]. Degenerate oligonucleotide primers were designed based on respiratory burst oxidase homolog (Rboh) proteins, the NOX homologues in plants, from *Arabidopsis thaliana* and *Nicotiana tabacum* [44, 82]. RT-PCR employing these primers on two day-old seedlings of *S. asiatica* yielded a mixture of products which BLAST analyses supported as potential NOX fragments. Employing gene specific primers designed from these sequences and the SMART RACE

cDNA Amplification Kit (Clontech), three full length putative NOX homologs were cloned from *S. asiatica*. The *Striga asiatica* NADPH Oxidases: *SaNOX1, SaNOX2,* and *SaNOX3* were assigned accession numbers DQ431679, DQ431678 and DQ431677 respectively. Using specific primers derived from the full length cDNA for each *SaNOX*, the complete genomic sequence, as well as the promoter region were obtained by PCR of genomic DNA [96].

3.2.3 Intron-exon analysis of putative SaNOX sequences

Intron-exon analyses of the genomic DNA for the three *SaNOX* sequences were performed with the SPIDEY (http://www.ncbi.nlm.nih.gov/IEB/Research/Ostell/Spidey/) software package. The first six exons of *SaNOX1* (12 exons) code for the calcium binding EF-hand domains and the transmembrane helices while the remaining exons code for the FAD and NADPH binding domains [82]. In both *SaNOX2* (8 exons) and *SaNOX3* (5 exons), the start of the first exon coincides with positions within exon 5 from *SaNOX1*. The final exon of *SaNOX2* (exon #5) combines exon 11 and 12 from *SaNOX1* while *SaNOX3* divides the last exon *SaNOX1* (#12), into two exons (#7&#8). From these initial results, only *SaNOX1* appears to maintain the canonical architecture among plant NADPH oxidases while both *SaNOX2* and *SaNOX3* appear to be N-terminal truncations. Such truncations have not previously been observed in plants and only rarely in eukaryotes. The novelty of these truncations as well as the potential importance of these genes in semagenesis prompted further analysis (Figure 3.3).

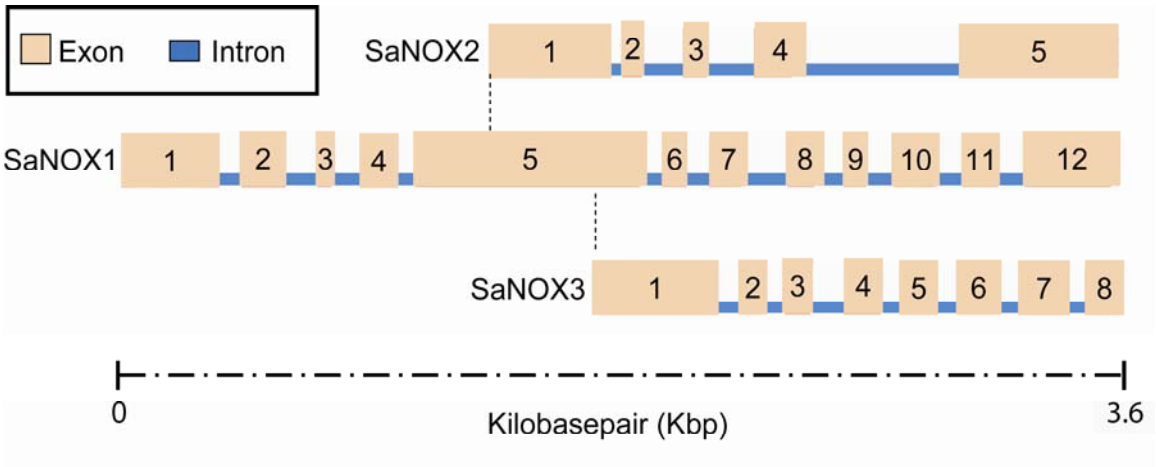

Figure 3.3: *Exon-intron analysis of SaNOX1, SaNOX2, and SaNOX3.* Cartoon of exon-intron positions are determined by comparing the mRNA of each gene to its genomic sequence using SPIDEY (http://www.ncbi.nlm.nih.gov/IEB/Research/Ostell/Spidey/). Boxes (peach) represent exons and horizontal lines (blue) represent introns. Start and end points are for the genomic sequence. Exon 1 of *SaNOX2* and *SaNOX3* start 'inside' exon 5 of *SaNOX1*.

3.2.4 Bioinformtic analysis of putative SaNOX sequences

The predicted protein sequences for SaNOX1, SaNOX2, and SaNOX3, were compared to both AtRbohA as well as $gp91^{phox}$, the primary catalytic subunit of NOX from *Homo sapiens*. CLUSTALW sequence alignments as well as Kyte-Doolittle hydropathy plots, to map transmembrane sections, confirmed the overall sequence homology as well as the conservation of critical regulatory and catalytic components (Figure 3.4 & 3.5). For example, the histidine residues in transmembrane helices 3 and 5 associated with heme binding [97, 98] as well as the C-terminal FAD and NADPH binding domains [40, 99, 100] were present in all three sequences. As expected from the previous intron-exon analysis (Figure 3.3), SaNOX2 and SaNOX3 are truncations of the canonical Rboh structure lacking both the Ca^{2+}-binding EF-hand domains as well as the first transmembrane helix. The EF-hand domains found in SaNOX1 are common to all known plant Rboh proteins as well as members of the NOX5, Duox1, and Duox2 families in animals [101, 102]. While a member of the NOX5 family in humans without an EF-hand domain has been isolated [94], no truncation also including the first transmembrane helix have previously been observed in any eukaryote.

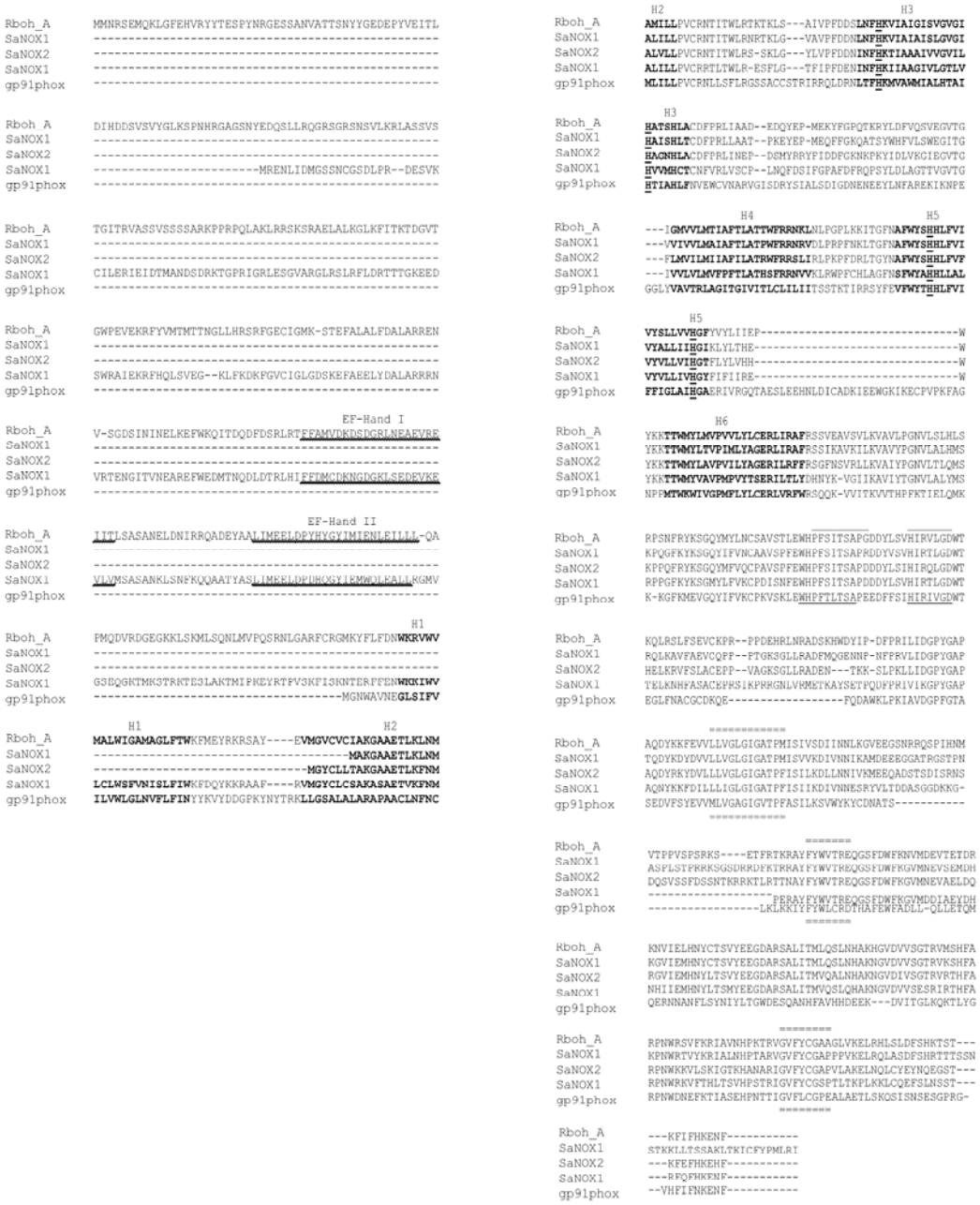

Figure 3.4: *CLUSTALW alignments of SaNOX1-3 with AtRbohA and gp91^{phox}*

Sequence of SaNOX1, SaNOX2, SaNOX3 are aligned with gp91^{phox} and AtRbohA (Rboh_A) by CLUSTALW and BLAST (See Methods). Critical domains conserved between the sequences are marked. Kyte-Doolittle hydropathy plots supported the assignment of six transmembrane helices in gp91^{phox}, SaNOX1, AtRbohA and five in SaNOX2 and SaNOX3. NADPH (=) and FAD (-) binding domains (BD) are also indicated.

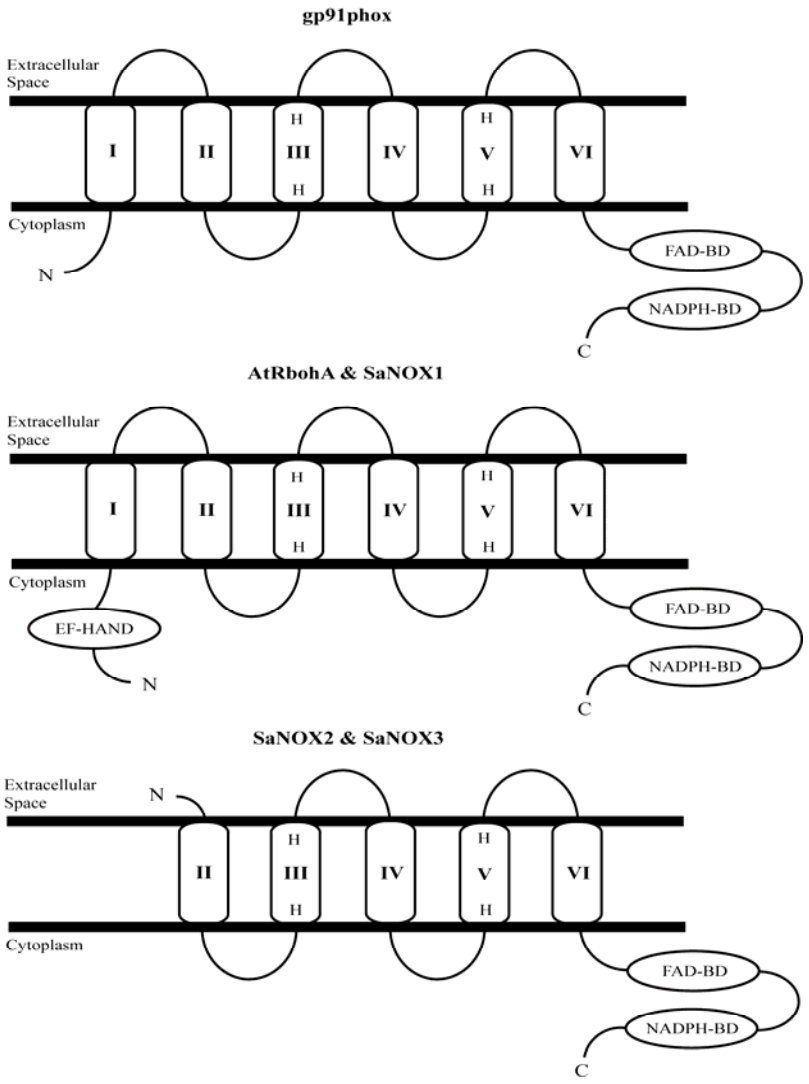

Figure 3.5: *Cartoon models based on CLUSTALW alignments*

Models built from CLUSTALW alignments seen in Figure 3.4. FAD, NADPH, and Ca^{2+} (EF-hand) binding domains shown in circles, putative transmembrane helices are numbered and conserved histidines are noted as 'H'. Structural models of gp91phox and AtRbohA previously established are also shown.

3.2.5 Localization of SaNOX expression

The conservation of the catalytic domains for ROS production in all three SaNOX sequences suggests any of these could be the oxidant source in semagenesis. Given that the production of ROS is specifically localized to the root tip in Striga, it seems reasonable that expression of the oxidant's source should be similarly localized. Gene specific primers for *SaNOX1*, *SaNOX2*, and *SaNOX3* were used to probe cDNA libraries by RT-PCR (30 cycles) along with primers for actin as a positive control for expression. The libraries were generated from either: germinated seedlings, stems and leaves, or flowers. The latter two libraries were produced from mature plants regenerated from callus (See Methods). As shown in Figure 3.6A, *SaNOX1* expression appears to be exclusively localized to the root of Striga, while *SaNOX2* and *SaNOX3* are found throughout the mature plant (Fig. 3.6B). Northern blot analyses further confirmed the presence of both *SaNOX1* and *SaNOX3* in roots, while attempts to detect *SaNOX2* failed, potentially due to low expression levels (Fig. 3.6C, 3.6D) [96].

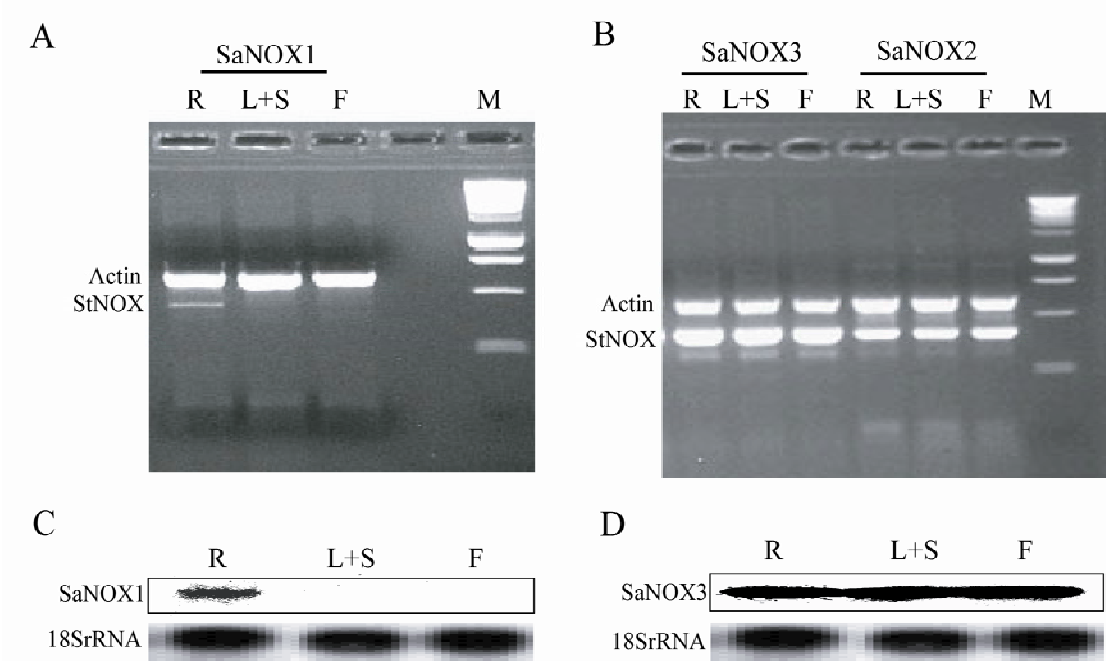

Figure 3.6: Tissue localization of *SaNOX1, SaNOX2, and SaNOX3*.

Tissues harvested from germinated seedlings (root) or mature cultured *S. asiatica* plants were screened for *SaNOX* expression by RT-PCR (A&B) and confirmed by Northern analyses using 18s rRNA as control (C&D). Lane labels are R: Root, L+S: Leaf + Stem; F: Flower; M: Marker. Data from: [96].

While the exclusive localization of *SaNOX1* to the germinated seedlings is promising, neither *SaNOX2* nor *SaNOX3* could be excluded as a potential source for ROS. Unfortunately, Striga seedlings are too small for analysis by further sectioning of the growing root, requiring an alternative technique to observe localization. One common method in plants is to place reporter genes such as β-glucuronidase (GUS) behind promoters for a target gene of interest. GUS staining, like the ubiquitous β-galactosidase blue-white screening technique used in *E. coli* studies, cleaves chromagenic substrates like X-gluc to yield blue-green deposits at the site of expression. As the promoter sequences for all three *SaNOX* genes had been identified but the parasite itself could not be transformed for expression analysis, Arabidopsis was pursued as a heterologous host to identify the sites of *SaNOX* expression. *A thaliana* is ideal for such experiments as it is easy to transform, has a short generation time, and the mechanics for visualization experiments are extremely well defined [103, 104].

Three Arabidopsis transformants, each expressing GUS behind the promoter for either: *SaNOX1*, *SaNOX2*, or *SaNOX3*, were evaluated for stain localization. As seen in Figure 3.7A&B, both the *SaNOX2* and *SaNOX3* promoters directed expression throughout the Arabidopsis transformants, whereas *SaNOX1* expression was localized to the root tip, the site of ROS production in Striga (Fig. 3.7C, 3.7D). It should be noted that differences in GUS staining intensity does not reflect variations in expression levels, as the staining times were not identical [96].

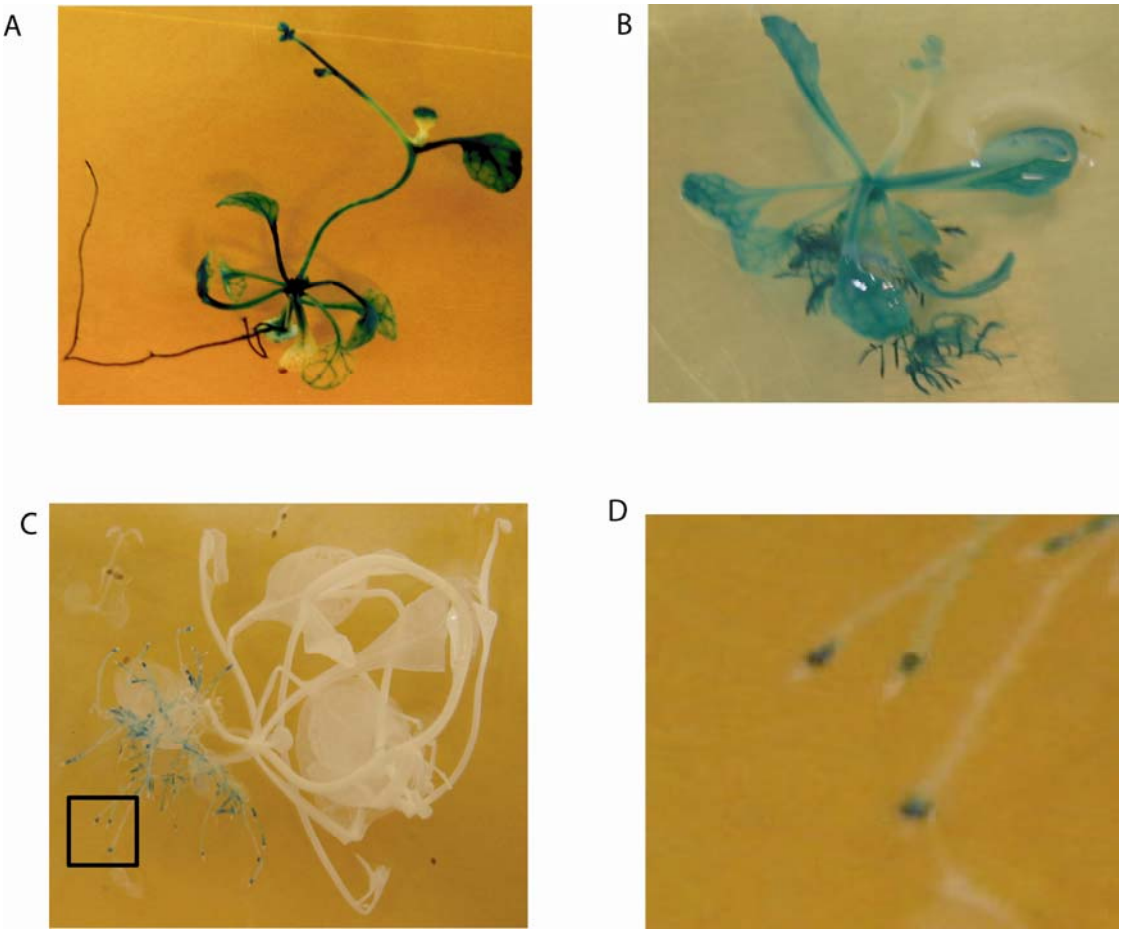

Figure 3.7: *SaNOX1 expression is localized to the root tip.*

Arabidopsis transformants expressing β-glucuronidase (GUS) behind the promoter sequences of (A) *SaNOX2*, (B) *SaNOX3*, and (C) *SaNOX1*. (D) Enlargement of boxed root tips in (C). Stain intensity does not reflect expression levels as staining times were not identical. Images from: [96].

3.2.6 Regulation of SaNOX genes in response to haustorial inducers

While short term exposures to haustorial inducing quinones result in the reversible down regulation of ROS production, sustained exposures ultimately lead to the terminal commitment to haustorium development and reduced ROS levels (Chapter 2). This commitment to reduced ROS suggests a change in the expression of the oxidant's source is likely to coincide with development. To evaluate this hypothesis, cDNA libraries developed at set time intervals in response to 10 μM DMBQ exposures, were probed for the effect on *SaNOX1*, *SaNOX2*, and *SaNOX3* expression. Initial screenings of these libraries quickly established that neither *SaNOX2* nor *SaNOX3* showed any changes in expression in response to DMBQ exposure at any time point in the libraries. Conversely, changes in *SaNOX1* expression are summarized in Figure 3.8B and compared to the results of ROS imaging at identical time points in Figure 3.8A. Noticeably, the down regulation of both ROS levels and *SaNOX1* expression reach their minima after two hours of 10μM DMBQ exposure. *SaNOX1* expression, like ROS levels, remained low throughout the 24hr period required for haustorium development. Similar exposures to the non-haustorial inducer tetrafluorobenzoquinone (TFBQ) had no effect on ROS production or *SaNOX1* expression.

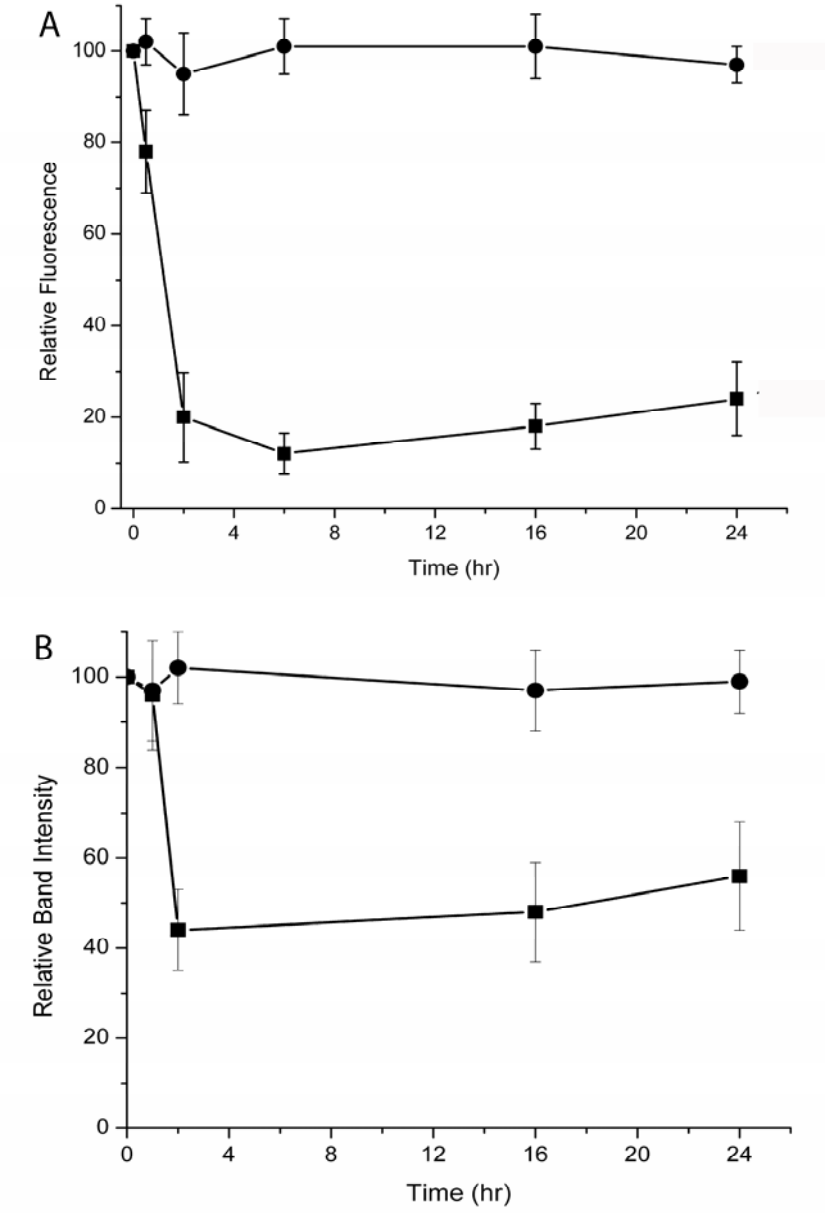

Figure 3.8: *ROS and SaNOX1 expression in response to DMBQ.*

Two day-old seedlings of Striga are incubated in solutions of either 10 μM DMBQ (■) or 10 μM TFBQ (●) for the indicated time points then washed and either (A) Imaged for ROS accumulation via H_2DCFDA or (B) screened for *SaNOX1* message accumulation by RT-PCR. Each data point is performed in triplicate and expressed as average ±SD. Actin standards were taken for each time point and were consistent. Figure B from [96].

3.2.7 SaNOX1 expression is coupled to the semagenesis chemostat

Although the absolute levels of H_2O_2 and *SaNOX1* mRNA are not readily compared in these assays, the similar time scale for their modulation by DMBQ supports the latter's involvement in the process of semagenesis. However semagenesis is a robust process in which ROS production oscillates over time to permit sustained signal generation while minimizing deleterious effects. It is therefore reasonable to assume that its source might display similar flexibility. Indeed, when DMBQ is removed from the seedlings after a 2 hr pre-exposure, both root tip H_2O_2 and *SaNOX1* expression rebound to initial levels (Fig. 3.9A&B). This dynamic flexibility in expression is consistent with both the robust 'chemostat' model for semagenesis developed in Chapter 2 as well as the parasite's ability to integrate the haustorial xenognosin over multiple exposures [31, 36-38].

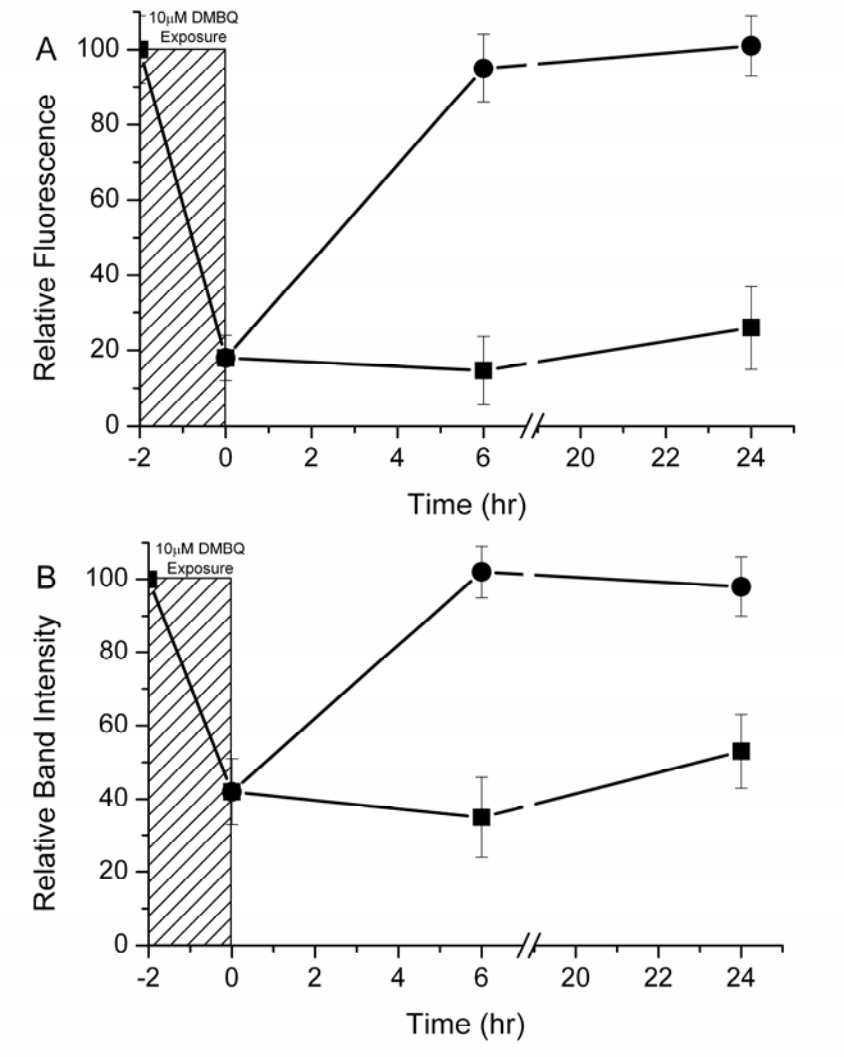

Figure 3.9: *SaNOX1 expression is reversible prior to commitment.*

Two day-old *S. asiatica* seedlings were (A) treated with 10 μM DMBQ for 2 hr (shaded area), washed, and incubated further with (■) or without (●) DMBQ. At each time point, 10 seedlings were scored for fluorescence via H_2DCFDA. Data are expressed as ±SD. (B) Seedlings are treated with DMBQ for 2 hr, washed, and incubated further with (■) or without (●) DMBQ. At the indicated times, sufficient seedlings for extracting RNA were screened for *SaNOX1* expression via RT-PCR. Data for 3.9B from [96].

3.2.8 Calcium regulation of oxidant production

The presence of N-terminal EF-hand domains on SaNOX1, as well as their noticeable absence in both SaNOX2 and SaNOX3, suggested an additional level of regulation that might be exploited for assigning the oxidant source. Ca^{2+} binding to EF-hand domains, like the putative ones in SaNOX1, have been shown to increase NOX5 activity in animals and a similar model has been proposed for the respiratory burst oxidases of plants [82, 93, 95, 102]. To determine if SaNOX1 could indeed bind calcium, the EF-hand domains were synthesized *in vitro*, purified, and incubated with $^{45}Ca^{2+}$ on nitrocellulose membranes [105]. Both domains were found to bind $^{45}Ca^{2+}$, while a 26aa control peptide showed no binding affinity (Figure 3.10) supporting the assignment of these domains and a potential role for $[Ca^{2+}]_{cyt}$ in regulating ROS production [96].

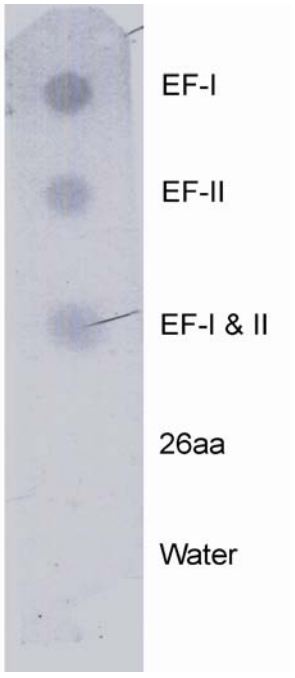

Figure 3.10: *Putative EF-hand domains bind calcium*

The sequences IFFDMCDKNGDGKLSEDEVKEVLVMS (EF-I) and LIMEELDPDHQGYIEMWQLEALLRGM (EF-II) were synthesized *in vitro*, purified by HPLC, and fixed to nitrocellulose membranes. Autoradiographs of dot blots following exposure to $^{45}Ca^{2+}$ are shown both separately and as a mixed spot. The control 26 amino acid peptide, YEVHHQKLVFFAEDVGSNKGAIIGLM, served as a negative control. Figure from [96].

Perturbations in $[Ca^{2+}]_{cyt}$ should effect the rates of dye activation, i.e. fluorescence accumulation. Assuming SaNOX1 activity is Ca^{2+}-dependent, elevated $[Ca^{2+}]_{cyt}$ should stimulate SaNOX1 activity, increasing relative fluorescence, whereas decreasing $[Ca^{2+}]_{cyt}$ should lower relative fluorescence. The brute force approach to elevating $[Ca^{2+}]_{cyt}$, via the addition of exogenous $CaCl_2$, does result in an increase in relative fluorescence as seen in Figure 3.11A. However like all other living organisms, plants maintain a rigorous buffering system to prevent excess ion accumulation, so a more elegant approach was sought.

Ionophores such as ionomycin or A23187, originally isolated from fungi, are capable of disrupting the calcium gradient across the membrane [106]. These anionic compounds bind Ca^{2+}, forming a neutral complex that can diffuse across the cell membrane. The bound calcium is then released into the cytoplasm where calcium levels are typically much lower. As seen in Figure 3.11B, relative fluorescence increased in a concentration dependent manner in response to treatments with the calcium salts of either ionomycin or A23187. Higher concentrations of both ionophores resulted in diminished root elongation and the accumulation of significant PI fluorescence, suggesting they were toxic. Furthermore, FDA fluorescence accumulation was unaffected by either $CaCl_2$ or ionomycin exposures confirming increased DCF fluorescence is not simply due to increased esterase activity in response to elevated $[Ca^{2+}]_{cyt}$. Neither $CaCl_2$ nor ionophore treatments significantly increased ROS production throughout the rest of the Striga root further implicating *SaNOX1*, as the ROS source. The increased production of ROS

appears NOX dependent as both DPI and PAO treatments successfully inhibited ROS production at the maximal concentrations of $CaCl_2$ and both ionophores (Fig. 7C).

Clearly the elevation of $[Ca^{2+}]_{cyt}$ increases ROS production as expected, however the model further suggests the reverse; that reduced $[Ca^{2+}]_{cyt}$ will limit ROS production. BAPTA-AM, a cell permeable Ca^{2+} chelator, diffuses into the cytoplasm where, like H_2DCFDA, it is activated by cytoplasmic esterases. BAPTA-AM treatments have previously been used in animal cells to inhibit activity of the calcium dependent NOX5 *in vivo* [102, 107, 108]. Exposure of day-old seedlings of *S. asiatica* to BAPTA-AM reduced ROS production (relative fluorescence) in a concentration dependent manner (Figure 3.11D). The BAPTA-AM concentrations employed here had no effect on FDA or PI fluorescence accumulation, arguing against changes in esterase activity or toxicity in these studies.

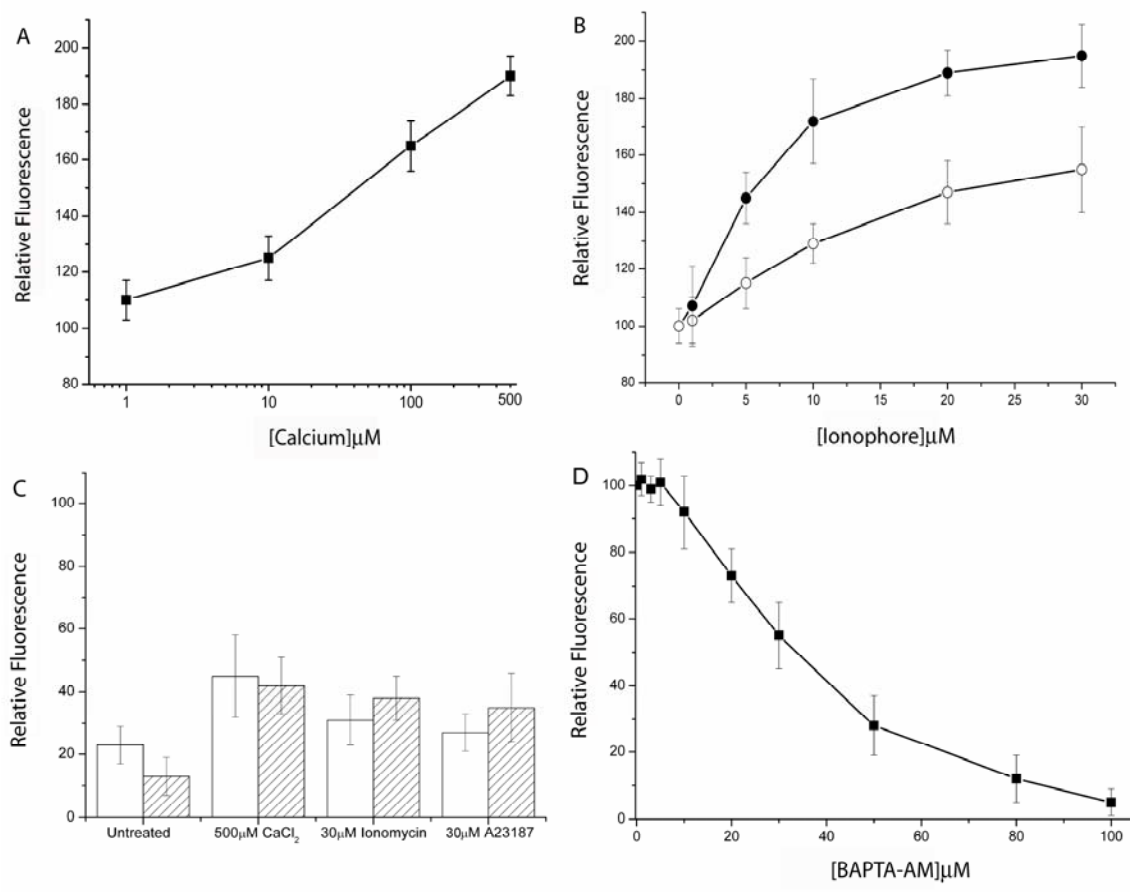

Figure 3.11: *Calcium regulation of ROS production*

One day-old *S. asiatica* seedlings were: **(A)** incubated with the indicated concentrations of $CaCl_2$ for 2 hr, washed, and scored for cytoplasmic H_2O_2. **(B)** Incubated with the indicated concentrations of the Ca^{2+} salts of: ionomycin (●) or A23187 (o) for 2 hr, washed, and scored. **(C)** Co-incubated for 2 hours with the maximal concentrations of either: $CaCl_2$ (500 µM), Ionomycin (30µM), or A23187 (25µM) with 10µM DPI (WHITE) or 0.1 µM PAO (SHADED) then washed, and scored. Untreated seedlings are seedlings treated with 10 µM DPI (WHITE) or 0.1 µM PAO (SHADED) only. **(D)** Incubated with the indicated concentration of the cell permeable Ca^{2+} chelator BAPTA-AM for 2 hr, washed and scored. All data points are expressed as ±SD. Fluorescence of seedlings loaded with dye only are set as 100 in all figures (See Methods).

3.3 Discussion

3.3.1 The contradiction of ROS signaling

While ROS have long been recognized as toxic byproducts of aerobic metabolism and critical components of an organism's defensive arsenal against invading pathogens, the last decade has witnessed the discovery of a diverse array of developmental processes regulated by these transient intermediates [56, 59, 60, 71]. The expanding functional roles for these toxic ROS intermediates pose inherent cost/benefit contradictions to the producing organism, and nowhere is this more apparent than in the semagenic events which control host/pathogen interactions in the parasitic angiosperm *Striga asiatica* [31, 38]. Here the host and pathogen reside within the same Kingdom, and yet a process intended for defense and vascularization in the host, i.e. ROS driven lignification, is employed for host recognition by the parasite. By exploiting the well-defined signal-induced developmental transitions of the parasite, the advancements in our understanding of reactive oxygen sources, and the transparency of the tissues undergoing developmental commitment, it seemed reasonable that a source for oxidant production in semagenesis could be isolated.

3.3.2 Pharmacological assays for ROS production

By coupling inhibitor assays to the ROS-sensitive fluorescence microscopy technique developed in Chapter 2, it was possible to evaluate potential oxidant sources *in vivo* (Table 3.1, Figure 3.1 & 3.2). These results suggested an NADPH oxidase as the likely source of H_2O_2 production at the root tip of *S. asiatica*. While DPI has regularly been employed for the inhibition of the Rboh proteins, phenylarsine oxide (PAO) induced inhibition has not been significantly explored in plants prior to these assays and therefore deserves more attention [56-58, 61, 62, 109].

3.3.3 PAO inhibition in plants

Phenylarsine oxide (PAO), which disrupts disulfide bonds, has previously been proposed to inhibit ROS production in human neutrophils by two distinct mechanisms. The first, by disrupting formation of the $p47^{phox}$/$gp91^{phox}$ (NOX) complex by binding to Cys85 and Cys86 of the $p47^{phox}$ binding motif: ^{85}<u>*CC*</u>STRXXRQL in $gp91^{phox}$ (NOX) [46]. While this subunit association is required for maximal activity in neutrophils neither this motif nor additional subunit associations appear to occur in NOX5, any of the SaNOX sequences, or the Rboh sequences used in homology cloning. Alternatively, inhibition in neutrophils also occurs at a CXC motif located between the FAD and NADPH binding domains, but this motif is also not present in the plant sequences evaluated.

How then does PAO inhibit the production of ROS? Two CXC motifs, conserved among the SaNOX, as well as most of the Rboh sequences, located proximal to either helix II or III may provide alternate sites for the disruption of protein activity. While

inhibition at the first site may simply disrupt protein structure, the latter motif, adjacent to helix III, may either disrupt heme assembly or oxygen association. Therefore, while the previously observed sites for PAO activity in neutrophils are absent in plants, alternative inhibition sites potentially exist. Ultimately, the reversibility of this inhibitor may provide a powerful tool for characterizing ROS production in development.

3.3.4 Genetic screens for oxidant source, localization and regulation

The inhibitor assays prompted the design of oligonucleotide primers based on conserved regions of known Rboh proteins, which were then used to clone 3 putative NADPH oxidase sequences: *SaNOX1*, *SaNOX2*, and *SaNOX3* from a cDNA library of germinated Striga seedlings. Sequence specific primers were then used to obtain both the full length genomic sequence as well as the promoter region for each gene. Extensive bioinformatic analysis supported the assignment of these sequences as NADPH oxidases while also confirming the unique truncations of SaNOX2 and SaNOX3 predicted by intron-exon analysis (Figure 3.3-3.5). While these truncated sequences may yet prove critical in later stages of parasitism, given their ubiquitous expression in the mature parasite, future studies will be required to elucidate this.

Tissue localization via RT-PCR and Northern blot analyses, as well as GUS staining in Arabidopsis transformants, found only *SaNOX1* to be localized to the growing root tip (Figure 3.6 & 3.7). cDNA libraries constructed in response to DMBQ treatments confirmed only *SaNOX1* expression was regulated in a robust manner consistent with the chemostat model for ROS production proposed in Chapter 2 (Figure 3.8 and 3.9). The

changes in *SaNOX1* expression appears specific for haustorial inducing xenognosins as similar libraries generated while exposed to the non-inducer TFBQ showed no regulation.

3.3.5 Ca^{2+} regulation of ROS production

The presence of calcium binding EF-hand domains on SaNOX1 suggested $[Ca^{2+}]_{cyt}$ may play a role in regulating ROS production during semagenesis. Ca^{2+} regulation has previously been observed in members of the NOX5 sub-family, which are most homologous to the Rboh proteins of plants including the conservation of the EF-hand domains [93, 101, 102]. The functionality of these EF-hand domains was confirmed by *in vitro* synthesis and labeling on nitrocellulose membranes with $^{45}Ca^{2+}$ (Figure 3.10). Relative fluorescence levels were positively correlated with the increase or decrease of $[Ca^{2+}]_{cyt}$ (Figure 3.11). The lack of EF-hand domains on both SaNOX2 and SaNOX3 have not previously been observed, and suggest an alternative mechanism for regulating activity in these sequences. These findings all supported a model in which calcium regulated SaNOX1 provides the required oxidant for the process of semagenesis, and is down regulated during the commitment to parasitism.

3.3.6 SaNOX1 Expression attempts

Given the success of the GUS transformants in localizing *SaNOX* expression, it seemed reasonable to attempt to express *SaNOX1* in a heterologous host to confirm its activity. Unfortunately, Arabidopsis transformants with *SaNOX1* showed no significant increase in ROS production over wild type, as visualized by fluorescence accumulation. Nor did ROS levels appear significantly altered in *Saccharomyces cerevisiae* (yeast) transformants containing *SaNOX1*. In both cases, mRNA of *SaNOX1* was isolated confirming successful transformation [96]. This apparent lack of activity could arise from the absence of specific regulatory components and/or modifications such as glycosylation, phosphorylation, or additional subunits specific to Striga [62, 107, 110].

3.3.7 A model for the evolution and regulation of semagenesis

In both ROS mediated development and the oxidative burst response ROS are produced by NADPH oxidases, tightly regulated, and localized to the site of activity just as they are in semagenesis, suggesting either or both of these processes could be the evolutionary progenitor of this xenognosis. Support for an origin in plant development can be found in evidence that ROS production at the root tip is not unique to Striga, having previously been observed in roots of *Glycine max*, *Arabidopsis thaliana*, and *Zea mays* [58, 111]. Furthermore haustorial inducers have been shown to have an allelopathic effect, reducing growth in non-parasites, suggesting a conserved mechanism co-opted by parasites for the purposes of host detection [112].

If a mechanism for the detection of such products is conserved, then potentially a method for their production is also not specific to the parasites. Indeed, previous studies have established the importance of *AtRbohC* in providing ROS, not only to stimulate root hair growth, but to catalyze the crosslinking of monolignols to provide additional support to the swelling root hair [56, 62]. This reaction is essentially identical to semagenesis, and therefore the production of quinone side products seems reasonable. NOX proteins have also been implicated in the lignification of xylem elements further underscoring an intimate role for these proteins in development [79]. Moreover, the cross-linking of monolignols during the oxidative burst could easily result in the side production of haustorial inducing quinones. Indeed it may well be that such ROS mediated processes are regulated by the distribution of products resulting from the oxidation of the plant's cell wall or that of another's, in the case of semagenesis.

Ultimately these studies hint at the potential for a process discovered in the context of host detection, i.e. semagenesis, to play a critical role in regulating growth and development as well as the oxidative burst. Deciphering a role for this process among non-parasites clearly depends on our growing mechanistic understanding of reactive oxygen species accumulation and utilization in higher plant cells. The tight regulation of oxidant production coupled to the well defined phenotypic and genotypic responses to haustorial inducing quinones continues to make Striga an ideal system for characterizing this process. Chapter 4 will see the further elucidation of the regulation of semagenesis, the intimate coupling between vegetative growth and parasitic development, and the potential larger implications on plant biology.

CHAPTER 4 – Biochemical Regulation of Semagenesis

ROS, Calcium and Cytokinins in Xenognosis

"You have to learn the rules of the game. And then you have to play better than anyone else." – Albert Einstein

4.1 Introduction

4.1.1 Semagenesis/Xenognosis – Two sides of the same developmental coin

The preceding chapters have confirmed that similar to defense and/or developmental events, ROS production during semagenesis occurs via the activity of NADPH oxidases, is spatially restricted to the site of activity, and tightly regulated [56, 57, 60-63, 74, 79]. In the case of semagenesis, one critical regulatory component of this process is its products, the xenognostic quinones. As the perception of these compounds (xenognosis) is inversely correlated to oxidant production and positively correlated with haustorial organogenesis, it underscores the intimate coupling between oxidant production and the developmental event with which it is associated. As a result, the genetic screens and ROS assays developed in the preceding chapters are critical components of a toolbox which allows us to define not only oxidant production but to evaluate xenognosis and subsequent haustorial organogenesis. In this chapter, these new tools have been re-focused to further evaluate and temporally assign the role of three distinct components in semagenesis/xenognosis.

4.1.2 A Role for ROS loss in Haustorial Development

The loss of oxidant production during semagenesis is in sharp contrast with developmental events such as polar growth and vascular development in which ROS is necessary [56, 58, 79]. One reasonable hypothesis which emerges from these observations is that the reduction in ROS production is critical to haustorial development. Given protocols for evaluating, as well as altering oxidant levels within the parasite have already been established (Chapters 1-3), the necessity of oxidant loss for successful haustorium development can be readily evaluated.

4.1.3 Cytokinis – A role for endogenous hormones in xenognosis

Previous attempts to identify endogenous factors associated with xenognosis have implicated cytokinins in haustorial development, as micromolar concentrations of the hormone initiates organogenesis [26, 27, 70, 76, 113-116] (Figure 4.1). In addition to their potential role in haustorium development, these N-substituted derivatives of adenine have been implicated in regulating cell division and root morphogenesis [22, 117]. While these studies suggest quinone perception is mediated by endogenous hormones, alternative models outlined in Figure 4.2 cannot be excluded by the data currently available. In model A, quinone and hormone induced haustorial development are parallel but independent events which share common developmental markers. In model B, perception of the xenognostic quinones initiates a cytokinin driven pathway during signal transduction. The inverse of this model, that DMBQ is a downstream component of a cytokinin pathway, is unlikely as the commitment to haustorium development occurs before the accumulation of monolignols in the parasite. Finally, it is possible that the

interaction between quinone and hormone is not linear but rather that the two components are interdependent (Model C). Employing the techniques and results from Chapters 2 and 3, new experiments were initiated to resolve these conflicting models.

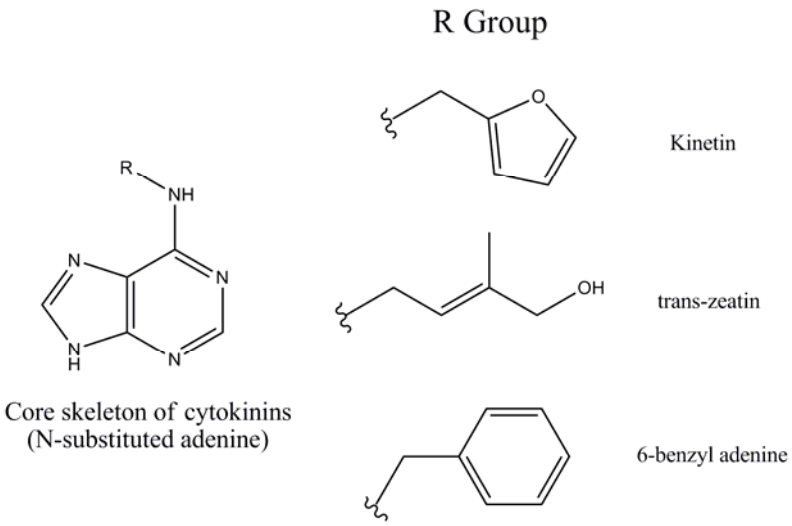

Figure 4.1: *Common Cytokinin structures*

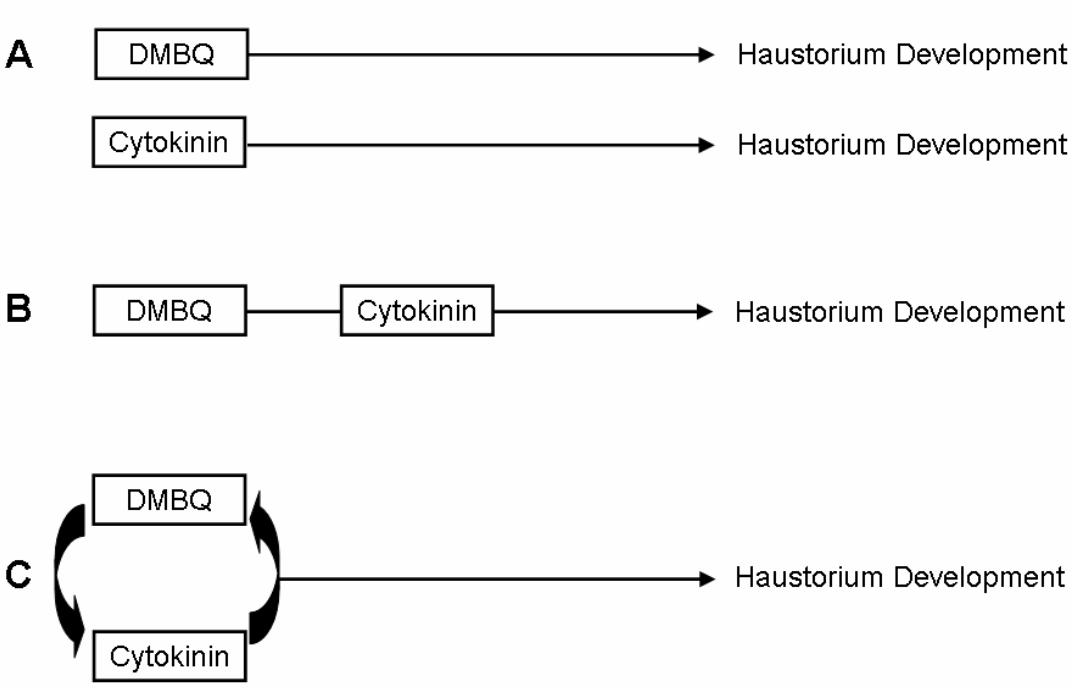

Figure 4.2: *Putative Models for Cytokinin and DMBQ integration*

(A) Independent processes: Quinone and Cytokinin are completely unrelated events with similar resulting phenotypes. (B) Linear developmental process: DMBQ perception triggers a downstream change in cytokinin activity resulting in haustorium development. (C) Interdependent processes: Haustorial inducing quinones and cytokinins are tightly coupled and dependent on each other for haustorium development and cannot be distinguished.

4.1.4 Calcium – Cation regulation of haustorial development

In semagenesis, as well as defense and development, oxidant production has been coupled to fluctuations in cytoplasmic calcium ($[Ca^{2+}]_{cyt}$) [118-120](Chapter 3). In addition, Ca^{2+}-channel inhibitors as well as chelators have been shown to inhibit haustorium development, confirming a role for this cation in xenognosis [76]. However, both the degree and point of Ca^{2+} regulation in semagenesis/xenognosis remains undefined. Studies employing genetic screens, ROS assays, and probes for cytokinin activity in conjunction with regulators of $[Ca^{2+}]_{cyt}$ were employed to resolve the critical point(s) of the cation's activity.

4.1.5 Developing a timeline for Semagenesis/Xenognosis

The potential time points for oxidant, calcium, and cytokinin regulation are detailed in Figure 4.3. The experiments in this chapter have exploited our growing understanding of xenognosis and semagenic ROS production to resolve the order and timing of these regulatory events. These studies expand our repertoire of *in vivo* probes for the regulation of semagenesis and ultimately the commitment to haustorium development. An expanded model for semagenesis and xenognosis, incorporating the data accumulated in this thesis is presented in the discussion.

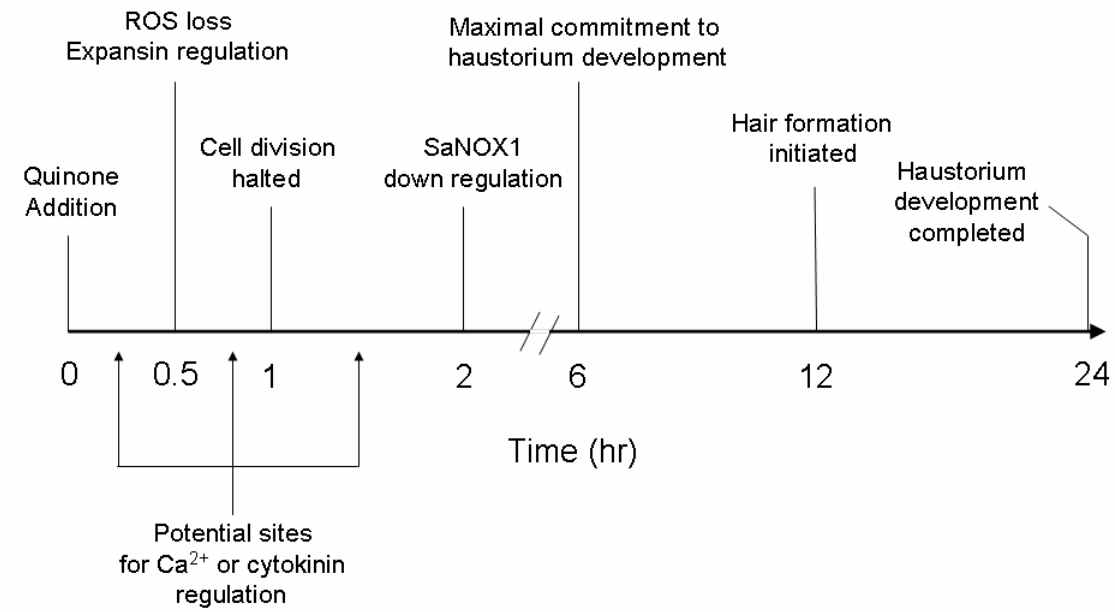

Figure 4.3: *Model for quinone perception resulting in haustorium development*

Phenotypic and genotypic changes associated with haustorium development are above the timeline. Both Ca^{2+} and cytokinins have been implicated in regulating this transition and as a result are likely to be involved within the first two hours of signal exposure as indicated by the arrows. The loss of ROS so early in the process suggests it may also be critical to the developmental transition.

4.2 Results

4.2.1 The role of ROS in xenognosin perception and haustorium formation

In contrast to the cell-impermeant catalase experiments, studies to determine if the loss of ROS was sufficient for haustorial induction were conducted with the cell-permeable superoxide dismutase mimic manganese (III) tetrakis (4-benzoic acid)porphyrin (MnTBAP) [121-124]. Increasing concentrations of MnTBAP, while lowering the overall oxidant concentration, asvisualized by H_2DCFDA, failed to induce haustorium development, suggesting that the loss of oxidant production alone is insufficient for organogenesis (Figure 4.4). Similar effects were also observed with the ROS scavenger KI.

While establishing that the loss of ROS is insufficient for haustorial development, ROS-scavenging experiments do not address the necessity of oxidant loss in organogenesis. However, day-old seedlings treated with 10 μM DMBQ and increasing concentrations of H_2O_2 developed haustoria normally (Figure 4.5A). Increased cellular ROS levels was confirmed by H_2DCFDA staining 1 hour after H_2O_2 addition (Figure 4.5A). Additional H_2DCFDA staining experiments after 24 hours confirmed that oxidant levels remained elevated throughout haustorial development. Furthermore, elevated H_2O_2 treatments (500 μM) had no effect on the rate of commitment to haustorium development by 10 μM DMBQ (Figure 4.5B). Taken together these results suggest that changes in ROS production, beyond their role in xenognosin production during semagenesis, are not related to the commitment to haustorium development and/or xenognosis.

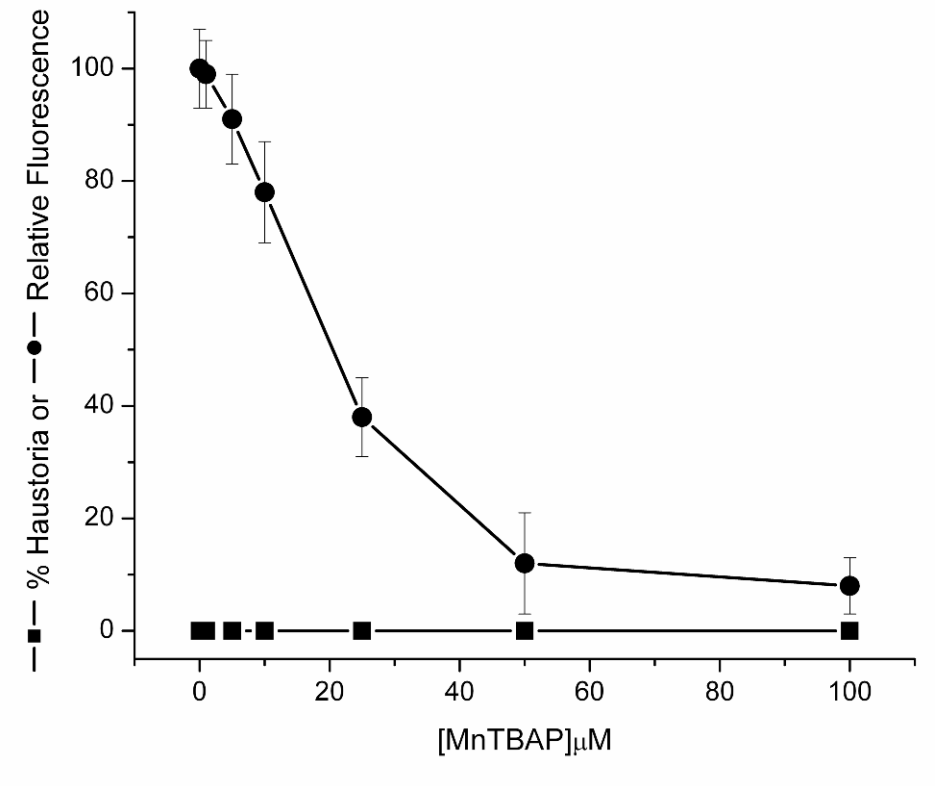

Figure 4.4: *Effects of MnTBAP on ROS and Haustorium development*

One day-old seedlings of *Striga asiatica* are incubated with the indicated concentration of MnTBAP for 24 hrs then scored for haustorium development (■). For each concentration 5 seedlings are isolated and scored for ROS production via H_2DCFDA (●). Experiments performed in triplicate and results expressed as average of trials +/- standard deviation as error.

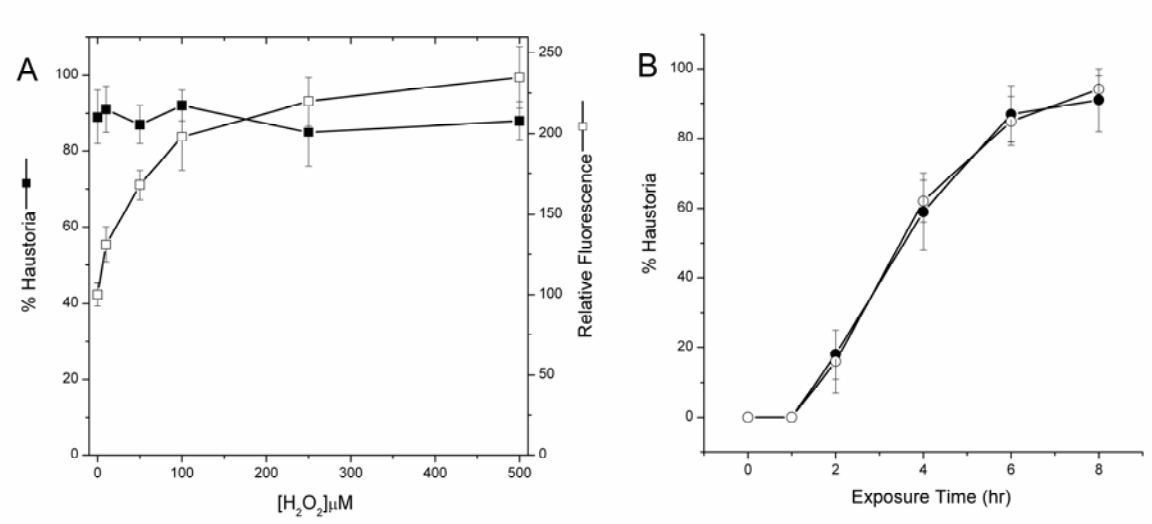

Figure 4.5: *Effects of H_2O_2 on haustorium development*

All experiments conducted on one day-old Striga seedlings. (A) Striga seedlings are incubated in the indicated concentration of H_2O_2 for 1 hour then scored for ROS production (□) or treated with 10 µM DMBQ and scored for haustorium developed after 24 hours (■). (B) Striga seedlings are placed in a solution of 10 µM DMBQ with (●) or without (○) 500 µM H_2O_2 for the indicated time, rinsed in triplicate, placed in 0.1 mM KCl, and scored for haustorium development after 24 hr. Results plotted as average of trials +/- standard deviation.

4.2.2 Cytokinin mediated haustorial development

While the efficacy of cytokinins as inducers of haustorium development has previously been established [26, 27, 113, 114], a more thorough analysis was critical for evaluating their coupling to xenognosis. As seen in Figure 4.6, day-old seedlings of *Striga asiatica* incubated in 10 μM solutions of DMBQ or the cytokinin 6-benzyladenine (6-BA) developed haustoria within a 24 hour period. At 10 μM 6-BA hair formation was more robust, consistent with a stimulatory effect for root hairs previously observed in *Medicago sativa* (alfalfa) [125].

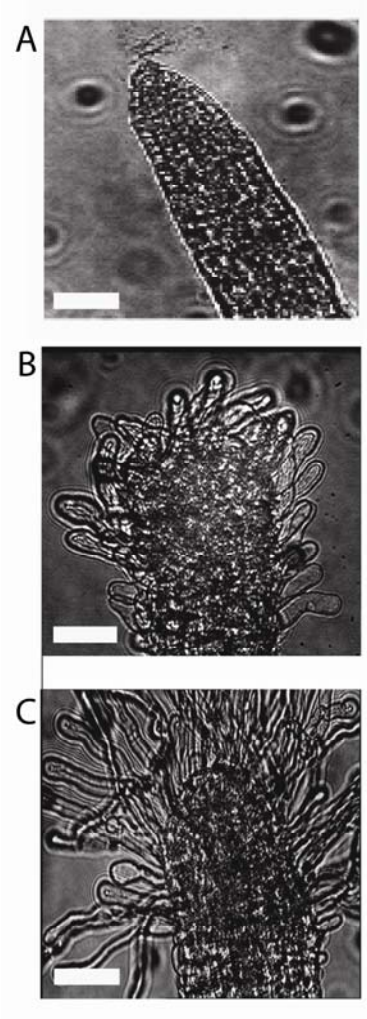

Figure 4.6: *Haustorium development in response to cytokinins* Day-old seedlings of *Striga asiatica* without treatment (A), or in solutions of: 10 μM DMBQ (B), or 6-BA (C) for 24 hours. At this point, seedlings were transferred to microscope slides for image collection. Bar = 100 μm

10 μM treatments with trans-zeatin or kinetin also induced haustorium development confirming the general efficacy of the cytokinins (Figure 4.7A). Such concentrations are abnormally high for hormone effects, which are typically active at submicromolar concentrations, and may not reflect a genuine role for cytokinins in this process [126]. However, as seen in Figure 4.7B, the cytokinins were potent inducers of haustorium development with observable activity at subnanomolar (10^{-10}) concentrations (Figure 4.7B). Like the xenognosic quinones, cytokinins require sustained exposures for commitment with a half maximal induction of haustorium development ($t_{1/2}$) of 4 hours for 10 μM 6-BA [34, 35] (Figure 4.7C). Interestingly, both hormone and xenognosin display similar minimum exposure times for developmental commitment and premature removal results in a recommitment to vegetative growth.

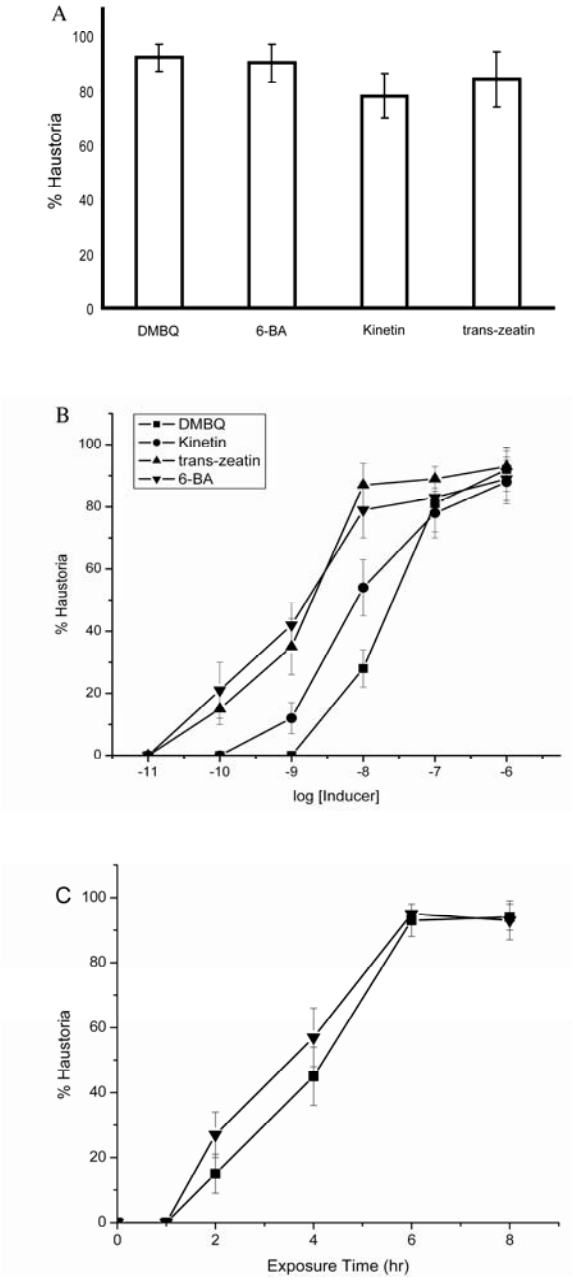

Figure 4.7*: Concentration and time dependence for haustorium formation.*

All experiments conducted in triplicate on day-old seedlings of *S. asiatica*. Samples were scored for haustorium formation after 24 hr with results expressed as average +/- standard deviation. Seedlings were: (A) Exposed to 10μM of the indicated compound, (B) incubated with a concentration series of the indicated compound, or (C) incubated in a 10 μM solution of either (■)DMBQ or (▼) 6-BA for the indicated time then washed in triplicate to remove inducer.

4.2.3 ROS and SaNOX1 expression regulated by cytokinins

The effects of cytokinins on ROS production were evaluated by 10 μM DMBQ or 6-BA exposures for set time intervals followed by H_2DCFDA imaging or evaluating changes in *SaNOX1* expression. As seen in Figure 4.8A&B, both ROS production and *SaNOX1* expression are down regulated by 6-BA in a manner comparable to DMBQ. Like DMBQ, the removal of 6-BA after only 1hr resulted in complete restoration in ROS production (Chapter 2) (Figure 4.9). Similar experiments evaluating the regulation of oxidant production with kinetin and trans-zeatin yielded similar results. These findings support a role for the cytokinins upstream of both ROS and *SaNOX1* expression regulation.

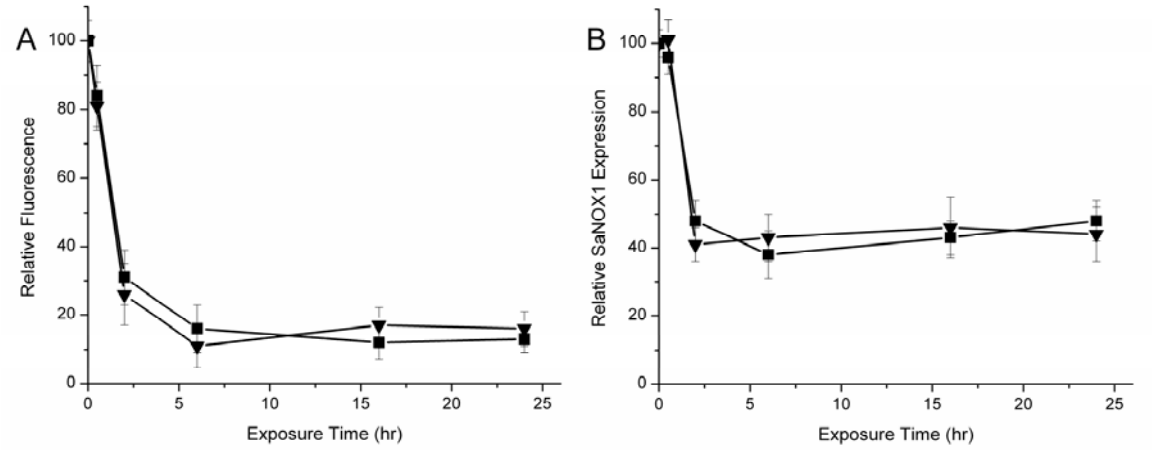

Figure 4.8: *ROS production and SaNOX1 expression in response to cytokinins.*

Day-old seedlings of Striga are incubated with 10 μM of either (■)DMBQ or (▼)6-BA for the indicated time. Seedlings are then washed and either: (A) imaged for ROS production or (B) treated for RT-PCR analysis of *SaNOX1* expression levels. Experiments in (B) conducted by Lizhi Liang.

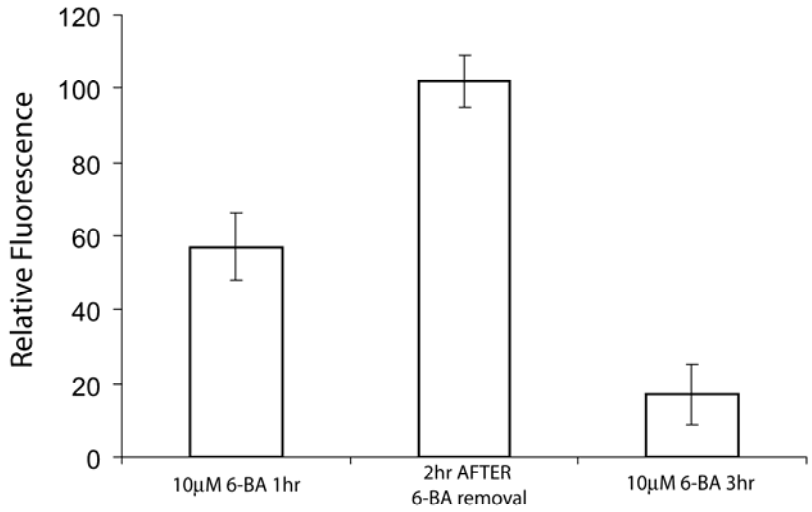

Figure 4.9: *Reversibility of ROS down regulation.*

Day-old seedlings of *Striga asiatica* are treated with 10 μM of 6-BA. After 1 hour the seeds are rinsed and a fraction isolated and imaged for ROS production. The remaining seedlings are returned to solution with or without zeatin and imaged for ROS after 2 hours. Experiments performed in triplicate. Results reported as average +/- standard deviation.

4.2.4 Evaluating cytokinin-xenognosin coupling by inhibitors

While the conservation of oxidant regulation in response to the cytokinins further defines haustorial development in response to hormone exposures they provide no additional information for resolving the proposed models. Employing inhibitors specific for either xenognosin or quinone further experiments were initiated to evaluate these models. As seen in Figure 4.11A, nebularine a known cytokinin inhibitor (anti-cytokinin), inhibited haustorium development by both DMBQ and 6-BA in a concentration dependent manner arguing against the independent model (A) but consistent with a role for the hormone downstream of quinone perception as proposed by model B.

Cyclopropylbenzoquinone (CPBQ), an inhibitor of haustorial xenognosis based on the redox potential of the inducing quinones, is specific for signal transduction, and should therefore have no effect on haustorium development by cytokinins [35]. However, similar concentration assays with CPBQ inhibited haustorial induction by both DMBQ and 6-BA (Figure 4.11B). The ability of the quinone specific inhibitor to block hormone induced haustorial development suggests the second (linear) model (B) to also be incorrect. Furthermore, treatments with CPBQ (10 μM) and nebularine (100 μM) also inhibited down regulation of ROS production by either 6-BA or DMBQ (Figure 4.12). Together these results suggest an intimate coupling between xenognosin and cytokinin (Model C), with the latter not simply a downstream component of the signal transduction pathway.

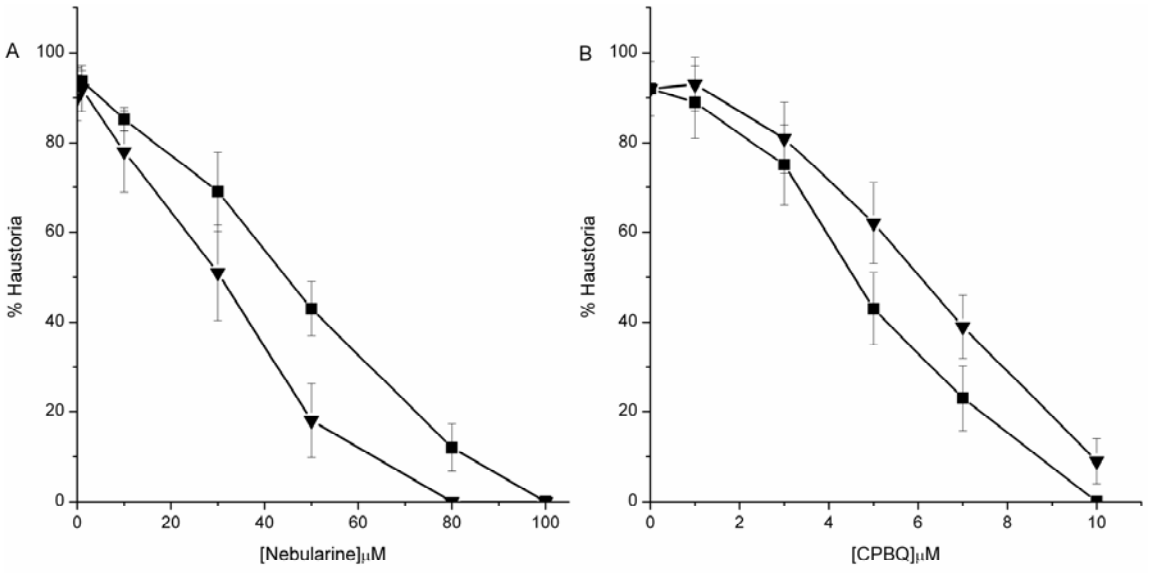

Figure 4.11: *Inhibition of haustorial induction by Nebularine and CPBQ*

Day-old seedlings of *S. asiatica* are treated with either: (■)10μM DMBQ or (▼) 6-BA in increasing concentrations of the anti-cytokinin Nebularine (A) or the redox-sensitive inhibitor of xenognostic quinones cyclopropylbenzoquinone (CPBQ)(B). Seedlings are scored for haustorium formation after 24 hours. Studies conducted in triplicate with results expressed as average of trials +/- one standard deviation.

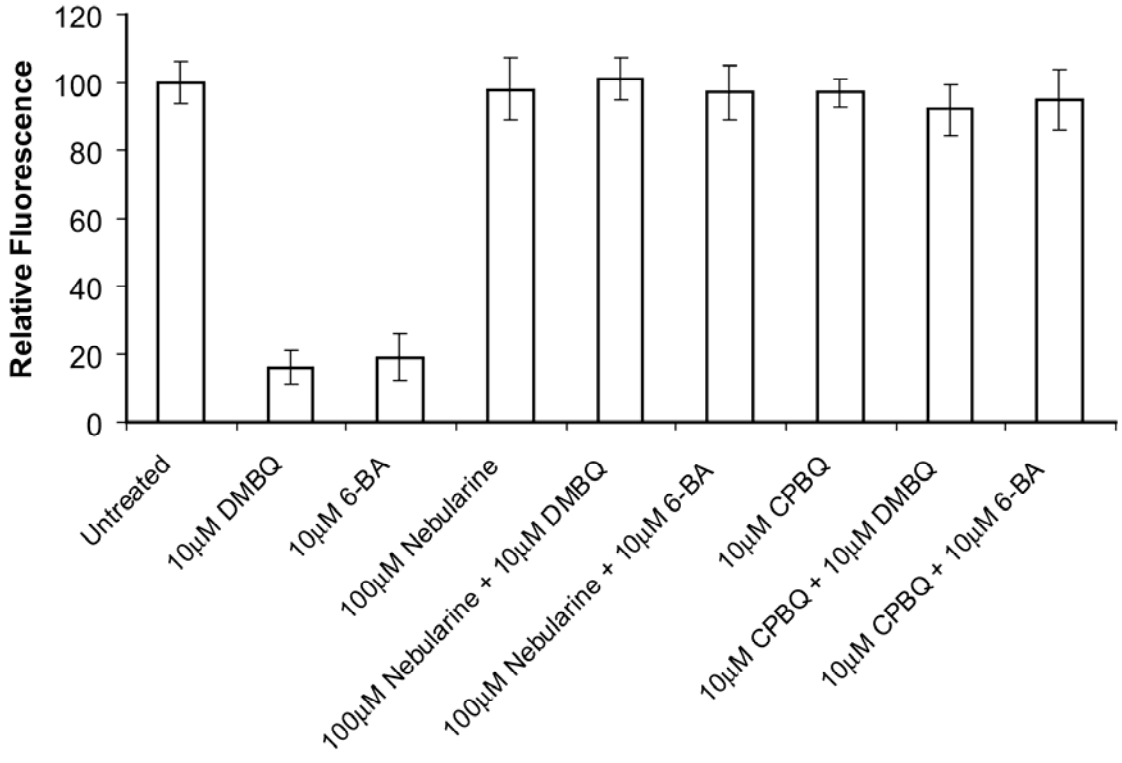

Figure 4.12: *Effects of inhibitors of haustorium development on ROS*

Day-old seedlings of *Striga asiatica* are incubated in 10 µM solutions of the haustorial inducers (DMBQ or 6-BA) with or without inhibitors (Nebularine and CPBQ) for 2 hours. Seedlings are rinsed in triplicate and imaged for ROS production by H_2DCFDA. Experiments performed in triplicate with results expressed as average +/- standard deviation.

4.2.5 Effects of Ca^{2+} channel inhibitors on ROS and SaNOX1

Calcium channel inhibitors have previously established a role for this cation in haustorial development [76]. Furthermore, a positive correlation between oxidant production and $[Ca^{2+}]_{cyt}$ was established in Chapter 3. Hypothesizing that changes in $[Ca^{2+}]_{cyt}$ for xenognosis and oxidant production were coupled, new experiments to evaluate this connection were initiated. Trivalent cations such as lanthanum (La^{3+}), which block Ca^{2+}-channels at the cell membrane, have previously been employed to study a variety of calcium mediated events (reviewed in [127]) including those previously described in *Striga asiatica* [76]. As seen in Figure 4.13, seedlings treated with 10 μM DMBQ alone showed reduced DCF fluorescence accumulation (4.13C&E) while those co-incubated with 10 μM $LaCl_3$ showed no loss in oxidant production (4.13D&E). 10 μM $LaCl_3$ also inhibited DMBQ induced down regulation of *SaNOX1* expression (4.13E). 6-BA induced down regulation of ROS production was also blocked by $LaCl_3$ treatments. These results are consistent with a change in $[Ca^{2+}]_{cyt}$ occurring downstream of the interaction between xenognosin and hormone but early enough in the signal transduction process to regulate semagenesis.

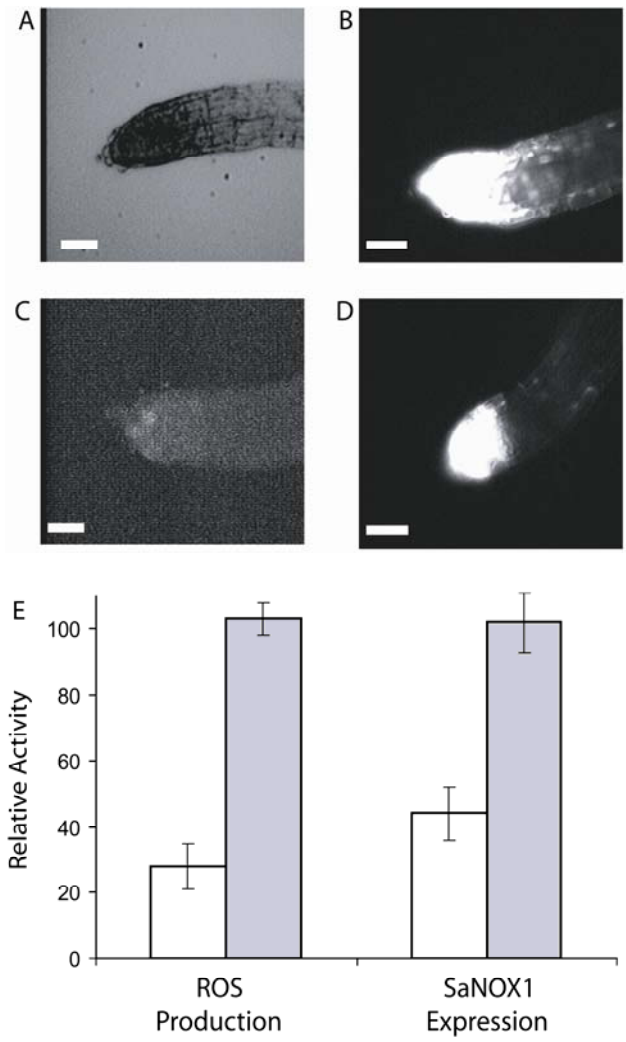

Figure 4.13: *Effects of Ca^{2+} channel blockers on ROS & SaNOX1 regulation*

Day-old seedlings of *Striga asiatica* are treated with: 10 μM DMBQ with or without 10 μM $LaCl_3$ for 2 hours. Seedlings are then imaged for ROS production or evaluated for changes in *SaNOX1* expression. (A-D) microscopy images: (A) Bright field image, (B) Untreated, (C) 10 μM DMBQ, (D) 10 μM DMBQ and 10 μM $LaCl_3$. (E) Summary of fluorescence change or *SaNOX1* expression in response to DMBQ (white) or DMBQ and $LaCl_3$ treatments (grey). Studies conducted in triplicate with results expressed as average of trials +/- one standard deviation as error.

The observed inhibition was not specific for $LaCl_3$ as the trivalent calcium channel inhibitors $GdCl_3$ and $AlCl_3$ both inhibited ROS loss in response to DMBQ exposures. Conversely, micromolar concentrations of Ruthenium Red and Verapamil, typically associated with the inhibition of organelle associated calcium channels, had no effect on ROS suggesting the channels involved in regulating oxidant production and *SaNOX1* expression were likely associated with the cell membrane and extracellular calcium stores [120, 127, 128]. Finally, at the concentrations employed, none of the inhibitors showed significant propidium iodide (PI) fluorescence accumulation arguing against any toxic effects arising from these compounds. These findings are consistent with the inhibition by $LaCl_3$ blocking Ca^{2+} fluctuations at the plasma membrane in response to either xenognosin or cytokinin.

4.2.6 Ca^{2+} channel inhibitors prevent haustorium development

If the calcium phenomenon which appears to regulate semagenic ROS in response to xenognosis plays a role in haustorium development, then similar inhibitory effects should be observed. Indeed, $LaCl_3$ treatments inhibited haustorial development by 10 μM DMBQ in a concentration dependent manner (Figure 4.14A). To determine if this inhibition occurred at the level of xenognosis, seedlings were incubated with 10 μM DMBQ, with or without 10 μM $LaCl_3$ for set times then washed and scored for haustorium development after 24 hours. As seen in Figure 4.14B, seedlings treated with 10μM $LaCl_3$ showed no response to DMBQ exposures while controls developed normally. Moveover, removal of $LaCl_3$ after 6 hours, via $CaCl_2$ washings, followed by re-exposing the seedlings to DMBQ for set exposure times resulted in haustorial

development at rates comparable to controls, suggesting calcium channel inhibition directly inhibited xenognosis. These results are consistent with those for ROS and SaNOX regulation supporting a common calcium fluctuation regulating these events.

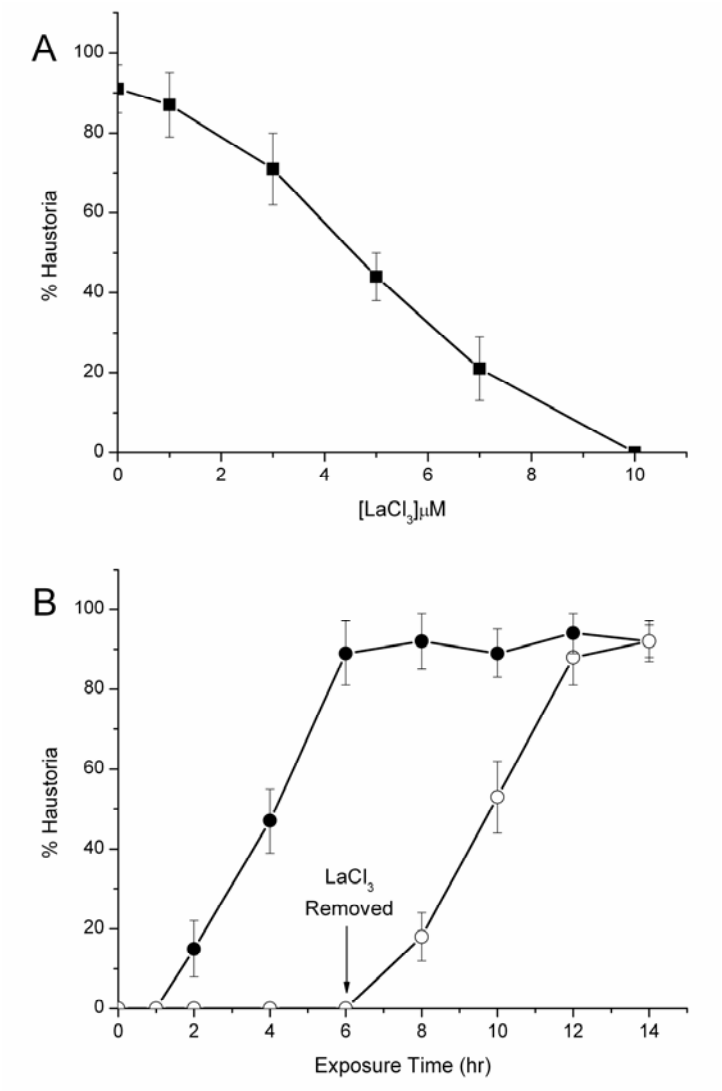

Figure 4.14: *LaCl3 inhibits xenognosin perception*

All experiments conducted on day-old seedlings of *Striga asiatica* in triplicate with results expressed as average +/- SD. (A) Seedlings treated with 10 µM DMBQ and the indicated concentration of $LaCl_3$ then scored for haustorium formation after 24 hours. (B) Seedlings treated with 10 µM DMBQ with (●) or without 10µM LaCl3 (○) for the indicated exposure time then rinsed and scored for haustorium formation. After 6 hours seedlings treated with DMBQ and $LaCl_3$ are washed and placed in a solution of 10µM DMBQ and experiment continued normally.

4.2.7 Ca^{2+}-Ionophores 'reset' developmental commitment

In both root hairs and pollen tube growth, Ca^{2+} gradients accumulate in the cytoplasm driving development and a similar mechanism was hypothesized to be at work in haustorium development [56]. Such gradients can easily be dissipated by the use of calcium ionophores such as ionomycin, which was previously used to alter cytoplasmic calcium ($[Ca^{2+}]_{cyt}$) levels to regulate the activity of SaNOX1 (Chapter 3). A 30 μM solution of ionomycin inhibits quinone induced down regulation of ROS and even restores oxidant production in seedlings pre-incubated with DMBQ for one hour (Figure 4.15). Ionomycin treatments also prevented the down regulation of *SaNOX1* expression.

To further evaluate this calcium phenomenon in the context of haustorium development, ionophore effects on organogenesis were studied. Ionomycin inhibited 10μM DMBQ haustorial induction in a concentration dependent manner (Figure 4.16A). In addition, seedlings pre-treated with DMBQ for two hours then exposed to 30 μM ionomycin show no commitment to haustorium development (Figure 4.16B). However, re-exposure to DMBQ following the ionophore's removal allows organogenesis to progress normally. These results suggest calcium dynamics are reversible during xenognosis and critical in developmental commitment.

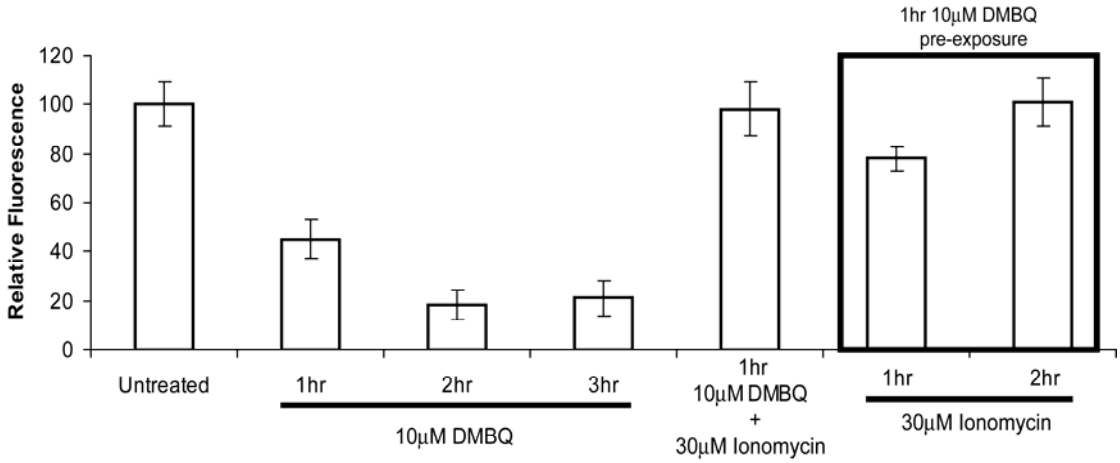

Figure 4.15: *Ionomycin effects on ROS production*

All experiments performed on day-old seedlings of *S. asiatica* in triplicate. Results expressed as average +/- standard deviation of relative fluorescence. Seedlings are treated with DMBQ for the indicated time (1-3 hours) or with DMBQ and ionomycin for 1 hour then imaged, via H_2DCFDA, for ROS production. BOX: Seedlings are pre-treated with DMBQ for 1 hour then ionomycin is added for the indicated time before H_2DCFDA imaging.

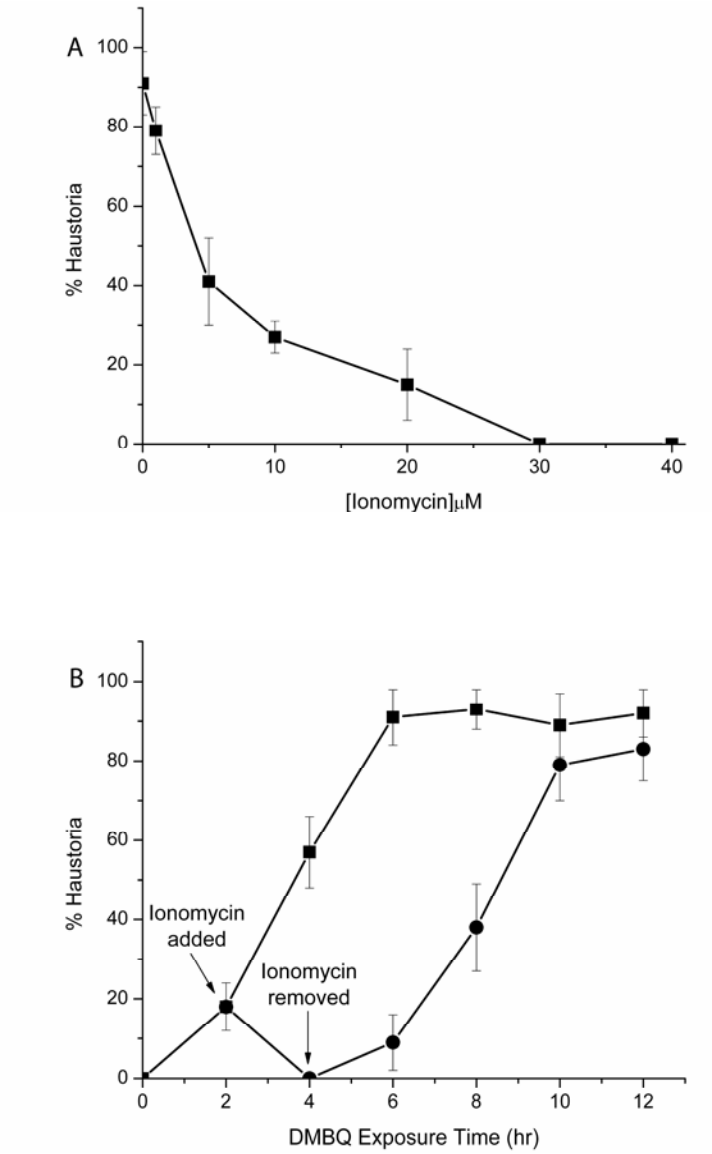

Figure 4.16: *Ionophore effects on ROS production and haustorium formation.*

All experiments conducted on day-old seedlings of *S. asiatica* in triplicate with results expressed as average +/- standard deviation. (A) Seedlngs incubated in the indicated concentration of ionomycin and scored for haustorium development after 24hr. (B) Seedlings are treated with 10μM DMBQ for 2 hours then 30 μM ionomycin is added. At the indicated time points ionophore and/or DMBQ is removed by triplicate washings. The seedlings are scored for haustorium formation after 24 hours.

4.2.8 Ca^{2+} chelation inhibits haustorium formation

The inhibitory activity of $LaCl_3$ and ionomycin suggests an increase in cytoplasmc calcium, arising from an influx of Ca^{2+} from extracellular stores, was critical for both ROS regulation as well as the commitment to haustorium development. Chealtion of extacellular Ca^{2+} with EGTA inhibited haustorium development supporting this hypothesis (Figure 4.17A). This inhibition could be rescued by the removal of the chealtor followed by the addition of a solution of 100 μM $CaCl_2$ (Figure 4.17B). Chelation of cytoplasmic calcium via the cell permeable BAPTA-AM also inhibits haustorium development in a concentration dependent manner (Figure 4.18).

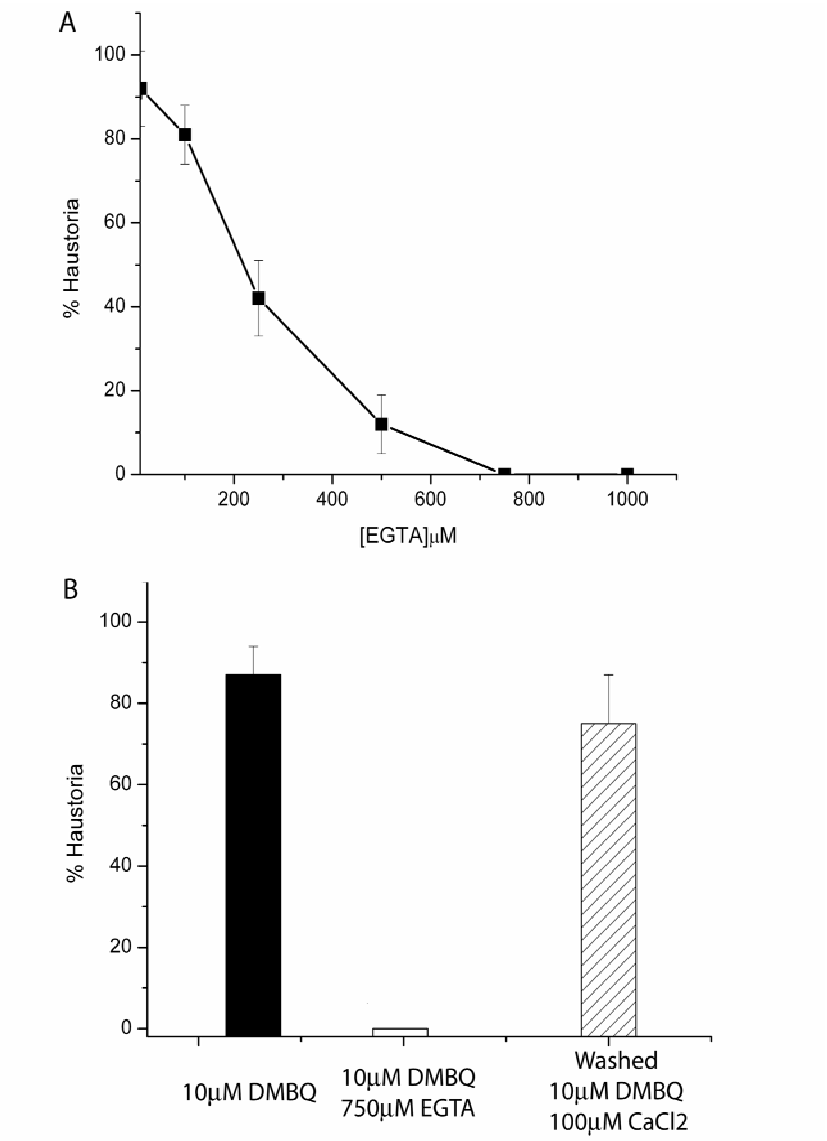

Figure 4.17: *EGTA inhibits haustorium formation.*

(A) Day-old seedlings are incubated with 10μM DMBQ and the indicated concentration of EGTA. Seedlings were scored for haustorium formation after 24 hours. (B) Seedlings are treated with 750 μM EGTA for 2 hours then washed and placed in a buffer containing either 10 μM DMBQ (white) or 10 μM DMBQ and 50 μM $CaCl_2$ (hatched). Seedlings are scored for haustorium formation after 24 hours and compared to seedlings exposed only to 10 μM DMBQ (black).

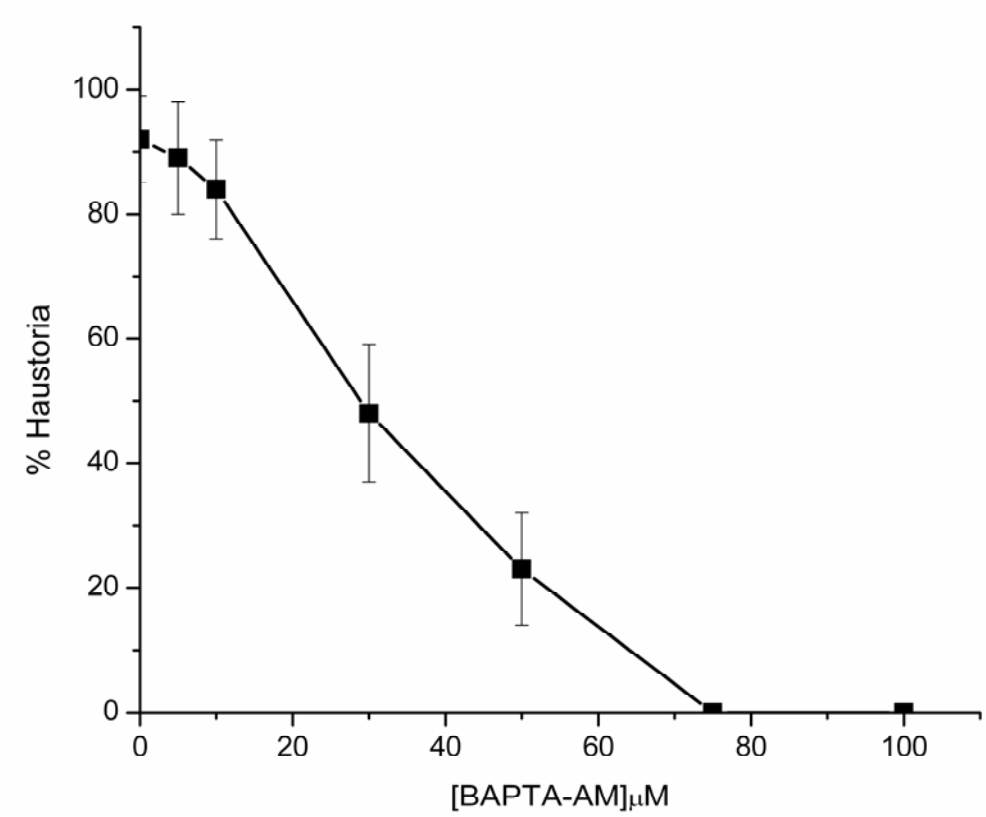

Figure 4.18: *BAPTA-AM inhibits haustorium development*

Day-old seedlings of *Striga asiatica* are treated with the indicated concentration of BAPTA-AM and 10 μM DMBQ then scored for haustorium formation after 24 hours. Experiments performed in triplicate with results expressed as average +/- standard deviation.

4.2.9 Imaging Ca^{2+} dynamics

Fluo-4 is a common fluorescent Ca^{2+} indicator that has previously been used to image free Ca^{2+} in both cardiac and stem cells of humans, rats, and mice (Figure 4.19) [129-132]. This negatively charged dye associates with free Ca^{2+} resulting in a significant increase in fluorescence which, unlike H_2DCFDA, provides a dynamic probe for changes in Ca^{2+}. Due to its anionic character, Fluo-4 is cell impermeant however the netural acetoxymethyl ester analogue, Fluo-4 AM, is able to diffuse into the cell where, like H_2DCFDA, esterase activity traps the negatively charged dye in the cytoplasm. The excitation/emission spectra of Fluo-4 AM is similar to H_2DCFDA and fluorescence images were acquired by similar methods. Day-old seedlings of *S. asiatica* were loaded with 50 μM Fluo-4 AM for 30 minutes then washed to remove excess dye, and transferred to a 6-well microscope slide. Compounds were added directly to independent wells permitting real time *in vivo* imaging of calcium dynamics. As seen in Figure 4.20, the addition of DMBQ stimulates an increase in fluorescence across the root tip over 30 minutes.

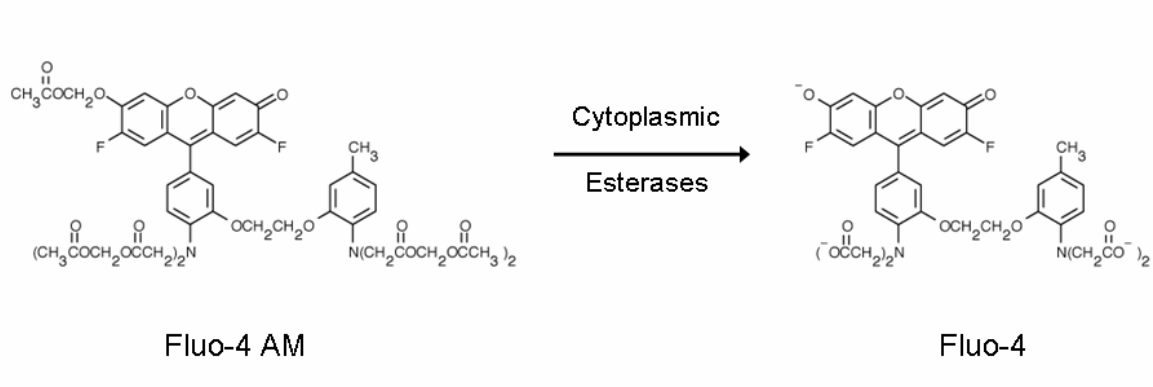

Figure 4.19: *Fluo-4 AM a fluorescent probe for* $[Ca^{2+}]_{cyt}$

Neutral Fluo-4 AM is fluorescent, cell permeable, and with no discernable affinity for Ca^{2+}. Cleavage by cytoplasmic esterases yields the active probe (Ex: 488 nm/Em: 535 nm) whose fluorescence increases upon Ca^{2+} binding.

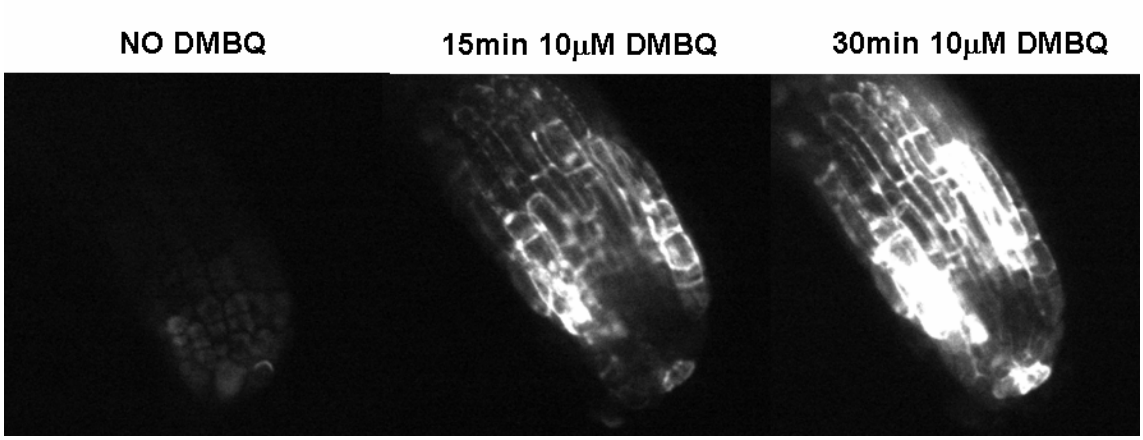

Figure 4.20: *Fluo-4 AM imaging of cytoplasmic calcium dynamics*

Day-old seedlings of *S. asiatica* are treated with 10 μM Fluo-4 AM for 30 min then washed to remove excess dye, and transferred to 6 well microscope slides in 250 μl of 0.1 mM KCl. DMBQ was then added (0.2μl) from stock to produce a 10 μM DMBQ final solution. Seedlings were imaged at successive time intervals on a fluorescence microscope excited with a blue light.

Pixel intensity at the root tip was calculated and plotted as relative fluorescence as a function of time. As seen in Figure 4.21A seedlings show an increase in fluorescence within 5-10 minutes of DMBQ or trans-zeatin addition which plateaus within 30 minutes. Like the regulation of ROS, calcium flux appears specific to haustorial inducing quinones as non-inducers, like TFBQ and Naphthoquinone, had no significant effect (4.21B). Pre-incubation with 10 μM $LaCl_3$ inhibited fluorescence elevation in the presence of DMBQ and trans-zeatin as did CPBQ pre-treatments (Figure 4.22). Chelation of extracellular calcium with 750 μM EGTA also prevented the accumulation of fluorescence in response to DMBQ exposure. Attempts to extend image collection to longer time intervals, past 30 minutes, was complicated by Fluo-4 photobleaching.

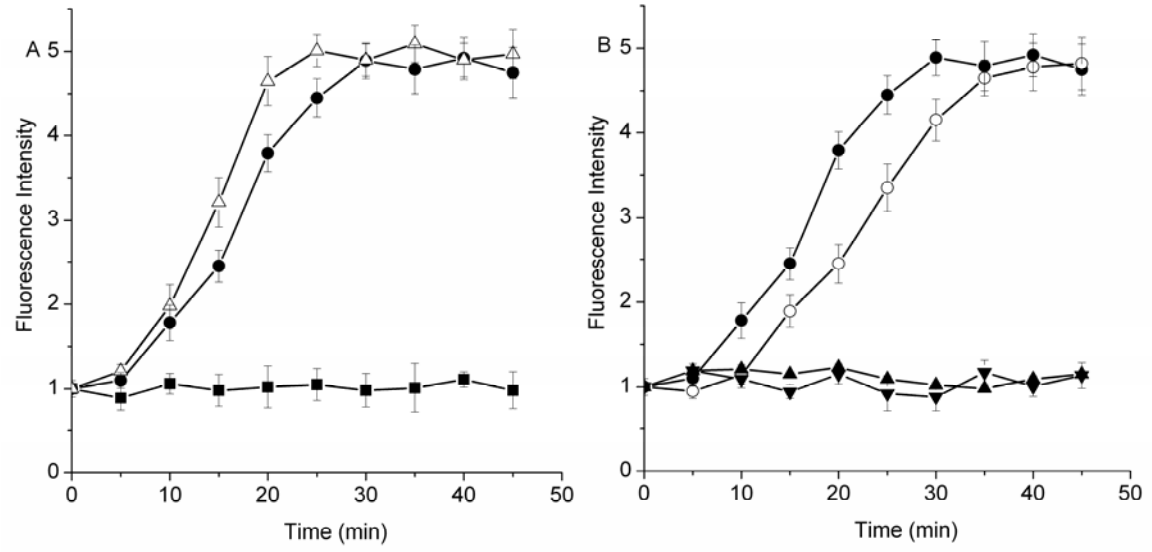

Figure 4.21: *Effect of haustorial inducers vs non-inducers on calcium dynamics*

Seedlings of *S. asiatica* are incubated with 10µM Fluo-4 AM for 30 minutes then washed and transferred into 6 well microscope slides, 3 seedlings/well (250µl vol.). (A) 10µM of either: (●) DMBQ or (△) trans-zeatin then imaged at successive time points and compared to (■) untreated samples. (B)Similar experiments were conducted on (○) benzoquinone, (▲) TFBQ, and (▼) Naphthoquinone. Experiments performed in triplicate and expressed as average +/- standard deviation.

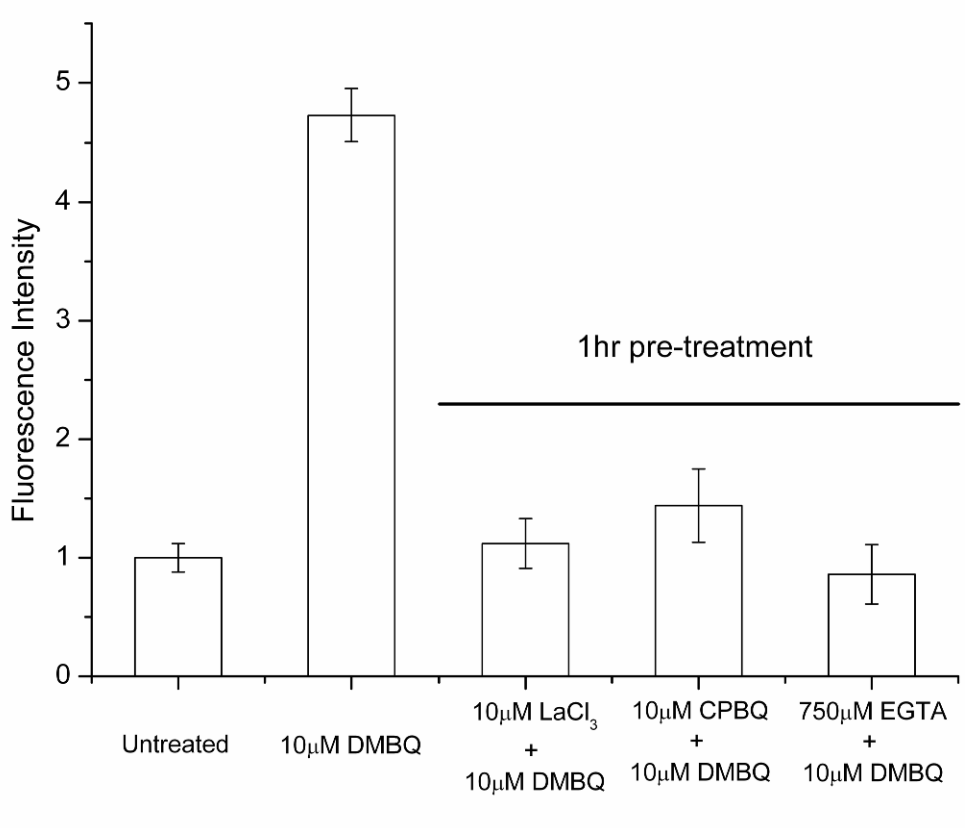

Figure 4.22: *LaCl3, EGTA, and CPBQ effects on Fluo-4 AM fluorescence*

Day-old seedlings of *S. asiatica* are incubated for 30 min in either: 10 μM $LaCl_3$, 10 μM CPBQ, or 750 μM EGTA at which point sufficient Fluo-4 AM is added from stocks to create a 10 μM solution and incubation continues for another 30 minutes. At the end of this hour DMBQ, samples are washed to remove excess Fluo-4 then transferred to 6-well microscope slides in 250 μl. Sufficient DMBQ then added from stock to produce a 10 μM solution. Seeds are imaged after 30 minutes and compared to DMBQ only seedlings (30 minutes) and untreated samples (Fluo-4 AM only).

4.2.10 Employing photocaged calcium to trigger haustorium formation

The calcium imaging assays support a model in which elevations in cytoplasmic calcium are necessary for the induction of haustorium development. However, such fluctuations may or may not be sufficient for this process. One potential way to evaluate this is through the artificial generation of a calcium spike via cell permeable photocaged Ca^{2+}-ionophores like DMNP-EDTA. Like previous acetoxymethyl esters it permeates the cell and is trapped in the cytoplasm by esterases. Photolysis opens the 'cage' resulting in the release of calcium generating a sudden spike in Ca^{2+}_{cyt}. Previously, DMNP-EDTA has been used to study calcium effects in nerve and muscle cells and to study root hair formation [133-136]. Cells loaded with 50 μM Fluo-4 and 50 μM DMNP-EDTA were excited to decage calcium then imaged for fluorescence increase. While increased Fluo-4 fluorescence established calcium release was successful it failed to induce haustorium development. These initial studies suggest calcium alone is insufficient to induce haustorium formation, although higher concentrations or additional dynamics may be necessary.

4.3 Discussion

4.3.1 Identifying regulatory components in xenognosis

The H_2DCFDA assay, the expression of *SaNOX1*, and the development of the haustorium provide viable markers for monitoring xenognosis/semagenesis. Coupled to prior studies these markers provided an opportunity to evaluate a time line for the events which regulate both ROS and organogenesis. Further clarification of the physiological responses which define this continuum between xenognosis and haustorium development provides insight into the nature of the host-parasite interface, the larger picture of interorganismal signaling, and parasitic evolution.

4.3.2 ROS in xenognsosis

Based on the similarities to polar growth events and the coupling of oxidant production to vegetative growth in the parasite it was hypothesized that ROS production was either necessary or sufficient for haustorial development. However, neither the scavenging nor the exogenous addition of ROS significantly altered haustorium development (Figure 4.5 & 4.6). While xenognosis may regulate ROS production, haustorial development is clearly independent of the oxidant.

4.3.3 Cytokinin effects on ROS, xenognosis, and haustorium development

Cytokinins are well established inducers of haustorium development in germinated seedlings of *Striga asiatica* suggesting a role for this hormone in parasitic development [113, 114]. Cytokinins also regulated ROS production, *SaNOX1* and expansin expression in a manner consistent with the xenognosins (Figure 4.9&4.10)[70]. These results were consistent with a model for xenognosis in which quinone perception stimulates downstream cytokinin activity. However, inhibitors specific for the redox potential of the xenognostic quinones inhibit ROS regulation and haustorium development by both DMBQ and cytokinins suggesting this simple model might be incorrect (Figure 4.11&4.12)[35].

While the exact interaction between xenognosins and cytokinins remains undefined, previous studies suggest several potential points of overlap that may explain the shared activity of these compounds. For example, cytokinin dehydrogenase, an enzyme responsible for regulating levels of the hormone throughout the cell appears to employ endogenous quinones, like ubiquinone, as electron acceptors [137] (Figure 4.23). Xenognostic quinones may prevent cytokinin degradation allowing the hormone to accumulate to higher levels stimulating organogenesis in a model consistent with the haustorial inducing activity of exogenous cytokinins. Alternatively, quinones and cytokinins could interact though a number of the redox sensitive components in the cell as the hormone has previously been implicated in their regulation [138, 139]. Finally, some specific receptor may exist which is capable of integrating both signals (Figure 4.24).

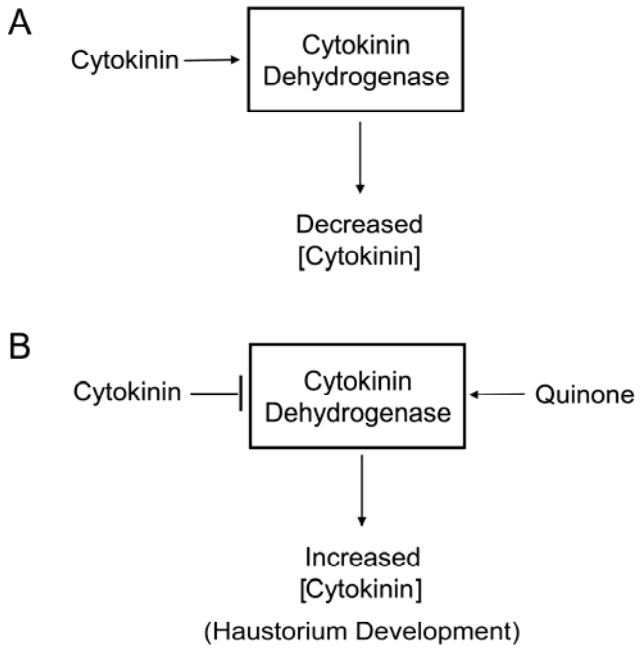

Figure 4.23: *Cytokinin dehydrogenase model for quinone activity*

(A) Cytokinin dehydrogenase catalyzes hormone degradation preventing over accumulation. (B) Xenognostic quinones compete with endogenous electron acceptors preventing cytokinin degradation. Hormone accumulation stimulates haustorium development.

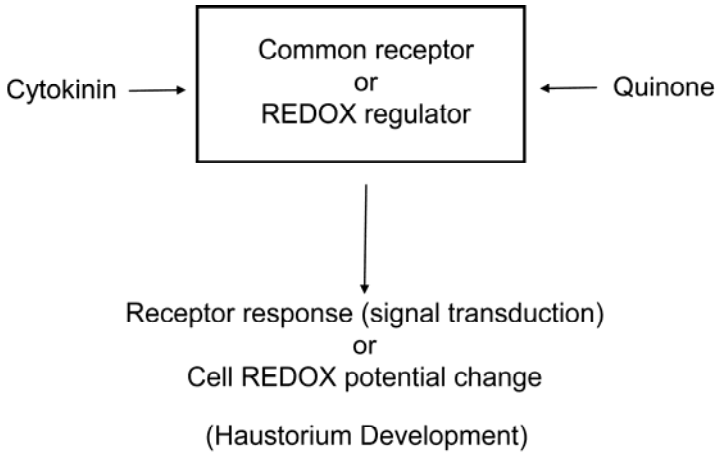

Figure 4.24: *Shared regulator or receptor model*

Quinone and cytokinin perception occur through a common receptor or directly effect similar REDOX regulators resulting in haustorium development.

4.3.4 Ca^{2+} effects on ROS, xenognosis, and haustorium development

Calcium has previously proven important in the ultimate development of the haustorium as well as changes in expansin expression and was further evaluated for its impact on development. Trivalent cation inhibitors of Ca^{2+}-channels like lanthanum trichloride ($LaCl_3$) successfully inhibited the down regulation of ROS production, *SaNOX1* expression, and the initiation of haustorium development by DMBQ and cytokinins (Figure 4.12 & 4.13). This inhibition also suggested that variations in $[Ca^{2+}]_{cyt}$ relative to the extracellular stores may regulate this process [120]. A series of ionophore and chelator assays further supported an increase in $[Ca^{2+}]_{cyt}$ from an extracellular source as critical to xenognosis (Figure 4.14-16). The fluorescent $[Ca^{2+}]_{cyt}$ reporter Fluo-4 AM determined that the $[Ca^{2+}]_{cyt}$ increase was rapid, beginning within 5 minutes of either quinone or cytokinin addition (Figure 4.19-4.21).

The development of Fluo-4 AM as an *in vivo* probe for Ca^{2+} dynamics during xenognosis provides an additional marker for studying the parasite's response to the interorganismal signals generated at the host-parasite interface. Unlike H_2DCFDA, in which dye activation is irreversible, increased Fluo-4 fluorescence is dependent on the non-covalent, and therefore reversible, interaction with free Ca^{2+}, permitting the same seedling to be visualized for changes in $[Ca^{2+}]_{cyt}$ over multiple time points. Like the ROS assay, calcium detection proved reasonably facile and robust, further underscoring the advantage of using fluorescent probes for physiological effects in *S. asiatica*.

These assays reveal several interesting facts about both semagenesis and haustorium development. First and foremost, the elevation of cytoplasmic $[Ca^{2+}]_{cyt}$ from an extracellular source is critical to the regulation of both processes. However it remains unclear if Ca^{2+} alone is sufficient to regulate these events as experiments with photocaged calcium failed to induce haustorium development. Such assays are complicated as the calcium released by photolysis may be below a necessary threshold for this process. Rather, haustorium development may require sustained Ca^{2+} exposures as opposed to a short term calcium spike or wave. This would be consistent with the rapid increase and then plateau of Fluo-4 fluorescence upon DMBQ or cytokinin addition.

Secondly, the loss of ROS production in the presence of elevated $[Ca^{2+}]_{cyt}$ in response to DMBQ is in sharp contrast to prior assays in which the increase of cytoplasmic calcium significantly increased oxidant production. This suggests that the reduction in oxidant production prior to the down regulation in gene expression may not be directly regulated by calcium binding to the EF-hand domain of SaNOX1. Rather, Ca^{2+} most likely regulates an additional component such as phosphorylation or Rac/Rop GTPase activity which controls oxidant production [75, 107, 140]. A temporal separation between increases in $[Ca^{2+}]_{cyt}$ and loss of ROS has previously been observed in roots of alfalfa in response to NOD-factors, the bacteria derived polysaccharides which initiate the legume-rhizobia symbiosis, another critical interorganismal signaling process [141, 142].

Third, the rapid increase in cytoplasmic calcium in response to DMBQ is the earliest event in the perception of haustorial inducing signals, other than the interactions with cytokinin regulatory components, detected thus far. Cytoplasmic calcium flux occurs ahead of both ROS and gene regulation, and potentially even the halt in cell division (<1 hr) previously observed by the uptake of ^{3}H-thymidine [115]. Ca^{2+} is clearly an upstream regulator of the first and second of these events and a potential role for the latter is reasonable given the cation's role as a regulator in the cell cycle [119, 129].

4.3.5 A refined model for xenognosis and the regulation of semagenesis

While several questions remain as to the mechanism by which calcium and cytokinins are integrated into haustorial xenognosis, these experiments provide a more detailed model for signal perception. First, the accumulation of xenognosins, as a result of the oxidation of cell wall phenols by ROS during semagenesis, initiates host detection. Perception of the haustorial inducing quinones appears directly connected to cytokinins through an as of yet unefined mechanism. However, regardless of the nature of this interaction the most immediate downstream event appears to be the opening of cytoplasmic Ca^{2+} channels permitting the influx of calcium from the extracellular space. Such stimulation is certainly reasonable as both redox sensitive compounds and/or cytokinins have previously been shown to stimulate Ca^{2+} channels in mosses [143-145]. The rapid and sustained increase in $[Ca^{2+}]_{cyt}$ (5-30 min) appears necessary for changes in gene expression, ROS loss, and other potential regulatory events. The loss of ROS, in the presence of elevated $[Ca^{2+}]_{cyt}$ suggests an additional regulatory mechanism controls oxidant activity. Prior to developmental commitment, removal of the xenognosin restores

both the phenotypic and genotypic responses associated with vegetative growth and most likely dissipates the growing calcium gradient across the cell membrane.

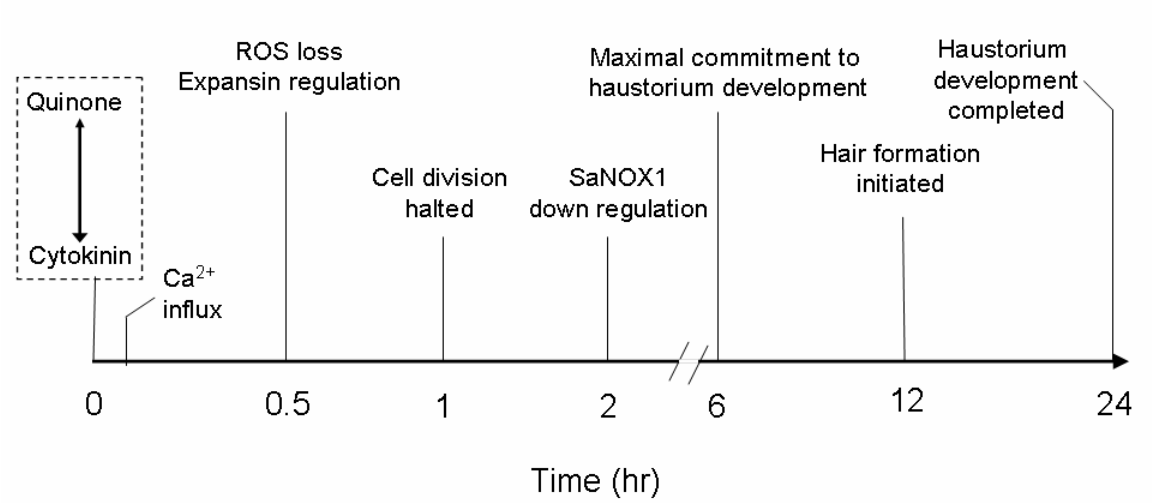

Figure 4.25: *Expanded model for xenongnosis/haustorial organogenesis*

Events above the timeline are known events that occur during the process of haustorium development. Dashed-box: The inability to separate quinone from cytokinin activity as inducers suggests these components are linked in some intimate but as of yet undefined way.

4.3.6 Conclusion

In this chapter, further studies elucidated the circuitry necessary for xenognosin perception suggesting both cytokinins and calcium played critical roles in this process as well as in semagenesis. Given the diverse array of functions regulated by both hormone and cation the evolutionary origins of this parasitic process remain unclear. However these studies do provide additional targets for evaluating xenognosin-mediated development for future studies. Finally, these studies highlight the intimate connection between ROS, calcium dynamics, and development in response to the xenognostic quinones. The conservation of this triumvirate in non-parasites underscores the use of Striga for evaluating growth and development of plants in general. Moreover, this conservation suggests developmental responses in non-parasites could provide insight into xenognosis and subsequent haustorial organogenesis. In chapter 5 model non-parasites such as Arabidopsis and Tobacco will be evaluated for their responses to the xenognostic quinones to provide the foundation for comparative analysis.

CHAPTER 5 – Evaluating the Origins of Semagenesis

'Semagenesis' In Non-Parasites

"All our knowledge has its origins in our perception." – Leonardo da Vinci

5.1 Introduction

In refining the model for semagenesis, evidence has continued to accumulate suggesting it is the evolutionary co-opting of a ROS mediated defense or developmental process focused externally for the detection of a prospective host. The cross-linking of monolignols by NADPH oxidases in both defense and development, an event likely to yield *p*-benzoquinones as side products, supports the potential for such products as a more general response in plants [56, 57, 79, 95] (Chapter 3). Previously, Yoder *et al.* proposed that the detection of the xenognostic quinones evolved out of a role for such compounds as allelopathic, or interorganismal, regulators of development [112]. This argument was supported by the inhibitory effects of the quinone juglone (Figure 5.1) on plant growth, as well as changes in gene expression in *Arabidopsis thaliana* in response to haustorial inducers [16, 112]. However, these studies failed to propose a mechanism for this allelopathic activity or how this mechanism might be connected with the process of xenognosis.

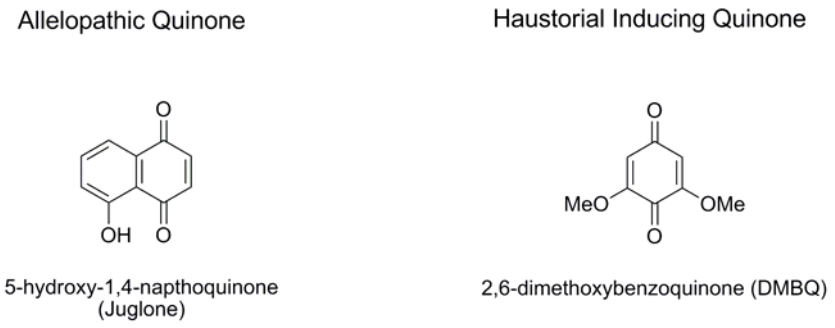

Figure 5.1: *Allelopathic quinone juglone and haustorial inducing quinone*

The well-defined signaling between parasitic plants and their hosts underscores the importance of further evaluating the effects of xenognostic quinones in non-parasites. The conservation of such responses would not only help to define evolutionary origins for the general function of these quinones, but also provide a wealth of new systems amenable to genetic manipulation in which to evaluate the larger impact and evolutionary origins of semagenesis and xenognosis. With regards to the more immediate studies of the host-parasite interface a response to the xenognosins in prospective host plants would confirm the products of semagenesis are not limited to serving as xenognosins for haustorial development, adding an additional level of complexity to the exchanges of signals at the host parasite interface.

The model which has emerged over the preceding chapters provides a framework in which to evaluate general response in plants to the haustorial inducing quinones. In this chapter the tools developed over the course of this thesis, along with growth assays and new molecular probes, will be applied to non-parasites to evaluate these responses. The results will be discussed within the context of parasitic evolution, xenognosis, and the nature of the host-parasite interface.

5.2 Results

5.2.1 Growth effects of haustorial inducing xenognosins on non-parasites

To evaluate the effect of xenognostic quinones on non-parasites, seeds of the model plants *Nicotiana tabaccum* (tobacco) and *Arabidopsis thaliana* were grown on solid media plates of 2% Gelrite, 50% Murashigie Skoog media (MS), and increasing concentrations of DMBQ for 9 days. While seeds germinated comparably to controls at concentrations up to and including 50 μM, these levels declined significantly at higher exposures (Figure 5.2). To distinguish between the suppression of germination and toxicity, the ungerminated seeds exposed to 100 μM DMBQ were washed (3X) in 50% MS media and transferred to DMBQ free plates. The transferred seeds failed to germinate after 1 month and the roots of seedlings germinated at 100 μM and 200 μM DMBQ were blackened and accumulated substantial propidium iodide (PI) fluorescence, confirming toxicity at these concentrations. Conversely, PI fluorescence in 50 μM DMBQ treated seedlings was comparable to untreated samples. Based on these fluorescence results, in conjunction with the germination and growth assays, 50 μM DMBQ was selected as the maximal concentration for evaluating quinone activity among non-parasites.

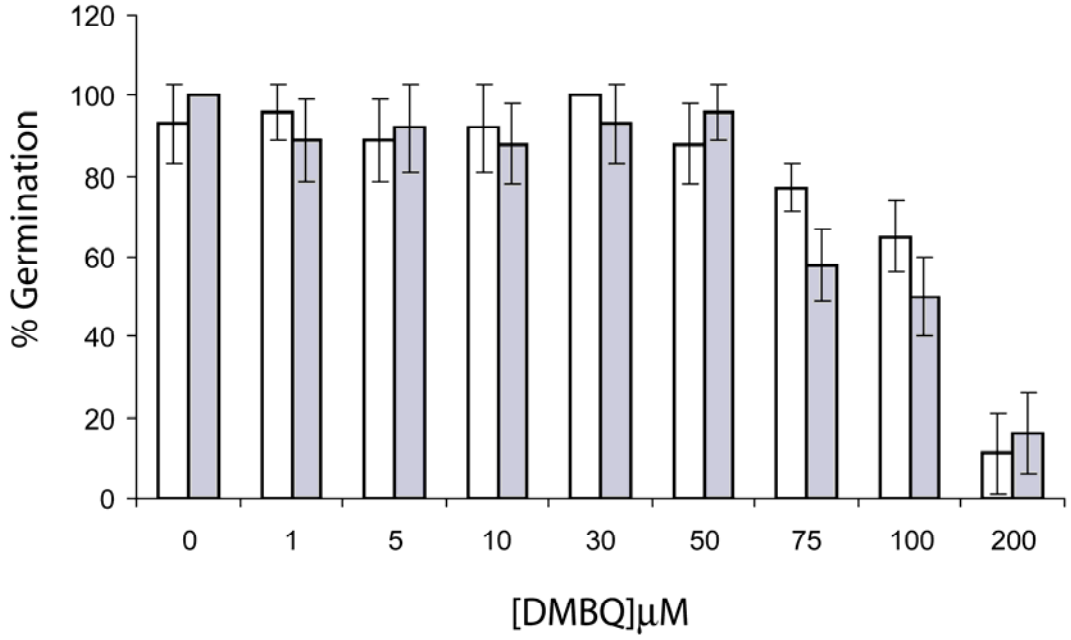

Figure 5.2: *Effects of DMBQ on non-parasite germination*

Sterilized seeds of *Arabidopsis thaliana* (grey) or *Nicotiana tabaccum* (white) were plated on Murashigie & Skoog (MS) plates (50% MS, 2% gelrite, 5 seeds/plate) and scored for germination after 9 days. Results are expressed as average of 5 trials with +/- SD as error.

Conservation of a quinone response through allelopathy, as proposed in the Yoder model, would most likely be observable in a reduction in growth and development in non-parasites. To test this model the germinated seedlings were then evaluated for DMBQ effects on root length, as well as the number and length of root hairs. In addition, cotyledon emergence, the distance from tip to tip of the first emerging leaves, a common indicator of toxicity and/or growth, were also characterized [146-148]. DMBQ effects were evaluated after 9 days of growth and normalized to untreated seedlings. As seen in Figure 5.3A-C, DMBQ exposures decreased root length, as well as the number and size of the root hairs in a concentration dependent manner. No significant effects on cotyledon emergence were observed between 1 and 50 μM exposures while higher concentrations showed diminished growth. The effects of DMBQ exposures on the roots of tobacco are shown in the Scanning Electron Micropscopy images (SEM) in Figure 5.4. While these results support DMBQ as an inhibitor of root growth, any effects associated with shoot growth are inherently complicated by the toxicity of the concentrations employed to produce these effects.

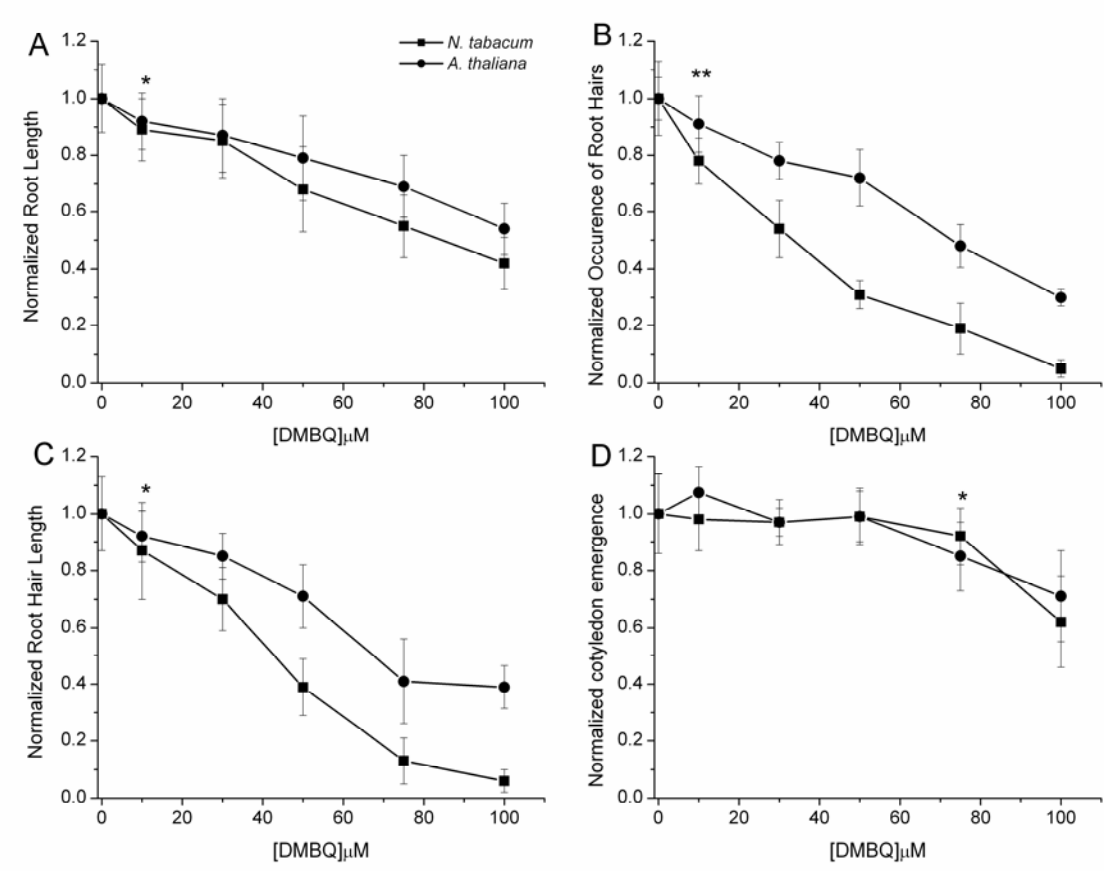

Figure 5.3: *Effects of DMBQ on non-parasite growth*

Nicotiana tabacum (■) and *Arabidopsis thaliana* (●) seeds are germinated and grown under the same conditions as Figure 5.2 are evaluated for effects on: root length (A), number of root hairs (B), root hair length (C), and the distance between tips of cotyledons (D). Results are average of 5 seedlings repeated 5 times with +/- SD as error. * = Statistically different by Student's t-test 97% confidence. ** = 99% Confidence.

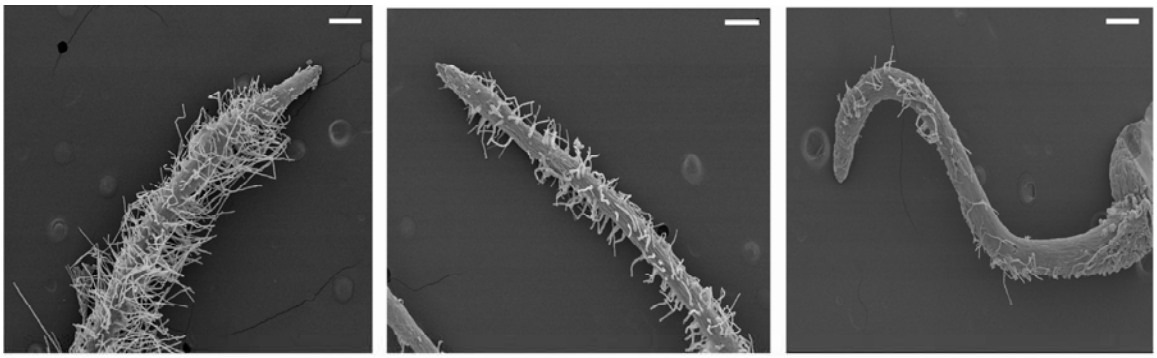

Figure 5.4: *DMBQ effects on tobacco root growth*

Scanning electron microscopy (SEM) images of 9 day-old tobacco seedlings growth on 0, 10, and 50μM DMBQ (See Methods). Bar = 286 μm

5.2.2 Evaluating DMBQ decomposition

While successfully establishing a working concentration range for DMBQ assays, the observed affects may be skewed by quinone degradation and turnover. To address this concern, tobacco seedlings were grown on plates of 10, 30, or 50 μM DMBQ and replated at 3, 5, and 7 days. As seen in Figure 5.5, root development in replated samples showed no significant variation from controls (single platings) suggesting the DMBQ concentration remains constant throughout the 9 day growing period. The potential that root hairs are lost (torn off) during replatings seems unlikely as these samples were comparable to their single plated counterparts at every concentration.

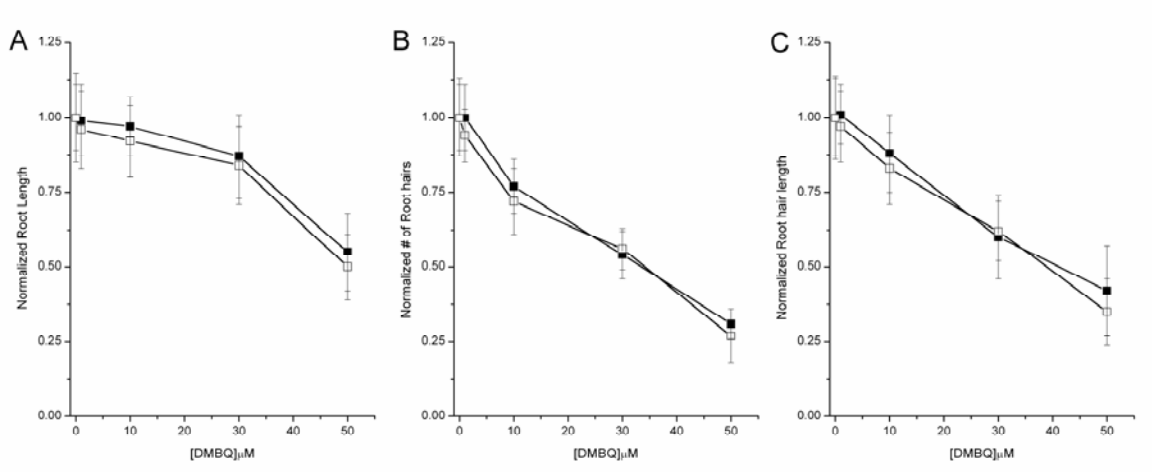

Figure 5.5: *Tobacco seedling replating experiments*

Tobacco seeds are plated on 50% MS plates with the indicated concentration of DMBQ. At days 3, 5, and 7 the growing seedlings are transferred to freshly prepared plates of the equivalent DMBQ concentration. After 9 days, growth in replated seedlings (□) are compared to single plated samples (■) for effects on root length (A), number of root hairs (B), and root hair length (C). Results are average of 5 seedlings repeated 3 times with +/- SD as error.

5.2.3 Evaluating the activity of other quinones in non-parasites

To further evaluate the connections between xenognosis and allelopathy, a structure-activity relationship (SAR) study was completed on tobacco with quinones within the redox window for haustorial induction (-250 mVto 0 mV)[35]. Tobacco seeds were germinated and grown on plates of 50 μM quinone for 9 days then scored for effects on root development. The results summarized in Table 5.1, establish that quinones within this redox window reduce root development in tobacco, including structures whose steric constraints preclude them from haustorial induction in Striga (Chapter 1). Neither germination nor cotyledon emergence were significantly affected by these quinone exposures. Repeating these growth assays at 10 μM and 30 μM with haustorial inducing *p*-benzoquinone and methoxybenzoquinone, as well as the non-inducer *t*-butyl benzoquinones further confirmed the concentration dependence of the quinone responses in tobacco.

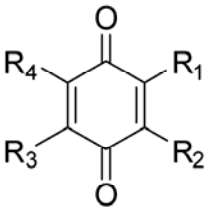

R1	R2	R3	R4	Root Length	Root Hair #	Root Hair Length	HI
H	H	H	H	0.51 +/- 0.06	0.39 +/- 0.1	0.47 +/- 0.21	✓
OCH_3	H	H	H	0.59 +/- 0.09	0.41 +/- 0.08	0.58 +/- 0.11	✓
OCH_3	OCH_3	H	H	0.47 +/- 0.15	0.29 +/- 0.12	0.45 +/- 0.12	✓
OCH_3	H	OCH_3	H	0.56 +/- 0.12	0.43 +/- 0.07	0.49 +/- 0.08	×
OCH_3	H	H	OCH_3	0.55 +/- 0.13	0.31 +/- 0.05	0.42 +/- 0.15	✓
$C(CH3)_3$	H	H	H	0.58 +/- 0.11	0.48 +/- 0.14	0.55 +/- 0.14	×
$C(CH3)_3$	H	H	$C(CH3)_3$	0.61 +/- 0.09	0.45 +/- 0.11	0.31 +/- 0.07	×
OH	H	OH	H	0.42 +/- 0.17	0.25 +/- 0.05	0.55 +/- 0.16	✓
			Untreated	1.0 +/- 0.15	1.0 +/- 0.13	1.0 +/- 0.09	

Table 5.1: *Quinone effects on plant root growth*

Tobacco seeds are germinated and grown on 50 μM of the indicated quinone for 9 days then scored for effects on root growth. The results are normalized to untreated samples set at 1. Results are the average of 5 seeds/plate repeated 5 times with error bars representing +/- standard deviation. HI: huastorial inducer.

Building on these initial SARs results these assays were extended to quinones outside the redox window for haustorial induction. Studies of the more electronegative naphthoquinone and 2-hydroxynaphthoquinone showed substantially reduced germination, less than 25%, at 50 μM (Figure 5.6). Washing and replating of the ungerminated seeds failed to restore germination and the emerging roots of the few seedlings which did germinate were stunted, blackened, and accumulated substantial PI fluorescence supporting this concentration (50 μM) as toxic. However at lower concentrations, treatments with the naphthoquinones inhibited germination and root elongation (Figure 5.6) without PI fluorescence accumulating to levels above controls. Similar inhibitory trends were observed for root hair number and length [112]. Conversely, the more electropositive tetrafluorobenzoquinone (TFBQ) while having no effect on germination or hair growth showed stimulatory effects on root elongation (Figure 5.6). However, over the 9 days, both TFBQ stocks and plates turned a faint purple suggesting reduction and/or degradation of the quinone. As the nature and concentration of these products are unknown, further TFBQ studies were not pursued.

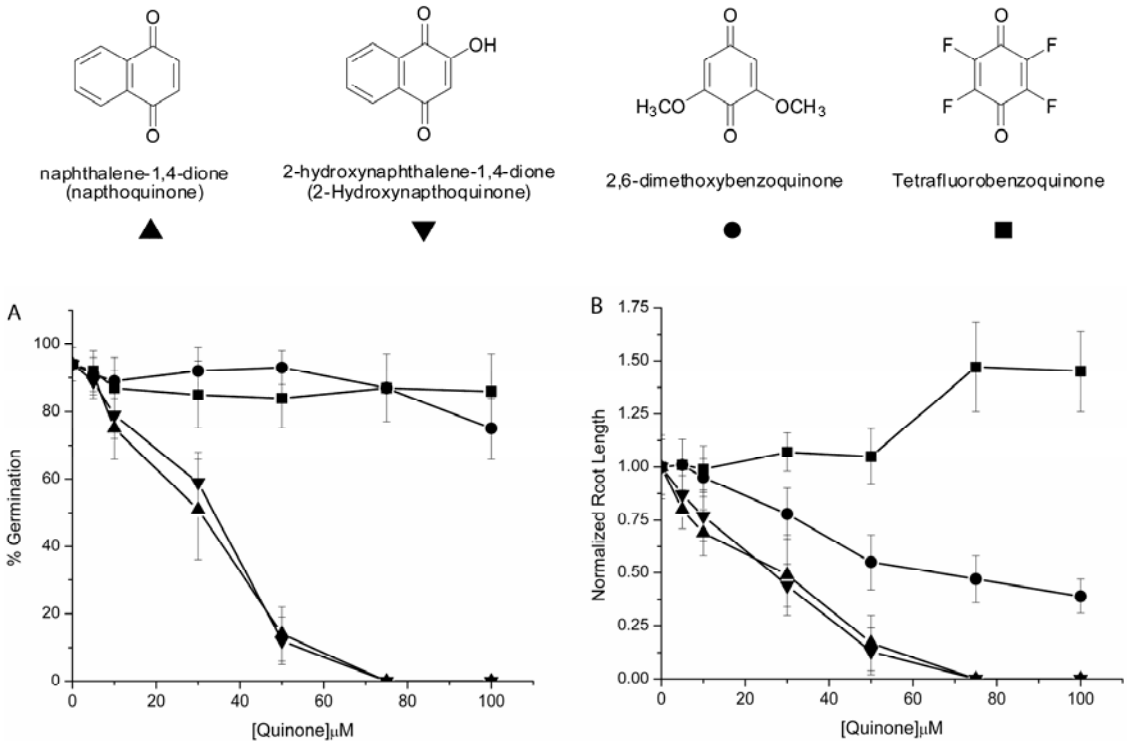

Figure 5.6: *TFBQ and Naphthoquinone effects on tobacco*

Seeds of tobacco are placed on solid media plates of the indicated concentration of quinone (5 seeds/plate). Seeds are scored for germination and root length after 9 days. Results are expressed as average of 15 seeds with error as +/- standard deviation.

5.2.4 Monolignols and root development

The localization of ROS at the root tip of Striga, proximal to the monolignol and peroxidase rich host root surface, creates a microenvironment in which haustorial inducing quinones can be generated (Chapter 1). Given the constitutive production of ROS and the numerous peroxidases throughout the roots of plants, the exogenous application of monolignols should drive quinone accumulation resulting in a comparable phenotype. As seen in Figure 5.7, tobacco seeds grown on coniferyl and sinapyl alcohol, phenolic precursors for methoxybenzoquinone and DMBQ respectively, reduced root development. The more potent inhibitory activity of coniferyl alcohol, versus its methoxybenzoquinone product, on root hair number was consistently observed and may represent some additional activity of the monolignol in this process. While these results are consistent with the oxidation of monolignols to quinones, as in Striga, the results are complicated by the necessity of ROS in root development.

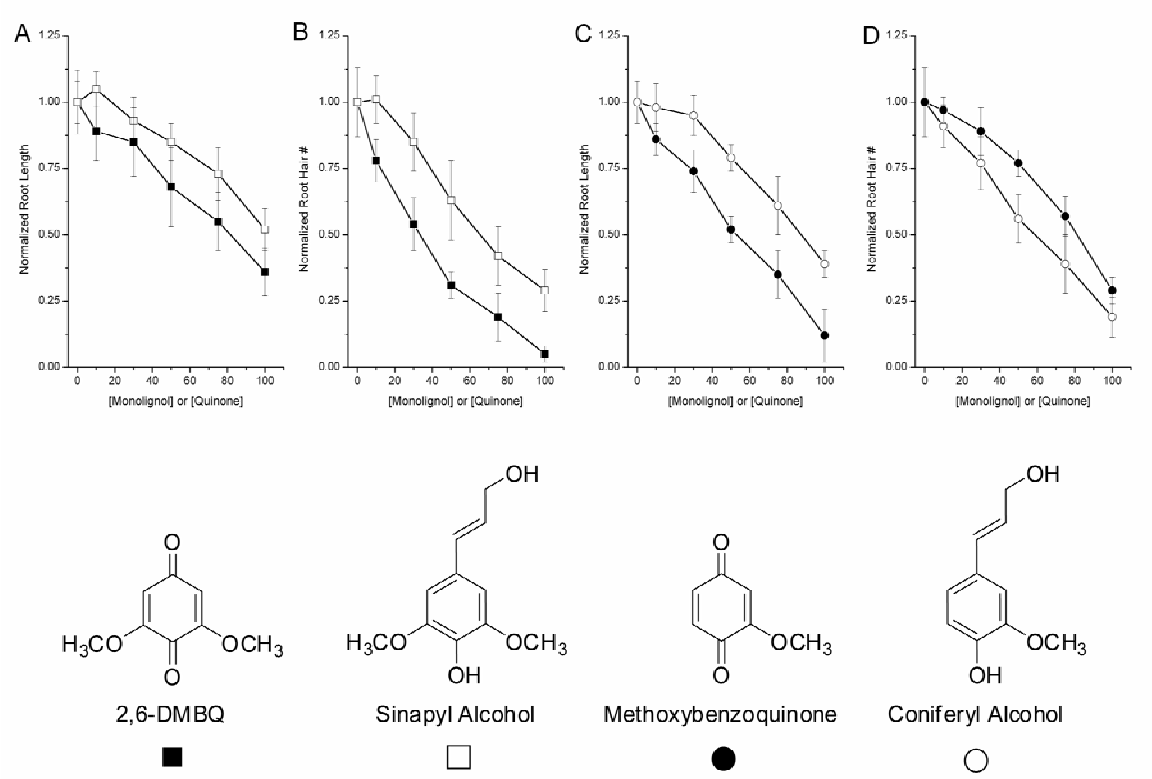

Figure 5.7 *Effects of monolignols on tobacco root development*

Tobacco seeds are plated on increasing concentrations of the indicated quinone or monolignol for 9 days then scored for root length (A&C) and root hair number (B&D). Results are expressed as average of 15 seeds (5 seedlings/plate) with error as +/- standard deviation.

5.2.5 Evaluating the generality of DMBQ inhibition

Given the ubiquity of both ROS and monolignols among both monocots and dicots the potential generality of this response was explored. Seeds of the dicot *Ocimum basilicum* (Basil) as well the monocots *Zea mays* (corn) and *Sorghum bicolor* (Sorghum), both hosts for Striga, were grown in Magenta boxes with 50μM DMBQ. The effects of these treatments on both root length and root hair number, relative to the untreated samples, are shown in Table 5.2 and are consistent with the results observed for both Arabidopsis and Tobacco. As in previous studies such exposures had no significant effect on germination or cotyledon emergence. Finally, seedlings of *Zea mays* grown on coniferyl or sinnapyl alcohol showed a similar reduction in growth. Taken together these growth assays support conservation of both semagenesis as well as xenognosis across multiple families in the Plantae Kingdom.

Plant	Monocot (M) or Dicot (D)	Root Length	Root Hair #
Arabidopsis thaliana	D	0.79 +/- 0.11	0.65 +/- 0.1
Nicotiana tabaccum	D	0.68 +/- 0.15	0.39 +/- 0.09
Ocimum basilicum	D	0.75 +/- 0.08	0.54 +/- 0.11
Sorghum bicolor	M	0.81 +/- 0.12	0.71 +/- 0.13
Zea mays	M	0.83 +/- 0.16	0.68 +/- 0.11

Table 5.2: *Effects of DMBQ on other non-parasites*

Seeds of each plant are germinated and grown on solid media plates (50% MS media, 2% Gelrite) with 50 μM DMBQ for 9 days, then scored for root length and root hair number. Results are the average of 15 seedlings with error expressed as +/- standard deviation.

5.2.6 Evaluating oxidant production in non-parasites

To this point, these studies have focused on evaluating the conservation of the xenognosin as well as semagenesis. However, while the concentration dependent inhibition of root development in response to the products of semagenesis is in sharp contrast to their role in the parasite, where they induce haustorium development, it is consistent with a decrease in ROS production [58]. Given the importance of oxidant regulation in development, as well as the ease of its detection, ROS seemed an ideal physiological response for evaluating mechanistic conservations in the response to xenognosins.

While the fluorescence assays previously used to probe Striga seedlings provided information as to the localization and regulation of oxidant production, dye diffusion and photobleaching prevented them from functioning as high throughput screens. An assay permitting multiple seedlings to be screened while facilitating general localization of oxidant production was sought. Nitroblue tetrazolium (NBT), a cell impermeant stain, that forms insoluble blue/black deposits upon contact with ROS, has previously been employed to observe oxidant production in root tips, root hairs, pollen tubes, and to evaluate photo-oxidative stress in leaves [57, 58, 62, 149] (Figure 5.8). Since NBT deposition occurs at the site of oxidation, this dye is not subject to diffusion or photobleaching permitting multiple seeds to be evaluated simultaneously.

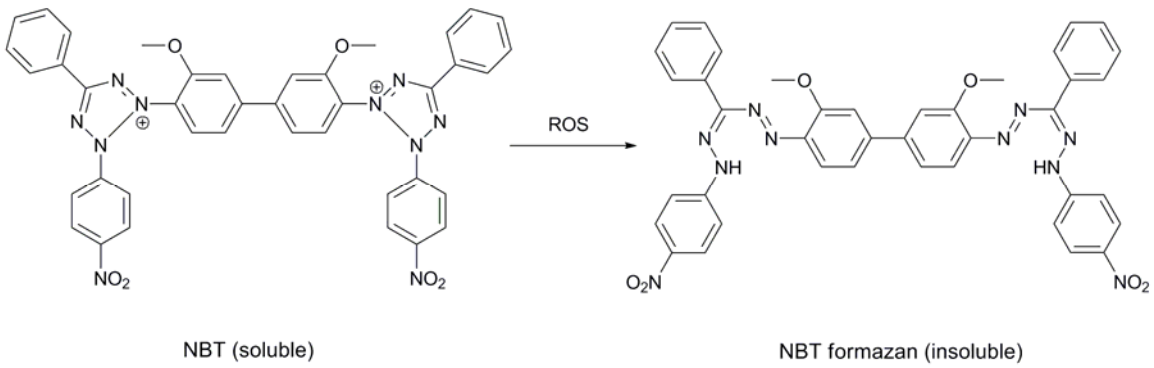

Figure 5.8: *NBT oxidation to insoluble NBT formazan*

Nine day-old seedlings of tobacco were exposed to a 200μM NBT solution for 10 minutes, washed to remove excess dye, and scored by bright field microscopy. Deposits accumulated along the vascular tissue of the root and at the tips of both the root and elongating root hairs, known sites of ROS production and NBT deposition [58]. Six hour pre-treatments in 30 or 50 μM DMBQ showed no significant change in oxidant accumulation in either the vascular tissue or the root hairs. However, the root tips of DMBQ treated seedlings accumulated significantly more stain than controls, suggesting a substantial increase in oxidant production at the site of the root meristematic tissues (Figure 5.9).

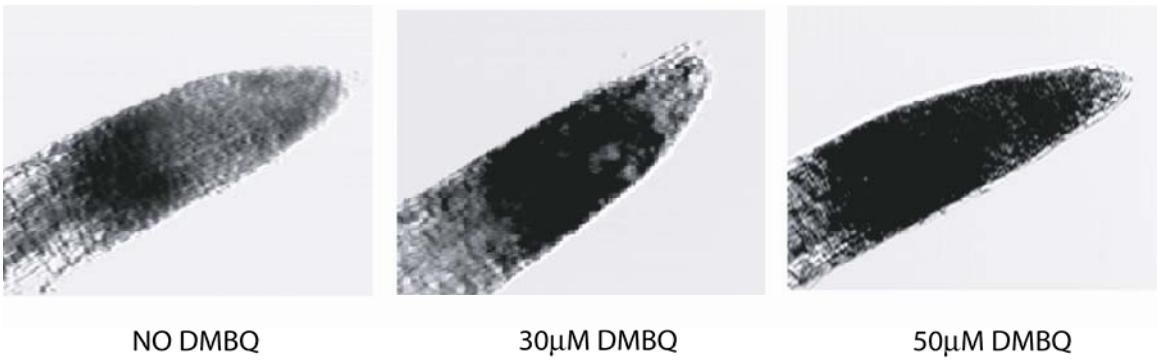

Figure 5.9: *NBT staining of tobacco seedlings*

9 day-old tobacco seedlings are transferred into 6 well plates (15 seedlings/well) and 5 ml of the indicated concentration of DMBQ for 6 hours. Seedlings are then incubated in 200 μM NBT for 10 minutes, rinsed to remove unreacted NBT, and scored.

To confirm NBT deposition was due to oxidant production, as well as to evaluate it within the context of ROS accumulation in Striga, tobacco seedlings were incubated in 50 μM DMBQ solutions along with 100 μM KI, a ROS scavenger or 10 μM DPI an NADPH oxidase (NOX) inhibitor prior to NBT staining (Chapter 2&3). As seen in Figure 5.10, both treatments reduced stain accumulation in the DMBQ induced tobacco seedlings. These treatments also reduced NBT accumulation in both the vascular tissue as well as elongating root hairs, sites at which a NOX is the known ROS source [56, 79]. These responses were consistent with those observed in Striga with the DCF fluorescence assays, supporting the use of either cytoplasmic (H_2DCFDA) or extracellular (NBT) probes for evaluating oxidant production in roots (Chapters 2&3). However, in sharp constrast to the response observed in Striga, oxidant production at the root tip was positively correlated with increasing DMBQ concentrations over the 6 hour incubation period (Figure 5.11A). At 50 μM DMBQ, NBT stain accumulation reached maximal

levels after 4 hours (Figure 5.11B) and this elevation appears to be sustained as longer exposure times, up to 24 hours, showed comparable staining.

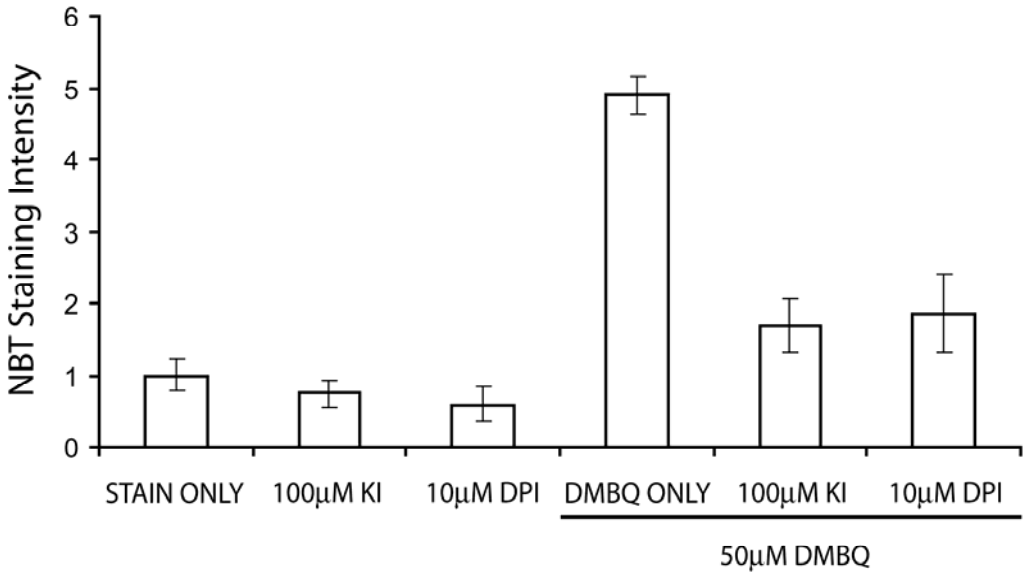

Figure 5.10: *NBT accumulation and ROS.*

Nine day-old tobacco seedlings are transferred to 6 well plates and incubated with or without 50 µM DMBQ and either 100 µM KI or 10 µM DPI for 6 hours. Samples are stained with 200 µM NBT for 10 minutes, scored, and results reported as the average of 15 seedlings +/- standard deviation as error.

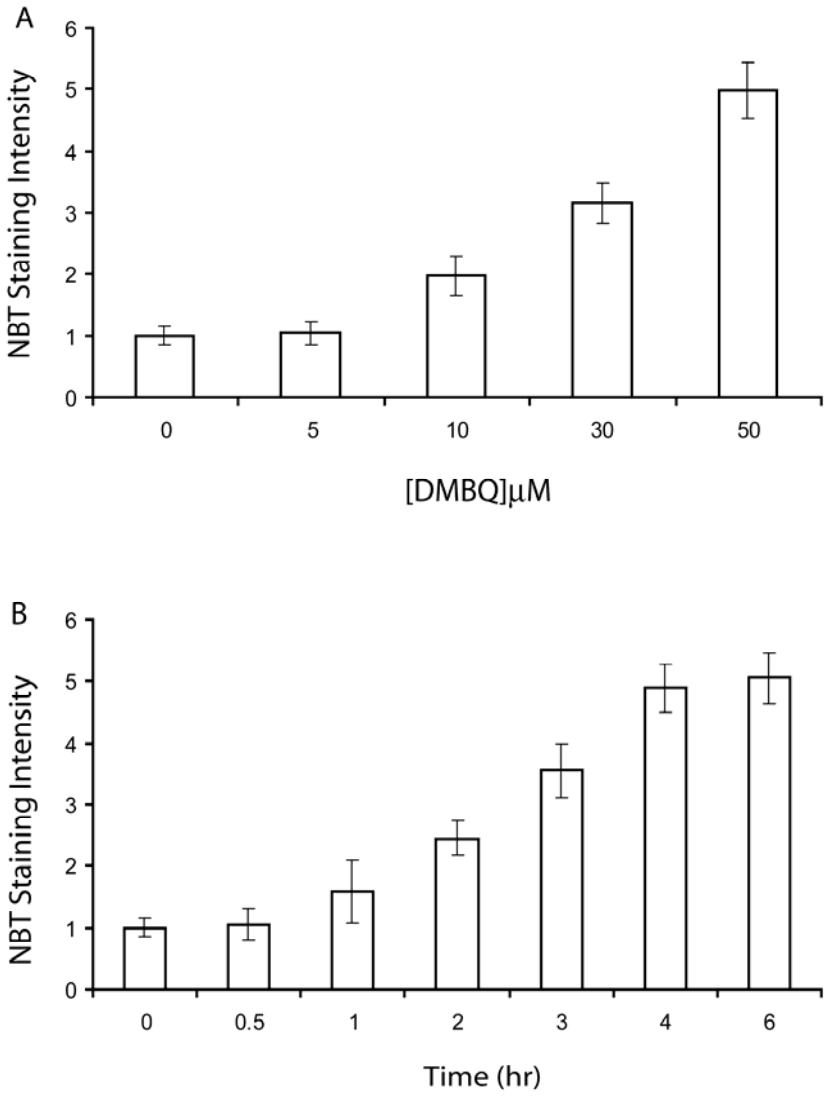

Figure 5.11: *Response to DMBQ is time and concentration dependent.*

Nine day-old tobacco seedlings grown on solid media were stained with 200 µM NBT for 10 minutes and scored for deposition. (A) Tobacco seedlings exposed to the indicated concentration of DMBQ for 6 hours. (B) Seedlings incubated in 50µM DMBQ for the indicated time period. Results expressed as ratio of stain accumulation in treated seedlings versus untreated seedlings. Staining results are the average of 15 seedlings with error expressed as +/- standard deviation.

5.2.7 H_2O_2 effects on root development

The results are consistent with an increase in oxidant production reducing root elongation and inhibiting root hair initiation and development. However, as seen in Figure 5.12, increasing concentrations of H_2O_2 stimulated root hair initiation in tobacco but had little effect on either root hair length or root elongation (Figure 5.12). Concentrations above 1mM H_2O_2 proved toxic to the growing seedlings and were excluded from these assays. Based on these studies a simple increase in oxidant production is insufficient to explain the growth and development effects on roots seen in response to quinone exposure.

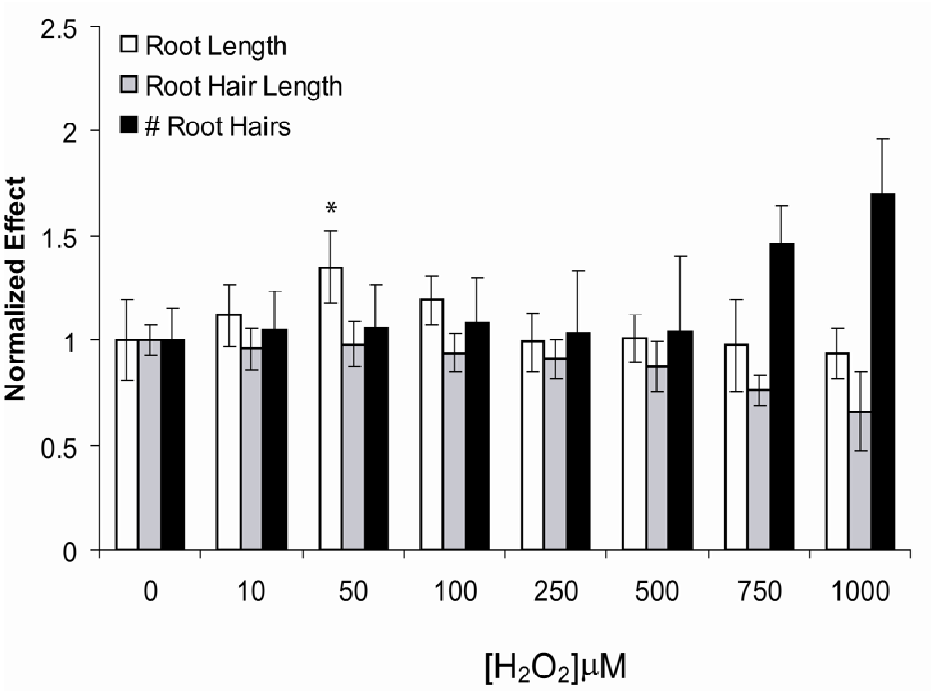

Figure 5.12: *Effects of H_2O_2 on tobacco root development*

Tobacco seeds are germinated on plates of the indicated concentrations of H_2O_2 and scored for root development after 9 days. Results are average of 15 seedlings +/- standard deviation as error. *= Statistically different by Student's t-test at 99% confidence.

5.2.8 Ca^{2+} regulation of oxidant production in plant roots

Having established the conservation of oxidant regulation in response to DMBQ additional studies using physiological markers identified in the preceding chapters were initiated. The down regulation of ROS accumulation in Striga is dependent on the increase of cytoplasmic calcium (Chapter 4). Similarly, a 1hr pre-treatment with 20 μM of the Ca^{2+} channel inhibitor $LaCl_3$ or chelation of extracellular calcium with 100 μM EGTA inhibited the increase in ROS in response to DMBQ (Figure 5.13). Disruption of Ca^{2+} gradients across the cell membrane by 30 μM treatments with the calcium ionophore ionomycin similarly prevented accumulation of NBT stain (Figure 5.13). These findings are consistent with an increase in $[Ca^{2+}]_{cyt}$ in response to DMBQ.

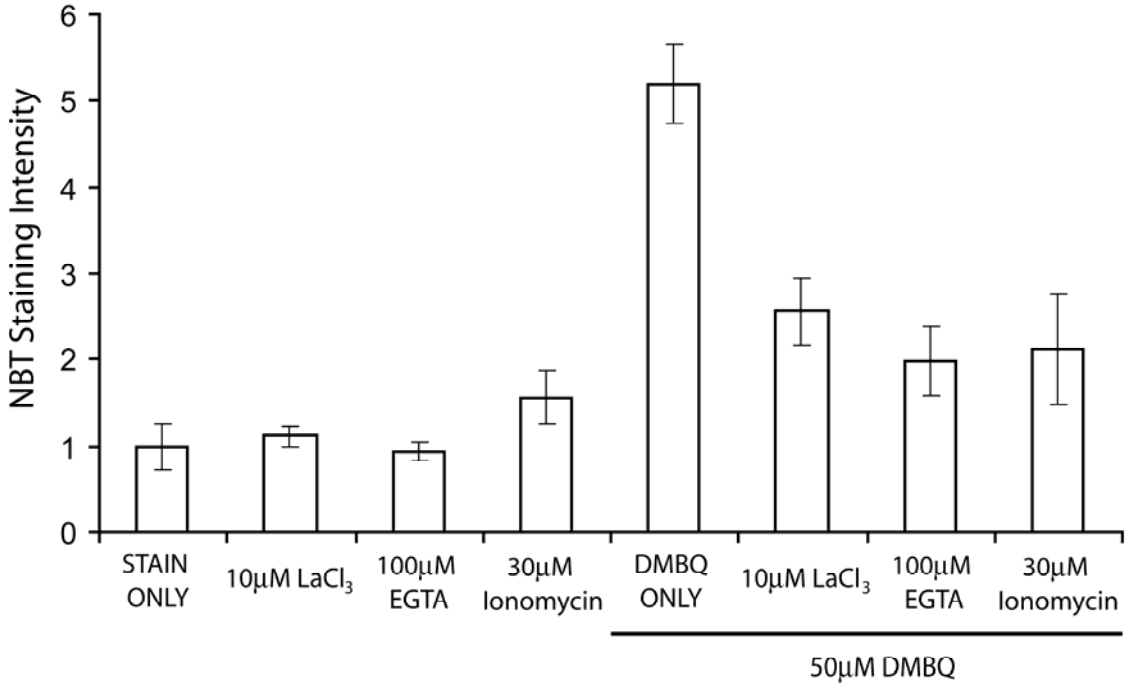

Figure 5.13: *Effects of Ca^{2+} regulators on oxidant accumulation in tobacco roots*

Nine day-old tobacco seedlings grown on solid media are transferred to wells with the indicated concentration of $LaCl_3$, EGTA, or ionomycin. After 1 hour, half the sample is exposed to 50 µM DMBQ for 6 hours. Both fractions are then incubated in 200 µM NBT and evaluated for stain deposition. Results are an average of 15 seedlings with error expressed as +/- one standard deviation.

5.2.9 Calcium imaging in response to DMBQ

The dynamic calcium flux in response to DMBQ exposure was imaged in the parasite via the fluorescent probe Fluo-4 AM and the same technique was exploited for visualizing activity in tobacco roots. Seedlings of tobacco pre-loaded with Fluo-4 AM exhibited a similar increase in fluorescence throughout the root after a 30 minute exposure to 50 μM DMBQ (Figure 5.14). Pre-treatment with either 20 μM $LaCl_3$ or 100 μM EGTA limited fluorescence accumulation in response to DMBQ, consistent with an increase in $[Ca^{2+}]_{cyt}$ from extracellular sources as a result of quinone exposure. Similar fluorescence increases were observed with methoxybenzoquinone and *t*-butyl benzoquinone, confirming this response was not specific to DMBQ.

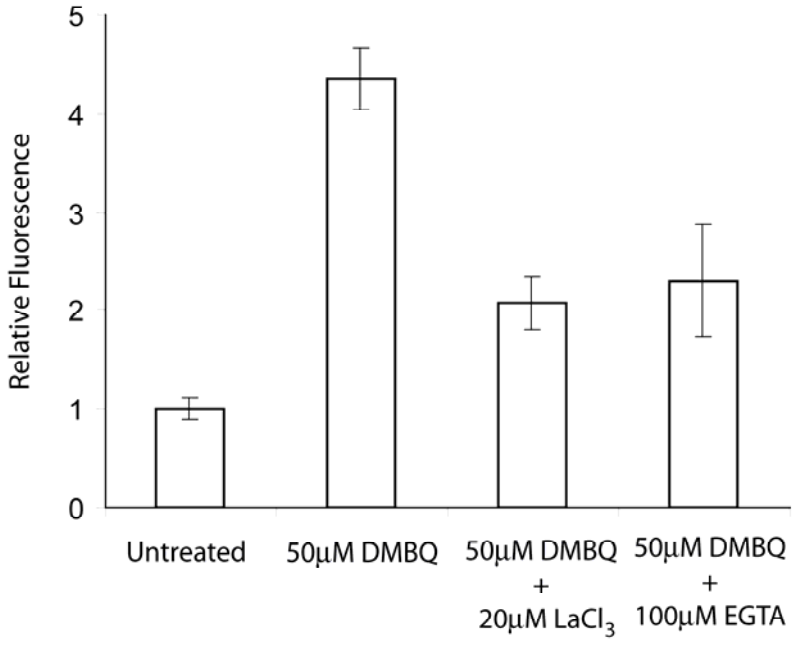

Figure 5.14: *Fluo4 fluorescence of tobacco seedlings.*

Nine day-old seedlings of tobacco grown on solid media plates are transferred to wells and loaded with 50 µM Fluo-4 AM for 30 minutes, washed to remove excess probe, and imaged. DMBQ is added directly to samples and fluorescence scored after 30 minutes. $LaCl_3$ and EGTA are added at the same time as Fluo-4 AM. (A) Untreated. (B) 50 µM DMBQ. (C) 20 µM $LaCl_3$ + 50 µM DMBQ. (D) 100 µM EGTA + 50 µM DMBQ.

5.2.10 Inhibiting plant root development

Previously, CPBQ has been employed as an inhibitor of haustorium development, Ca^{2+} flux, and ROS regulation [35, 150] (Chapter 4). Activation of this inhibitor is dependent on its reduction to the semiquinone allowing CPBQ to also serve as a viable reporter for a conservation of the mechanism of quinone perception (Figure 5.15) [151]. While tobacco roots grown on increasing concentrations of CPBQ alone showed some reduction in root development, co-incubation with DMBQ ameliorated the effects of the latter in co-incubation assays (Figure 5.16A). 50 μM CPBQ exposures also ameliorated growth effects of 50 μM benzoquinone or *t*-butyl benzoquinone. That such co-incubations do not produce cumulative inhibitory effects further argues against the quinone effect merely arising as a result of toxicity.

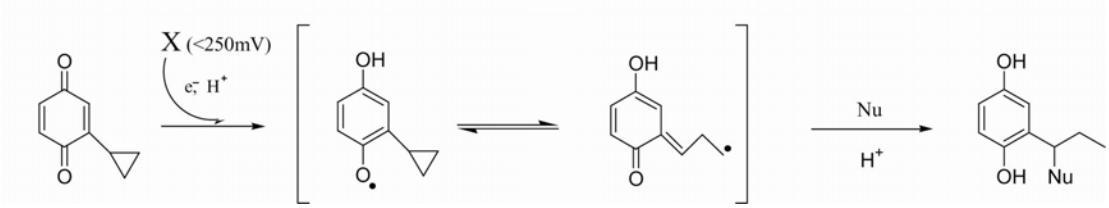

Figure 5.15: *Proposed mechanism for CPBQ activation and inhibition*

One-electron reduction of CPBQ to the semiquinone results in radical driven ring open of the cyclopropyl creating a site for both Michael addition and radical binding to the enzyme.

To determine if the CPBQ repression of DMBQ effects extended to oxidant production at the root tip, seedlings were pre-treated with CPBQ for 1 hour followed by the addition of 50 μM DMBQ for 2 hours. Like its effect on root growth, CPBQ induced a slight increase in oxidant production, observed by NBT staining, but limited oxidant accumulation in response to DMBQ exposure (Figure 5.16B). Similar experiments with 50 μM CPBQ and 50 μM methoxybenzoquinone or *t*-butyl benzoquinone had similar results with CPBQ limiting ROS accumulation at the root tip. In conjunction with its effects on root development these studies support the conservation of a reduction event in the perception of the quinones.

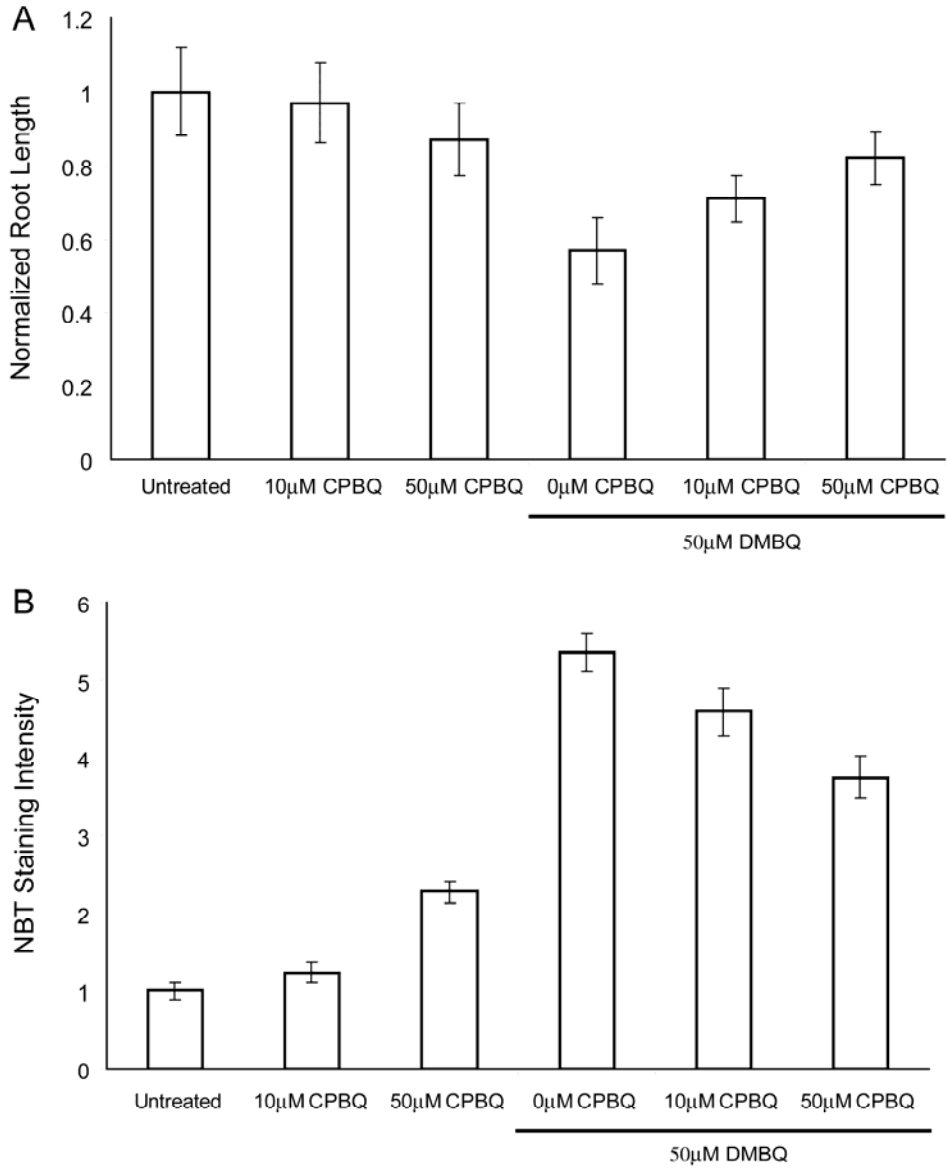

Figure 5.16: *CPBQ Effects on root growth and ROS accumulation*

(A) Tobacco seeds are germinated and grown for 9 days on the indicated concentration of DMBQ and/or CPBQ then scored for root length. (B) Nine day-old tobacco seedlings are transferred to a 6 well plate and co-incubated with the indicated concentrations of CPBQ and DMBQ. After 6 hours the seeds are stained for ROS production with NBT. Results expressed as the average of 15 seedlings +/- one standard deviation.

5.3 Discussion

5.3.1 Effects of haustorial inducing quinones on plants

The evidence accumulated throughout the previous chapters, along with prior studies, suggests both semagenesis and xenognosis likely evolved out of conserved processes in non-parasites. Using the model and tools developed in the preceding chapters in conjunction with new assays, the response of the haustorial inducing quinones on the non-parasites *Nicotiana tabaccum* and *Araibdopsis thaliana* were evaluated. These studies successfully identified several convergent responses between parasites and non-parasites as well as several, potentially critical, points of divergence.

In all plants tested, both parasitic and non-parasitic, perception of the xenognostic quinones reduced root elongation. Similarly, all plants showed a similar reduction in elongation in response to the monolignols, the phenolic precursors of the xenognostic quinones, supporting the hypothesis that the oxidation of these compounds is not a parasite specific process. Unfortunately, evaluating the model for phenol oxidation (semagenesis) in non-parasites is complicated by the importance of ROS in root development precluding the ROS scavenging experiments which identified semagenesis in Striga. As a result a shared mechanism of inhibition between these compounds cannot be excluded. In addition, roots of both Striga and Tobacco responded to the presence of the quinones by increasing cytoplasmic calcium from extracellular stores. Finally and potentially most importantly, is the apparent conservation of CPBQ as an inhibitor of these quinones, supporting a common reduction event in quinone perception in plant roots.

Conversely, oxidant production at the root tip appears to be differentially regulated as quinone perception appears to have opposite effects in parasites and non-parasites. Similarly, quinone exposures which induce swelling and hair formation in parasites reduced both root hair growth and elongation among non-parasites. Furthermore, the steric constraints which restrict the haustorial inducing activity of quinones do not appear to be conserved in the non-parasites. Attempts to expand these studies to evaluate the redox window which defines haustorial induction was complicated by quinone degradation as well as alternative allelopathic mechanisms. However, the conservation of the upper limits of this window are supported by the apparent activity of CPBQ.

In addition, while both Tobacco and Striga roots showed an increase in $[Ca^{2+}]_{cyt}$ in response to quinone exposure, this increase appears restricted to the root tip in the latter. Such specific localization in the parasite is particularly interesting given these tissues distal of the root meristem, do not initiate polar growth (i.e. root hair formation). The apparent absence of a quinone response in tissues that are not producing ROS may prevent haustorium development at points along the parasitic root at distances precluding successful host attachment.

5.3.2 Differential effects in response to xenognosin exposure

While the effects of these quinones on ROS production at the root tip are opposite in parasites and non-parasites, it is noteworthy that oxidant production throughout the remainder of the root appears unaffected. Given the role of quinones as electron carriers in biological systems the activity of these compounds may well be coupled to redox events which are differentially regulated in these distinct cell types. Indeed cell proliferation, at the root tip, and hair growth display variable sensitivities to redox active compounds such as ascorbic acid [152]. Alternatively, increased cytoplasmic calcium in the absence of the quinone increases oxidant production in Striga, and such Ca^{2+}-sensitive NADPH oxidases may be localized in greater numbers at the root tip.

5.3.3 Ca^{2+} as an inhibitor of growth

While an influx of cytoplasmic calcium can explain the observed increase in oxidant production at the root tip, is Ca^{2+} potentially involved in the overall reduction of root growth and development? The polar (directional) growth in root hairs is driven by a calcium and ROS gradient which forms at the site of extension. The general increase in cytoplasmic calcium throughout the prospective hair cell likely disrupts this gradient limiting both elongation and initiation of the hair (Figure 5.17). Indeed, this is the mechanism by which the fungal alkaloid hypaphorine inhibits hair growth [153]. Elevations in cytoplasmic calcium have also been associated with the inhibition of root elongation although a mechanism for this is less clear [154].

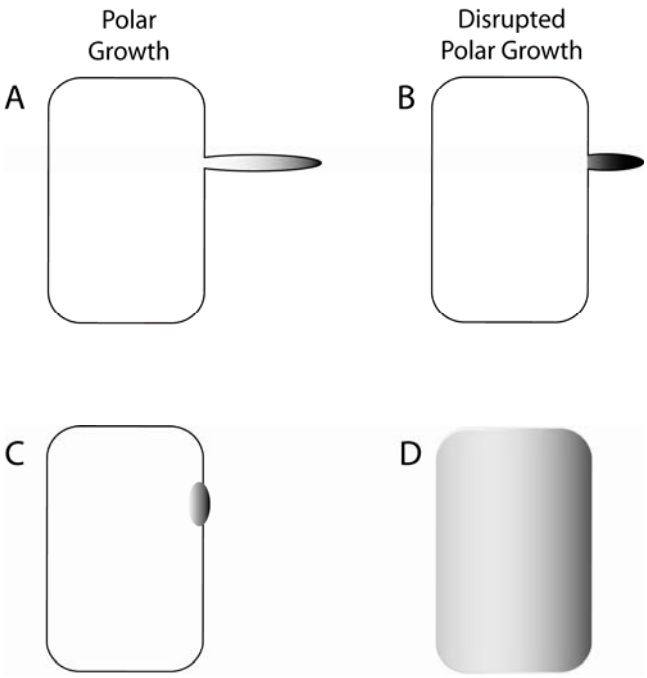

Figure 5.17: *Disrupting polar growth by Ca^{2+} influx*

(A) Root hair elongation follows the calcium gradient, shown from white (low) to black (high). (B) Disruption of this calcium gradient halts root hair growth. (C) A site of elevated cytoplasmic calcium initiates hair formation. (D) Disruption of this gradient also prevents hair initiation.

5.3.4 From Xenognosis to Allelopathy to the Oxidative Burst

The results clearly support a conserved mechanism between both parasites and non-parasites for at least the perception, if not the generation of benzoquinones. The fact that quinone effects are observed in both monocots and dicots suggests this may be an early, evolutionarily speaking, regulatory mechanism. Moreover, the inhibitory effects of these quinones on root growth and development appears to arise from changes in cytoplasmic calcium, much like hypaphorine. While consistent with the evolution of xenognosis out of a process associated with allelopathy, the potential association with the oxidative burst response cannot be excluded. However, regardless of its evolutionary origins these results clearly confirm that the products of semagenesis, i.e. the haustorial inducing xenognostic quinones, are detectable by the host surfaces at which they are generated. Such findings not only underscore the aforementioned importance of the tight regulation of oxidant production in the process of semagenesis (Chapter 2) it potentially adds an additional level of complexity to the host-parasite interface. In the conclusion, these results will be coupled to those of the preceding chapters to refine the model of semagenesis and further explore the rules which define oxidant production in signaling and development among eukaryotes.

CHAPTER 6 – Conclusion

"When I am working on a problem I never think about beauty. I only think about how to solve the problem. But when I have finished, if the solution is not beautiful, I know it is wrong." – Buckminster Fuller

The elucidation of a role for ROS in the interorganismal signaling processes which define successful host attachment in parasitic plants is in sharp contrast to the more traditional role for these powerful oxidants in defense. This contradiction was further complicated by the ever expanding roles for ROS in eukaryotic development. In this context, the obvious question which emerged was how does a parasite employ ROS for host detection, while avoiding the alternate roles for such oxidants? In evaluating this process, I have confirmed that as in defense and development, semagenic ROS production is tightly regulated at both the biochemical and genetic level. These results now permit semagenic oxidant production to be evaluated within the larger context of ROS in eukaryotic biology.

The first and most readily observable similarity in these processes is the localization of ROS production to the site of activity. Such oxidant localization defines polar growth in development, limits defense responses to the site of insult, and ensures the oxidation of host monolignols occurs proximal to the tip of the parasite where the products are exploited to induce haustorium development. The physical separation of distinct ROS driven processes, coupled to their short life time and endogenous oxidant scavengers, limits potential overlap between these events.

In addition to spatial localization, such oxidant dependant processes employ a common enzymatic source, the NADPH or respiratory burst oxidases (NOX or Rboh). In plant NOX, as well as members of the NOX5 protein family in animals, Ca^{2+} binding EF-hand domains couple enzymatic activity to cytoplasmic concentrations of the divalent cation. Given the importance of calcium dynamics in regulating growth, defense, and now semagenesis/xenognosis, the unusual truncations of these regulatory domains as well as the first transmembrane helix in SaNOX2 and SaNOX3 are intriguing and worthy of further study. In both defense and development, oxidant production is under regulation of additional components such as kinases, a fact which may be exploited in the future for further defining semagenesis. Alternatively, the studies herein suggest this robust and now well-defined process of semagenesis can be exploited for the identification of additional regulatory components at work in other ROS-dependent processes. Moreover these studies have provided the foundation for evaluating both the evolutionary origins as well as generality of semagenesis.

Given its similarities to the oxidative burst response, the origins of semagenesis may well lie in the defense response of eukaryotes. This is further supported by the observation that the oxidative cross-linking of monolignols, i.e. lignification, can yield the haustorial inducing quinones as side products. The absence of these precursors in Striga ensures semagenesis is limited to the detection of proximal roots. While preventing self-parasitism, i.e. attachment to other Striga seedlings, such a scheme for host detection eliminates host specificity, given the prevalence of monolignols in the roots of terrestrial plants. However, the benefit of coupling host detection to such a critical component of

plant architecture almost certainly restricts the options available to host plants for the evolution of new strategies for avoiding potential parasites. Moreover, by coupling germination to xenognosins, the obligate parasites like Striga, overcome this limitation as any roots encountered by the growing parasite are likely to be from a viable host.

In addition to its molecular origins, the studies herein suggest the chemistry which defines semagenesis, i.e. the oxidation of monolignols to quinones, as well as the mechanisms for their perception are generally conserved in plants. These initial studies confirm such quinones regulate oxidant production at the root tip, as well as calcium dynamics, and appear dependent on a similar reduction mechanism for activity. Moreover, the upper limits for quinone perception defined in Chapter 2 (50μM) appear conserved although the lower limits in Striga (0.1μM) are 100 fold less than that reported here for tobacco (10μM). While larger sample sizes and additional studies may yet establish activity in tobacco at the lower limits observed in Striga, such sensitivity may simply be due to the absolute dependence of the parasite on successful host detection and subsequent haustorial development. Interestingly, these studies establish that host plants like sorghum and corn, i.e. monocots, are far less sensitive to the products of semagenesis suggesting the parasite can probe their surfaces without triggering the developmental effects observed in dicots. In addition to suggesting a fundamental divergence between monocots and dicots with regards to the regulation of root growth and development, the reduced sensitivity in host plants may have been a critical factor in the evolution of host selection.

In considering a more general role for these compounds in root growth and development it is important to note that the effected sites, i.e. growing root tips and root hairs, are young tissues with little monolignol content in which ROS accumulate. Therefore, like the root tip of Striga these tissues are capable of using ROS as a probe for adjacent tissues with higher monolignol content such as the roots of an adjacent plant. Indeed, the process exploited by Striga for xenognosis may simply be a broader process by which growing roots explore their environment and avoid potential competitors. This model, shown in Figure 6.1, is identical to the model proposed for semagenesis. In this model the reduction, or halt in root elongation, is common to all plants and this response has simply been further extended in parasites to regulate haustorium development. In non-parasites this reduction in root development could lead to a shift in directional growth away from a potential competitor and/or stimulate lateral root growth to further compensate. Root hair growth could be similarly reduced proximal to adjacent roots.

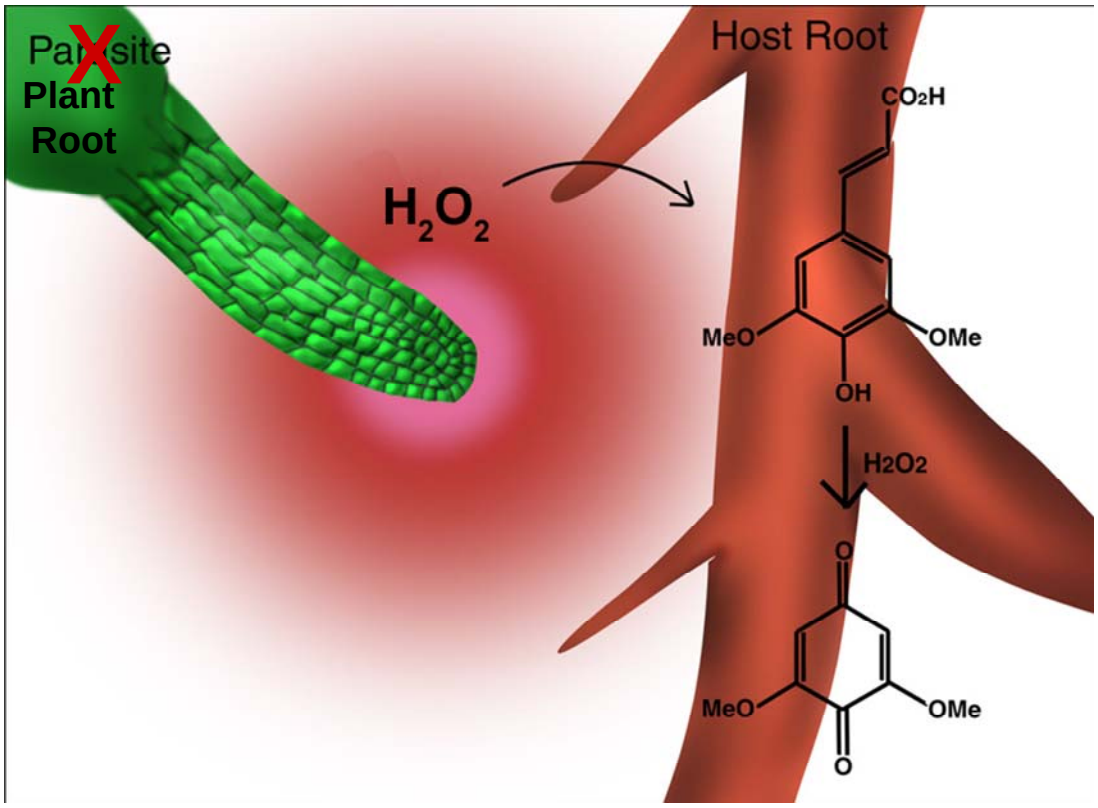

Figure 6.1: *A common model for semagenesis in all plants*

The growing root tip (or root hair tip) of a terrestrial plant generates H_2O_2 establishing a gradient of ROS (red). As this ROS comes in contact with the roots of another plant it, along with root bound peroxidases, catalyzes the oxidation of monolignols to quinones which are then released into the rhizosphere. These quinones serve as allelopathic signals alerting the growing tip of the plant to a potential competitor.

In conclusion, it would appear that in defining semagenesis a more general mechanism by which roots can explore their surroundings has been discovered. By refining the dialogue between host and parasite a chemical Rosetta Stone has been developed, permitting a potentially older and far more broadly employed plant-plant interaction to be translated (identified). With regards to parasitic evolution, this conservation suggests this transition may be even more facile than originally thought. Most importantly, the broader dialogue discovered here may prove critical in understanding the complex interactions between plant development and their interactions with their environment.

Materials & Methods

M.1 Reagents & Materials

All fluorescent probes were purchased from Molecular Probes (Carlsbad, CA). Murashgie and Skoog media (MS) and Gelrite was purchased from Caisson Labs (North Logan, UT). MnTBAP was purchased from A.G. Scientific (San Diego, CA). SMART™ RACE cDNA Amplification Kit was purchased from Clontech (Mountain View, CA). DNeasy Plant Mini Kit was purchased from Qaigen (Valencia, CA). All other chemicals were obtained from Sigma Aldrich (St. Louis, MO). Lab-Tek 8 Chamber Microscope slides were purchased from Fischer Scientific (Pittsburg, PA)

Striga asiatica seeds were obtained from Drs. R.E. Eplee and Rebecca Norris (U.S. Department of Agriculture, Witchweed Methods Development Laboratory; Oxford, NC) All Striga work was done under the auspices of the USDA quarantine licenses awarded to Emory University. Seeds of *Arabidopsis thaliana* and *Nicotiana tabaccum* were purchased from Lehle Seed (Round Rock, TX). *Zea mays* and *Sorghum bicolor* were purchased from Territorial Seed Company (Cottage Grove, OR). *Ocimum basilicum* (sweet basil) was purchased from Pike Nurseries (Atlanta, GA).

M.2 Germination, Plant Growth, and Plant Culture

M.2.1 Striga pre-treatment & germination

Striga seedlings are pre-treated by washing the seedlings in the following order: 3% chromic acid for 3 minutes, a solution of 1% Tween-20 and 7% bleach for 7 minutes, and finally 70% ethanol for 1 minute. The seeds are then rinsed and placed in ddH_2O for 10-14 days in capped Erlenmeyer flasks. Following incubation seeds were germinated by 24hr exposures to 10^{-9}M strigol in 0.1mM KCl [31].

M.2.2 Regenerating Striga from culture

Full grown parasites were regenerated by transferring germinated day-old sterile seedlings of *Striga asiatica* to Magenta boxes containing full strength MS medium and 2% agar supplemented with either: 1 mg/L 6-BA and 0.1mg/L IAA or 1mg/L 6-BA and 0.5mg/L IAA. Seedlings were grown at 23°C with a 16 hr photoperiod/day. Regenerated shoots were visible after one week, and the resulting Striga plants typically produced closed flowers within 4-6 weeks. Despite regular agitation of the magenta boxes the flowers remained sterile.

M.2.3 Germination and growth of non-parasites

Non-parasites were sterilized by a 5-7 minute wash in a 5% bleach solution followed by triplicate washings with an equal volume of ddH_2O. Seeds were then transferred to either petri dishes or Magenta boxes containing 50% MS media, 2% Gelrite, and the indicated concentration of quinone or H_2O_2. Magenta Boxes and petri dishes were placed on grow racks at 23°C with a 16hr photoperiod. After 9 days

seedlings were scored for effects on root elongation, hair length, and hair number under a microscope while cotyledon distance was measured with a ruler. Results were normalized to untreated samples set as 1. In replating experiments seedlings were transferred onto fresh plates of the indicated DMBQ concentrations at 3, 5, and 7 days after initial plating. Growth assays are reported as average of 15 seedlings with error as +/- standard deviation.

M.3 Haustorial induction and inhibition

Unless otherwise stated haustorial induction assays were performed on day-old seedlings of *Striga asiatica* in 0.1mM KCl and scored for development 24 hours after the start of the experiment. Unless otherwise stated, experiments are the average of three experiments +/- standard deviation.

M.3.1 Induction assays

Seedlings were placed in 6 well plates (30 seedlings/well) with 5ml of 0.1mM KCl. Putative haustorial inducers were evaluated by addition from master stocks (0.01M or 0.001M in DMSO) to produce the final concentration desired then scored after 24 hours. For timed exposure assays, the putative inducer was applied for the indicated time interval then removed from the well followed by triplicate washings with 1ml 0.1mM KCl. The seeds were then placed in 5ml of 0.1mM KCl and scored for haustorium development after 24 hours. All induction assays were performed in triplicate with error bars representing standard deviation. CPBQ inhibition of haustorial development was

evaluated by co-incubation of the indicated concentration with 10μM of the haustorial inducer.

M.3.2 Evaluating H_2O_2 effects on haustorial induction

Seedlings of *S. asiatica* are incubated in 10μM DMBQ and the indicated concentration of H_2O_2 then scored for haustorium development. ROS scavenging effects were evaluated by the addition of increasing concentrations of MnTBAP from a 0.01M aqueous stock then scored for haustorium development.

M.3.3 Ca^{2+} inhibition of haustorium formation

Germinated seedlings were co-incubated in a solution of 10μM DMBQ and the given concentration of Ca^{2+} channel inhibitors: $LaCl_3$, $GdCl_3$, $AlCl_3$, Verapamil, or Ruthenium Red from 0.01M aqueous stocks then evaluated for haustorium development. Reversibility of trivalent cation inhibition was accomplished by triplicate washings with 1mM $CaCl_2$ followed by returning seeds to the 0.1mM KCl buffer. Restoration of haustorial inducing activity was evaluated by the re-addition of the haustorial inducer followed by normal time exposure assays.

Calcium chelators (EGTA and BAPTA-AM) and ionomycin are added from 0.01M aqueous stocks to produce the indicated concentration and co-incubated with 10μM DMBQ. Reversibility of calcium chelation was evaluated by washing EGTA treated seedlings with 100mM $CaCl_2$ in triplicate then reincubating in 0.1mM KCl and

10μM DMBQ or 6-BA. All assays were performed in triplicate with error bars representing standard deviation.

M.3.4 CPBQ and nebularine inhibition of haustorium formation

Day-old seedlings of Striga are incubated with the indicated concentration of Nebularine or CPBQ, from 0.01M DMSO stocks, along with 10μM DMBQ or 6-BA.

M.4 Visualization, localization, and analysis of ROS production

CM-H_2DCFDA, H_2DCFDA and FDA were dissolved in dimethylsulfoxide (DMSO) and stored in 100μl 10mM aliquots at -20 °C. NBT was dissolved into phosphate buffer to produce a 200μM working solution [58]. Fluorescence data points are collected in triplicate with errors bars representing the standard deviation between the images. Images were processed using the IDL software package or Adobe Photoshop. Images were loaded and the average pixel intensity (PI) at the meristem was determined and corrected for any background fluorescence.

M.4.1 Laser scanning confocal microscopy

One day-old *S. asiatica* seedlings were incubated in a staining solution of either: 10μM H_2DCFDA or FDA from stock in 0.1 mM KCl solution for 3 minutes, washed twice with 0.1mM KCl, and then transferred to a custom-made depression cell or a Lab-Tek 8 well slide. The cell was then mounted on a Zeiss LSM 510 laser scanning confocal microscope. The 488nm line of the Ar laser was used for excitation and emission was

collected in the 500 to 550 nm window. In order to minimize photobleaching, excitation was limited to approximately 10 sec/sample.

M.4.2 Fluorescence microscopy

Fluorescence images were collected on a Leica fluorescence microscope with an Argon lamp. Excitation was with a blue light filter. Exposure was minimized to the time required for image acquisition to limit photobleaching (approx 10sec/sample). Striga seedlings of the indicated age are incubated in solutions of 10μM CM-H_2DCFDA, H_2DCFDA or FDA for 3 minutes then rinsed in triplicate with 0.1mM KCl. Seedlings were then transferred to 8 Chamber microscope slides in 250μl 0.1mM KCl (LabTek) then imaged for fluorescence. Effects of haustorial inducers, ROS scavengers, and calcium perturbation (ionophores, chealtors) on ROS production are evaluated by pre-incubation with indicated compound for the set exposure time then staining with H_2DCFDA (as above) to evaluate oxidant production. Similarly, potential ROS inhibitors are added for set exposure times at the given concentrations then evaluated for oxidant production. Images are collected at 5, 10, and 15 minutes after the sample is loaded onto the microscope.

M.4.3 Calculating Arbitrary Fluorescence

Arbitrary fluorescence is calculated by comparing fluorescence intensity at the seedling tip for untreated (dye only) seedlings and those treated with the indicated compound times 100 (AFU = Treated/Untreated X 100).

M.4.4 Calculating Relative Fluorescence

To avoid dye translocation, only the initial rate of DCF accumulation is measured (5-15 minutes). The relative rate of fluorescence accumulation was determined by calculating the ratio of the pixel intensities (RPI) of the entire meristem at 15 and 5 min (RPI=15min/5min). This method normalizes ROS production to each seedling and the size of each seedling. To determine the effects of each tested compound on DCF fluorescence, the ratio for treated and untreated seedlings were compared and expressed as percent of control as a relative fluorescence (RF) scale ($RPI_{untreated}/RPI_{treated}$)x100. Each experiment was performed five times, and the results expressed as the average ± SD.

M.4.5 Transmission electron microscopy experiments (TEM) to localize ROS

Cytochemical localization of hydrogen peroxide was carried out following a procedure based on the production of cerium perhydroxides [74]. *S. asiatica* seedlings 18hr post germination were incubated in freshly prepared 5mM $CeCl_3$ in 0.1mM KCl for 2hrs. The seedlings were then fixed in 1.25% (v/v) glutaraldehyde/1.25% (v/v) formaldehyde in 50 mM sodium cacodylate buffer at pH 7.2 (CAB) for 1 hr. After fixation, the seedlings were washed twice for 10 min in CAB buffer and postfixed or not, as desired, for 45min in 1% (v/v) osmium tetroxide in CAB, followed by two additional washes in CAB buffer (10 min each). The samples were then dehydrated in a graded ethanol series (30, 50, 70, 80, 90 % EtOH) with 10min steps, followed by 3 changes of 100% dry ethanol and 2 changes of propylene oxide (PPO) all for 10 minutes each. The seedlings were then progressively embedded in epoxy plastic (Embed 812; Microscopy

Sciences, Inc.), placed in labeled Beem™ capsules, topped off with epoxy plastic and polymerized at 60 °C for 48 to 72hrs. Selected blocks were then thin sectioned (70 to 90 nm) using a diamond knife, collected onto 200 mesh copper grids or onto Formvar™ covered single slot copper grids and post stained or not, as desired. The post stains used were 3% Uranyl Acetate and 2% Lead Citrate. The thin sections were observed with a JEOL JEM-1210 transmission electron microscope at 80 kV. The images were recorded using Kodak™ 4489 EM film.

M.4.6 Nitrobluetetrazolium (NBT) assays

9 day-old seedlings of Tobacco or Arabidopsis are incubated in a 200μM NBT solution for 10 minutes then washed in triplicate and evaluated for stain accumulation. Longer time points or higher concentrations resulted in over staining. Concentration effects of DMBQ were evaluated by pre-incubating seedlings of either plant in increasing concentrations of the quinone for 6 hours then washing and staining with NBT. Temporal resolution of the ROS change was evaluated by pre-treatment with 50μM DMBQ for increasing exposure times then washing and staining for NBT. Controls for NBT activity were evaluated with pre-treatments of 100μM KI or 10μM DPI for 6 hours, with or without 50μM DMBQ, followed by washing and staining with NBT.

M.5 Propidium iodide staining – toxicity assays

Propidium iodide (PI) was stored as 10mM stock solutions (deionized H_2O and 5% DMSO). One day-old seedlings of *Striga asiatica* and three day-old seedlings of *Arabidopsis thaliana* are placed in media containing 10μM PI and 0.1mM KCl for 15 minutes and transferred to depression slides for scoring using a blue light filter cube for excitation. Fluorescence intensities were collected and compared to seedlings previously treated with 10mM Al for 8 hours. 10mM Aluminum solutions were prepared by slow addition of $AlCl_3$ to H_2O at 4°C to control heat evolution and then allowed to warm to room temperature. Striga and Arabidopsis seedlings are incubated in 10mM $AlCl_3$ for 8 hours prior to imaging for toxicity.

M.6 Molecular Biology

M.6.1 Cloning the respiratory burst oxidases

Total RNA was extracted from germinated seedlings of *S. asiatica* with the RNeasy Plant Mini Kit (Qiagen). Integrity of the isolation was analyzed by electrophoresis in a 8% formaldehyde/ 1.5% agarose gel. cDNA was generated using Superscript ^{TM} III Transcriptase (Invitrogen) at 50 °C. Based on the conserved regions of the Respiratory burst oxidases from *Arabidopsis thaliana* (RbohA) and *Nicotiana tabacum (*NtRbohA), several degenerate primers were made, the best pair are: forward 5'-GGCAYCCITTYTCWATYACITC-3' and reverse: 5'-GGHGTIGCWCCDATICCNARWC-3'. The degenerate primers were used to clone genes with 1.5-day-old Striga seedling cDNA. PCR products were isolated and three distinct gene sequences (*SaNOX1*, *SaNOX2*, and *SaNOX3*) were cloned with the help of TOPO TA Cloning Kit (Invitrogen). Whole cDNA sequences of the three genes were obtained with the help of SMART™ RACE cDNA Amplification Kit (Clontech). Based on cDNA sequences, three genomic sequences were obtained from *S. asiatica* DNA, extracted using the DNeasy Plant Mini Kit (Qiagen).

M.6.2 Cloning the SaNOX promoters and Arabidopsis transformation

A region approximately 1-1.5Kb upstream of the start codon for each *SaNOX* gene was cloned using tail PCR method. The promoter fragments were cut by SalI and XbaI, ligated with *PBI101* vector to get the promoter-directed β-glucuronidase (GUS) constructs. These constructs were introduced via vacuum transformation in Agrobacterium GV3101 and selected on MS plates with Kanamycin (50ug/ml).

M.7 Bioinformatic Analysis of SaNOX1, SaNOX2, and SaNOX3

BLAST analysis, CLUSTALW alignments, and Kyte-Doolittle hydropathy plots were performed using software available at the SDSC Workbench website (http://workbench.sdsc.edu/). SaNOX1, SaNOX2, and SaNOX3 were aligned with AtRbohA as well as the NOX5 and $gp91^{phox}$ sequences from *Homo sapiens* to assign the location of specific structural components. Kyte-Doolittle hydropathy plots for SaNOX1, SaNOX2, and SaNOX3 were compared to those for $gp91^{phox}$ and RbohA to predict the number of transmembrane helices. Intron-exon analysis was performed using the SPIDEY software package (http://www.ncbi.nlm.nih.gov/IEB/Research/Ostell/Spidey/) comparing the cDNA sequences for SaNOX1, 2, or 3 to its respective genomic DNA sequences. Exon and intron positions for each sequence were compared to that for RbohA by the CLUSTALW alignment.

M.8 Tissue Localization and Regulation of SaNOX expression

M.8.1 Tissue specific RT-PCR

To analyze the expression pattern of these genes, RT-PCR was performed on different tissues (root, shoot, leaf + flowers). RNA and cDNA were obtained as described above. In order to exclude genomic DNA contamination, RNA was pretreatment with DNase. In addition, after the cDNA syntheses, we check the contamination again with several genes' primers spanning the sides of an intron. This method was able to detect the genomic contamination easily according to the size of PCR products. The RT-PCR employed two primers for each gene (*SaNOX1, 2, and 3*) and two primers for internal control (Striga actin gene) 28, 30, and 30 cycles respectively with an annealing temperature of 58°C. PCR products were analyzed in a 2% agarose gel. The RT-PCR experiments for each gene were repeated in triplicate with different cDNA samples. Gene specific primers used in RT-PCR were: SaNOX1 reverse: 5'-ctgcaccggacgatgactatcttagc-3'; forward: 5'-ctgctatatcatccataacgcctttg-3' or reverse: 5'-cagatcttccgagggacgaatccgtaaaat-3'; forward: 5'- gccatgttgaatttgacggtctcggcag-3'. SaNOX2 reverse: 5'-ttgcctaagccatttgaccgcctca-3'; forward: 5'-cctaactgccttatgtgaatgctgagg-3'. SaNOX3 reverse: 5'- cgagctattggcatttcgtgttgagc-3'; forward: 5'- ccttgtggctttgacatgtgcagagcc-3'. Actin reverse: 5'-caggctgttctctccctttat-3'; forward: 5'tccgatccagacactgtactt-3'. Changes in the expression of *SaNOX1, 2, or 3* in response to quinone treatments was evaluated in a similar manner.

M.8.2 Northern analyses

Total RNA from the specific Striga tissue was extracted as above. Approximately, 10μg of each RNA sample was transferred to a nylon membrane, and probed with the P^{32} labeled three genes' whole cDNA sequence. Samples are washed 3 times and exposed to X-ray film (Kodak).

M.8.3 GUS assay

Arabidopsis transformants are vacuum infiltrated for 5 minutes in the staining solution (50mM sodium phosphate buffer PH 7.0, 0.2% triton-X-100, 1mM X-Gluc), incubated at 37°C, and fixed in 75% ethyl alcohol. Pictures were taken with a Canon digital camera.

M.9 Peptide synthesis and Calcium binding

3 peptide sequences were synthesized by standard Fmoc sold-phase synthesis method on a Rainin Symphony QUARTET multiplex solid-phase peptide synthesizer. The peptides synthesized were: IFFDMCDKNGDGKLSEDEVKEVLVMS **(**EF-I), LIMEELDPDHQGYIEMWQLEALLRGM (EF-II), and YEVHHQKLVFFAEDVGSNKGAIIGLM (control). Peptides were cleaved from Rink amide resin (Novabiochem) with 90% TFA, simultaneously de-protecting the side chains. The resulting C-terminal amidated peptides were extracted with cold ether and purified by reverse-phase HPLC on an Atlantis preparative C18 column (with the gradient ramped from 20% acetonitrile/0.1% TFA to 50% acetonitrile/0.1% TFA over 30 min). The final pure products were confirmed with MALDI-TOF on a Voyager-DE^{TM} STR Biosepctrometry Workstation. Peptides were immobilized onto nitrocellulose membrane and incubated with $^{45}CaCl_2$ as described previously [105].

M.10 Arabidopsis and Yeast transformants of SaNOX1

The entire cDNA sequence of *SaNOX1* was inserted into the *PBI1.4* plasmid under the 35S promoter or its wild type promoter. These constructs were transformed into the Columbia ecotype (Col-0) via *Agrobacterium tumefaciens* (See Above). For Yeast transformants, the whole cDNA sequence of *SaNOX1* was spliced into the *pCUY 315* plasmid behind the ADH1 promoter then transformed using the S.c. EasyComp™ Transformation Kit (Invitrogen). ROS production in Yeast and Arabidopsis transformants was evaluated with the CM-H_2DCFDA assay. To confirm expression, RNA from different tissue was extracted from Arabidopsis or Yeast transformants. cDNA were obtained via Superscript ^{TM} III Transcriptase (Invitrogen). RT-PCR results with gene specific primers were confirmed by sequencing. All experiments with *SaNOX1* tranformants use non-transformed Yeast and Arabidopsis as negative controls.

M.11 Ca^{2+} imaging

Day-old seedlings of *Striga asiatica* are loaded with 50μM Fluo-4 AM for 20 minutes at 4°C then returned to room temperature for 10 minutes. Seeds are then washed in triplicate with ddH_2O, transferred to a well of an 8 well microscope slide and resuspended in 250μl of phosphate buffer (pH: 6.1) and imaged for basal Ca^{2+} on a fluorescence microscope at set time points (Ex: 488/Em: 535nm). Effects of haustorial inducers were evaluated by the addition of sufficient compound from stock to produce a 10μM solution. Images are collected at 5 minute intervals to evaluate changes in fluorescence. The effects of Ca^{2+} chelation, Ca^{2+} channel inhibition, or CPBQ treatments on Fluo-4 fluorescence was evaluated by pre-incubating 10μM DMBQ and the indicated concentration of $LaCl_3$, EGTA, or CPBQ for 30 minutes. After 30 minutes Fluo-4 AM was added and incubation of dye continued as above. After an additional 30 minutes seedlings are washed and imaged for calcium fluorescence.

M.12 Scanning Electron Microscopy of tobacco roots

Tobacco roots were grown on untreated, 10μM DMBQ, or 50μM DMBQ plates for 9 days then transferred to a 0.1 M cacodylate buffer, pH 7.4, for 2 to 5 minutes at room temperature (RT). Roots were excised and placed in separate buffer filled vials. Buffer in root vials was exchanged for fixative and incubated overnight at 4°C (2.5% TEM grade glutaraldehyde in 0.1 M cacodylate buffer, pH 7.4). This is followed by two 5 minute washes in buffer followed by two 5 minute washes in distilled water. Samples were post-fixed for one hour in 1% Osmium Tetroxide (aqueous) at 23°C followed by two 5 minute washes in distilled water. Next was dehydration through steps of an ethanol series (10min each); 30%, 50%, 70%, 80%, 90%, and three steps of 100% dry ethanol. The samples were then placed into labeled Microporous Specimen Capsules (Ted Pella, Inc., Redding, California) filled with 100% ethanol, and then placed into the sample boat/holder, also filled with 100% ethanol. The samples in the holder were then sealed in the critical point drying (CPD) unit (E3100 by Polaron, sold by Energy Beam Sciences, Agawam, Massachusetts). The ethanol was then exchanged for liquid CO_2, under pressure, by allowing the liquid CO_2 to gently and continuously wash through the CPD chamber until the exchange was complete. The contents of the CPD unit were then brought to and through the critical point for CO_2 (31.5°C and 1073 psi) and then allowed to vent until the samples were completely dry. Dried samples were secured to labeled aluminum SEM stubs and sputter coated with 12 to 15 nm gold using an EMscope SC500 sputter coater (EMSCOPE Labs, Ltd., Kent, England, UK). The samples were imaged using a TOPCON DS130 field emission scanning electron microscope (FE-SEM) at 10kV.

M.13 Methoxybenzoquinone Synthesis

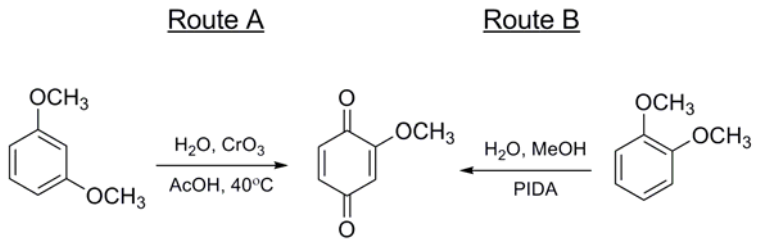

Figure M.1: *2 synthetic routes to methoxybenzoquinone*

M.13.1 CrO_3 synthesis of methoxybenzoquinone (Route A)

To a round bottom flask containing 30ml of acetic acid on ice being stirred, 3g CrO_3 (30mmol) is added. ddH_2O was added dropwise until CrO_3 was completely dissolved, typically 5ml. Reaction was stirred for 15 minutes then 1ml (7.6mmol) of 1,3-dimethoxybenzene was added. Mixture was allowed to come to room temperature then heated to 40°C for 3 days. Reaction was quenched with additional ddH_2O and extracted with CH_2Cl_2 (5x). The combined organic layers were rinsed with saturated $NaHCO_3$ and brine successively then dried over anhydrous $MgSO_4$. Removal of solvent under vacuum yields a dark yellow oil. 400mg (38%),of the rust colored product, was obtained by flash chromatography on silica (5:1 Hexane:EtOAc). ^{1}H and ^{13}C NMR spectra were collected on a Varian 400MHz. ^{1}H NMR ($CDCl_3$) δ 6.69 (s, 1H), 6.59 (s, 1H), 5.926 (s, 1H), 3.809 (s, 3H). ^{13}C NMR ($CDCl_3$) δ 188, 182, 158, 137, 135, 108, 57 ppm .

Haustorial inducing activity was confirmed by incubating day-old Striga seedlings in 10μM of the product then scoring for haustorium development (85% +/-9).

M.13.2 PIDA synthesis of methoxybenzoquinone (Route B)

To a three neck flask containing a solution of 25ml ddH_2O with 2.5% MeOH (625µl) under nitrogen, 640µl (0.69g, 5mmol) of 1,2-dimethoxybenzene (Veratrole) is added followed by 3.22g (10mmol) of PIDA under nitrogen by use of a powder addition funnel. The reaction is stirred at room temperature for 48 hours then diluted with ddH_2O, extracted with EtOAc (3X), and dried over $MgSO_4$. Removal of solvent under vacuum yields a dark yellow oil. 450mg (72%) of the rust colored product, was obtained by flash chromatography on silica (5:1 Hexane:EtOAc). ^{1}H and ^{13}C NMR spectra were collected on a Varian 400MHz. ^{1}H NMR ($CDCl_3$) δ 6.69 (s, 1H), 6.59 (s, 1H), 5.926 (s, 1H), 3.809 (s, 3H). ^{13}C NMR ($CDCl_3$) δ 188, 182, 158, 137, 135, 108, 57 ppm [155].
Haustorial inducing activity was confirmed by incubating day-old Striga seedlings in 10µM of the product then scoring for haustorium development (86% +/-5).

M.14 CPBQ Synthesis

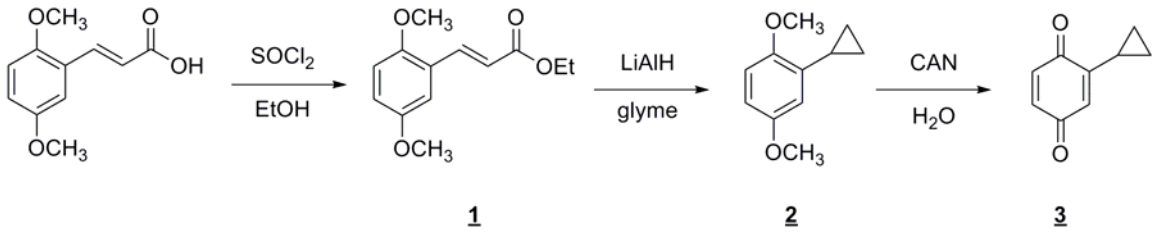

Figure M.2: *Synthetic scheme for cyclopropylbenzoquinone synthesis*

All ^{1}H and ^{13}C NMR spectra were collected on a Varian 400MHz.

M.14.1 2,5-dimethoxy cinnamyl ether ester (1)

10g of 2,5-dimethoxycinnamic acid (0.048mol) is dissolved in 150ml of 100% EtOH by sonication. To this stirring solution 5.25ml (0.072mol) of thionyl chloride ($SOCl_2$) is added dropwise over 30 minutes and run for 12 hours. Solvent is removed under vacuum yielding a viscous yellow oil. The oil was dissolved into ether (200ml) and washed successively with $NaHCO_3$ (20ml) and brine (20ml). The organic fraction was dried with $MgSO_4$ and removed under vacuum yielding a bright yellow oil which was purified by flash chromatography (5:1 Hex:EtOAc) yielding 9.4g of yellow product (83%). ^{1}H NMR ($CDCl_3$) δ7.95(d, J=16.1Hz, 1H), 7.02 (d, J=2.84Hz, 1H), 6.86 (d, J=8.9Hz, 1H), 6.8 (d, J=8.9Hz, 1H), 6.475 (d, J=16.1, 1H), 4.235 (q, J=7.1Hz, 2H), 3.8 (s, 3H), 3.75 (s, 3H), 1.311 (t, J=7.103, 3H). ^{13}C ($CDCl_3$) δ167.50, 153.61, 152.93, 139.90, 124.12, 119.15, 117.21, 113.41, 112.58, 60.64, 56.30, 56.0, 14.70.

M.14.2 2-cyclopropyl-1,4-dimethoxybenzene (2)

2.85g of $LiAlH_4$ (0.075mol) is dissolved in 100ml of glyme with molecular sieves under nitrogen in a three neck round bottom flask. To the stirring mixture 11.8g (0.05mol) of **1** dissolved in 100ml of glyme is added dropwise, under nitrogen, over a period of two hours. The stirring solution is then heated to reflux for 7 days. At this point the solution is cooled on an ice bath and diluted with 100ml ether. Excess hydride was consumed by the addition of 100ml H_2O dropwise over another hour. The mixture was suction filtered and washed with additional ether (3x50ml). The solvents were removed under vacuum producing a crude brown oil. The dried oil was vacuum distilled yielding a faint yellow oil which was further purified by flash chromatrography (5:1 Hex:EtOAc) resulting in 5.8g (65%) of a clear oil as the final product. ^{1}H NMR ($CDCl_3$) δ 6.77 (d, J = 8.81Hz, 1H), 6.65 (dd, J = 8.81Hz, 3.04Hz, 1H), 6.40 (d, J = 3.04Hz, 1H), 3.83 (s, 3H), 3.75 (s, 3H), 2.18 (m, 1H), 0.9 (m, 1H), 0.7 (m, 1H). ^{13}C NMR ($CDCl_3$) δ 154.3, 152.4, 133.77, 111.62, 111.59, 110, 57, 55, 10, 8, 6 [151, 156].

M.14.3 Cyclopropylbenzoquinone (3)

To a stirring solution of 1.78g (0.01mol) of **2** dissolved in 100ml H_2O and 20ml acetonitrile, 11g (0.02mol) of $(NH)_4Ce(NO_3)_6$ was added. The reaction mixture was stirred for 1 hour then diluted with 50ml H_2O and 50ml ether. The aqueous layer was washed with ether (3x50ml) and the organic fractions combined and dried with $MgSO_4$. Removal of the solvent under vacuum yielded a bright yellow oil. Purification by column chromatography (2:1 Hex:EtOAc) yielded 0.87g (59%) of yellow crystals. ^{1}H NMR ($CDCl_3$) δ 6.77 (s, 1H), 6.65 (s, 1H), 6.40 (s, 1H), 1.98 (m, 2H), 1.13 (m, 2H), 0.89 (m, 2H). ^{13}C NMR ($CDCl_3$) δ ^{13}C ($CDCl_3$) δ188, 185, 155, 140, 135, 125, 15, 10 [151].

References

1. Jackson, D.E. and F.L. Ratnieks, Curr Biol, 2006. **16**(15): p. R570-4.
2. Waters, C.M. and B.L. Bassler, Annu Rev Cell Dev Biol, 2005. **21**: p. 319-46.
3. Regnier, F.E. and J.H. Law, J Lipid Res, 1968. **9**(5): p. 541-51.
4. Prasanna, V., T.N. Prabha, and R.N. Tharanathan, Crit Rev Food Sci Nutr, 2007. **47**(1): p. 1-19.
5. Franklin, K.A. and G.C. Whitelam, Ann Bot (Lond), 2005. **96**(2): p. 169-75.
6. Zhu, J. and K.C. Park, J Chem Ecol, 2005. **31**(8): p. 1733-46.
7. Baldwin, I.T., et al., Science, 2006. **311**(5762): p. 812-5.
8. Preston, C.A., G. Laue, and I.T. Baldwin, J Chem Ecol, 2004. **30**(11): p. 2193-214.
9. Preston, C.A., H. Betts, and I.T. Baldwin, J Chem Ecol, 2002. **28**(11): p. 2343-2369.
10. Besserer, A., et al., PLoS Biol, 2006. **4**(7): p. e226.
11. Akiyama, K., K. Matsuzaki, and H. Hayashi, Nature, 2005. **435**(7043): p. 824-7.
12. Bauer, W.D. and U. Mathesius, Current opinion in plant biology, 2004. **7**(4): p. 429-33.
13. Gao, M., et al., Mol Plant Microbe Interact, 2003. **16**(9): p. 827-34.
14. Bauer, W.D. and J.B. Robinson, Current opinion in biotechnology, 2002. **13**(3): p. 234-7.
15. Hirsch, A., et al., Ecology, 2003. **84**(4): p. 858-868.
16. Jose, S. and A. Gillespie, Plant Soil, 1998. **203**: p. 191-97.
17. Macias, F.A., et al., J Agric Food Chem, 2004. **52**(21): p. 6402-13.

18. Kagan, I.A., A.M. Rimando, and F.E. Dayan, J Agric Food Chem, 2003. **51**(26): p. 7589-95.

19. Chang, M., et al., J Am Chem Soc, 1986. **108**: p. 7858-60.

20. Fate, G., M. Chang, and D.G. Lynn, Plant Physiol, 1990. **93**(1): p. 201-207.

21. Fate, G. and D.G. Lynn, J Chem Ed, 1990. **67**(6): p. 536-538.

22. Palmer, A., et al., Annu Rev Phytopath, 2004. **42**: p. 439-464.

23. Kuijt, J., *The Biology of Parasitic Flowering Plants*. 1969, Berkeley: University of California Press. 246.

24. Chang, M. and D.G. Lynn, J Chem Ecol, 1986. **12**: p. 561-579.

25. Yoder, J., Curr Opin Plant Biol, 2001. **4**(4): p. 359-365.

26. Riopel, J. and M. Timko, *Haustorial initiation and differentiation*, in *Parasitic Plants*, M. Press and J. Graves, Editors. 1995, Chapman&Hall: London. p. 39–79.

27. Riopel, L. and W. Baird, *Morphogenesis of the early development of primary haustoria in Striga asiatica.*, in *Parasitic Weeds in Agriculture*, L. Musselman, Editor. 1987, CRC Press: New York. p. 107–25.

28. Southgate, D. and D. Graham, *Growing Green: The challenge of sustainable agricultural development in Sub-Saharan Africa*. 2006, International Policy Network: London. p. 36.

29. Monteiro, C.A., *Understanding and redirecting the diet transition in the developing world*, in *UICC World Cancer Congress 2006*. 2006: Washington, DC.

30. Woomer, P.L., *Empowering African Farmers to Eradicate Striga from Maize Croplands*. 2006, African Agriculture Technology Foundation. p. 1-19.

31. Kim, D., et al., Chem & Biol, 1998. **5**(2): p. 103-117.

32. Lynn, D.G. and M. Chang, Annu Rev Plant Phys Plant Mol Biol, 1990. **41**: p. 497-526.

33. Albrecht, H., J.I. Yoder, and D.A. Phillips, Plant Physiol, 1999. **119**(2): p. 585-92.

34. Smith, C., M. Dudley, and D.G. Lynn, Plant Phys, 1990. **93**(1): p. 208-215.

35. Smith, E., et al., Proc Natl Acad Sci USA, 1996. **93**: p. 6986-6991.

36. Keyes, W., et al., Plant Phys, 2001. **127**(4): p. 1508-1512.

37. Keyes, W.J., *H_2O_2 as a Xenognosin. Exploiting Host Defenses for Host Detection*, in *Department of Chemistry*. 2002, University of Chicago: Chicago. p. 57.

38. Keyes, W.J., et al., Plant J, 2007. **51**(4): p. 707-716.

39. Roos, D., et al., Blood, 1996. **87**(5): p. 1663-81.

40. Segal, A.W., et al., Biochem. J., 1992. **284 (Pt 3)**: p. 781-8.

41. Krause, K.H., Exp Gerontol, 2007. **42**(4): p. 256-62.

42. Moller, I.M., Annu Rev Plant Phys Plant Mol Biol, 2001. **52**: p. 561-591.

43. Halliwell, H. and J. Gutteridge, *Role of Free Radicals and Catalytic Metal Ions in Human Disease: An Overview.* , in *Methods in Enzymology*, L. Packer and A. Glazer, Editors. 1990. p. 1-85.

44. Yoshioka, H., et al., Plant Cell, 2003. **15**(3): p. 706-718.

45. Torres, M.A., J.L. Dangl, and J.D. Jones, Proc Natl Acad Sci USA, 2002. **99**(1): p. 517-22.

46. Le Cabec, V. and I. Maridonneau-Parini, J Biol Chem, 1995. **270**(5): p. 2067-73.

47. Pan, J.-w., M.-y. Zhu, and H. Chen, Env Exp Bot, 2001. **46**: p. 71-79.

48. Nurnberger, T., et al., Cell, 1994. **78**(3): p. 449-460.

49. Orozco-Cárdenas, M.L., J. Narváez-Vásquez, and C.A. Ryan, Plant Cell, 2001. **13**: p. 179-191.

50. Doke, N., Phys Plant Path, 1983. **23**(3): p. 345-357.

51. Levine, A., et al., Cell, 1994. **79**: p. 583-593.

52. Apostol, I., P.F. Heinstein, and P.S. Low, Plant Phys, 1989. **90**: p. 109-116.

53. Bradley, D., P. Kjellbom, and C.J. Lamb, Cell, 1992. **70**(1): p. 21-30.

54. Allan, A.C. and R. Fluhr, Plant Cell, 1997. **9**: p. 1559-1572.

55. Edens, W.A., et al., J. Cell Bio., 2001. **154**(4): p. 879-891.

56. Foreman, J., et al., Nature, 2003. **422**: p. 442-446.

57. Potocky, M., et al., New Phytol, 2007. **174**(4): p. 742-51.

58. Dunand, C., M. Crevecoeur, and C. Penel, New Phytol, 2007. **174**(2): p. 332-41.

59. Pei, Z., et al., Nature, 2000. **406**: p. 731-734.

60. Joo, J., Y. Yun, and J. June, Plant Phys, 2001. **126**: p. 1055-1060.

61. Desikan, R., et al., Func Plant Biol, 2004. **31**(9): p. 913-920.

62. Jones, M.A., et al., J Exp Bot, 2007. **58**(6): p. 1261-70.

63. Kim, K.-N., et al., Plant Mol Bio, 2003. **52**: p. 1191-1202.

64. Yahraus, T., et al., Plant Phys, 1995. **109**: p. 1259-1266.

65. Naton, B., K. Hahlbrock, and E. Schmelzer, Plant Phys, 1996. **112**: p. 433-444.

66. Cathcart, R., E. Schwiers, and B. Ames, Anal Biochem, 1983. **134**: p. 111-116.

67. Ortega-Villasante, C., et al., J Exp Bot, 2005. **56**(418): p. 2239-2251.

68. Bolwell, G., et al., J Exp Bot, 2002. **53**(372): p. 1367-1376.

69. Blokhina, O., T. Chirkova, and K. Fagerstedt, J Exp Bot, 2001. **52**(359): p. 1179-1190.

70. O'Malley, R. and D. Lynn, Plant Cell, 2000. **12**(8): p. 1455-1465.

71. Lambeth, J., Nat Rev Immunol, 2004. **4**: p. 181-189.

72. Bokoch, G.M. and U.G. Knaus, Trends Biochem Sci, 2003. **28**(9): p. 502-508.

73. Peng, M. and J. Kuc, Phytopathology, 1992. **82**: p. 696-699.

74. Bestwick, C., et al., Plant Cell, 1997. **9**(7): p. 209-221.

75. Kawasaki, T., et al., Proc Natl Acad Sci USA, 1999. **96**: p. 10922-10926.

76. O'Malley, R., *Mechanisms Controlling Haustorial Organogenesis in Striga Asiatica*, in *Department of Chemistry*. 1996, University of Chicago: Chicago. p. 138.

77. Hammond-Kosack, K. and J. Jones, Plant Cell, 1996. **8**(10): p. 1773-1791.

78. Lamb, C. and R.A. Dixon, Annu Rev Plant Phys Plant Mol Biol, 1997. **48**: p. 251-275.

79. Barcelo, A., Planta, 2005. **220**: p. 747-756.

80. Matvienko, M., M. Torres, and J. Yoder, Plant Phys, 2001. **127**: p. 272-282.

81. Torres, M.A., J.D. Jones, and J.L. Dangl, Plant Phys, 2006. **141**(2): p. 373-8.

82. Torres, M.A., et al., Plant J, 1998. **14**(3): p. 365-70.

83. Lin, C.-M., et al., Planta Medica, 2002. **68**(4): p. 365-367.

84. Bolwell, G.P., et al., Free Rad Res, 1995. **23**(6): p. 517-32.

85. Montillet, J.L., et al., Plant J, 2004. **40**(3): p. 439-51.

86. Jarvinen, A., et al., J Biol Chem, 2005. **280**(8): p. 6595-601.

87. Gucciardo, S., et al., J Exp Bot, 2007. **58**(5): p. 1161-71.

88. Das, D.K., et al., Biochem Biophys Res Comm, 1987. **148**(1): p. 314-9.

89. Matsunaga, T., et al., Leuk Lymphoma, 1996. **20**(5-6): p. 487-94.

90. Davies, B. and S.W. Edwards, Biochem J, 1989. **258**(3): p. 801-6.

91. Pivovarov, A.S. and W. Egido-Villareal, Neurosci Behav Physiol, 1995. **25**(6): p. 483-7.

92. Obeso, A., A. Gomez-Nino, and C. Gonzalez, Am J Phys, 1999. **276**(3 Pt 1): p. C593-601.

93. Banfi, B., et al., J Biol Chem, 2001. **276**(40): p. 37594-601.

94. Cheng, G., et al., Gene, 2001. **269**(1-2): p. 131-40.

95. Groom, Q., et al., Plant J, 1996. **10**: p. 515-522.

96. Liang, L., et al., Plant Phys, 2008. **Submitted**.

97. Maturana, A., et al., J Biol Chem, 2001. **276**(32): p. 30277-84.

98. Quinn, M.T., M.L. Mullen, and A.J. Jesaitis, J Biol Chem, 1992. **267**(11): p. 7303-9.

99. Doussiere, J., G. Buzenet, and P.V. Vignais, Biochemistry, 1995. **34**(5): p. 1760-70.

100. Doussiere, J., et al., Biochemistry, 1993. **32**(34): p. 8880-7.

101. Edens, W.A., et al., J Cell Bio, 2001. **154**(4): p. 879-91.

102. Banfi, B., et al., J Biol Chem, 2004. **279**(18): p. 18583-91.

103. Tsukaya, H., et al., Mol Gen Genet, 1993. **237**(1-2): p. 26-32.

104. Lindsey, K., et al., Symposia of the Society for Experimental Biology, 1998. **51**: p. 1-10.

105. Keller, T., et al., Plant Cell, 1998. **10**: p. 255-266.

106. Abramov, A.Y., et al., J Neurosci, 2005. **25**(40): p. 9176-84.

107. Jagnandan, D., et al., J Biol Chem, 2007. **282**(9): p. 6494-507.

108. Reinehr, R., et al., Glia, 2007. **55**(7): p. 758-71.

109. Desikan, R., et al., FEBS Lett, 1996. **382**: p. 213-217.

110. Kobayashi, M., et al., Plant Cell, 2007. **19**(3): p. 1065-80.

111. Frahry, G. and P. Schopfer, Physiologia Plantarum, 1998. **103**: p. 395-404.

112. Tomilov, A., et al., eds. *Chemical signaling between plants: mechanistic similarities between allelopathy and host plant recognition by parasitic Angiosperms.* Chemical ecology: from genes to ecosystems, ed. M. Dicke and W. Takken. 2006, Springer: Berlin. 55-69.

113. Worsham, A., D. Moreland, and G. Klingman, Science, 1959. **130**: p. 1654-1656.

114. Williams, C., Nature, 1961. **189**: p. 378-381.

115. Keyes, W., et al., Plant Growth Reg, 2000. **19**(2): p. 217-231.

116. Wrobel, R.L. and J.I. Yoder, Gene, 2001. **266**(1-2): p. 85-93.

117. Kakimoto, T., Annu Rev Plant Biol, 2003. **54**: p. 605-27.

118. Long, J.C. and G.I. Jenkins, Plant Cell, 1998. **10**(12): p. 2077-86.

119. Poenie, M., et al., Nature, 1985. **315**(6015): p. 147-9.

120. Subbaiah, C.C., J. Zhang, and M.M. Sachs, Plant Physiol, 1994. **105**(1): p. 369-76.

121. Bao, F. and D. Liu, Neuroscience, 2004. **126**(2): p. 285-95.

122. Day, B.J. and J.D. Crapo, Toxicol Appl Pharmacol, 1996. **140**(1): p. 94-100.

123. Stull, N.D., D.P. Polan, and L. Iacovitti, Brain research, 2002. **931**(2): p. 181-5.

124. Cuzzocrea, S., et al., Free Radic Biol Med, 1999. **26**(1-2): p. 25-33.

125. Silverman, F.P., A.A. Assiamah, and D.S. Bush, Planta, 1998. **205**: p. 23-31.

126. Tomilov, A.A., et al., Plant Physiol, 2005. **138**(3): p. 1469-80.

127. Pingret, J.L., E.P. Journet, and D.G. Barker, Plant Cell, 1998. **10**(5): p. 659-72.

128. White, P.J., Biochim Biophys Acta, 2000. **1465**(1-2): p. 171-89.

129. Kapur, N., G.A. Mignery, and K. Banach, Am J Physiol Cell Physiol, 2007. **292**(4): p. C1510-8.

130. Zahradnikova, A., Jr., et al., J Physiol, 2007. **578**(Pt 3): p. 677-91.

131. Mork, H.K., et al., J Mol Cell Cardiol, 2007. **43**(2): p. 177-86.

132. Zima, A.V., et al., J Physiol, 2007. **584**(Pt 2): p. 601-11.

133. Kaplan, J.H. and G.C. Ellis-Davies, Proc Natl Acad Sci U S A, 1988. **85**(17): p. 6571-5.

134. Ji, G., et al., J Gen Physiol, 2006. **127**(3): p. 225-35.

135. Bibikova, T.N., A. Zhigilei, and S. Gilroy, Planta, 1997. **203**(4): p. 495-505.

136. Wymer, C.L., T.N. Bibikova, and S. Gilroy, Plant J, 1997. **12**(2): p. 427-39.

137. Frebortova, J., et al., Biochem J, 2004. **380**(Pt 1): p. 121-30.

138. Synkova, H., et al., Biologia Plantarum, 2006. **50**(1): p. 31-41.

139. Synkova, H., S. Semoradova, and L. Burketova, Plant Cell Tiss Org Cul, 2004. **79**: p. 169-179.

140. Apel, K. and H. Hirt, Annu Rev Plant Biol, 2004. **55**: p. 373-99.

141. Lohar, D.P., et al., New Phytol, 2007. **173**(1): p. 39-49.

142. Shaw, S.L. and S.R. Long, Plant Physiol, 2003. **131**(3): p. 976-84.

143. Miao, Y., et al., Plant Cell, 2006. **18**(10): p. 2749-66.

144. Schumaker, K.S. and M.J. Gizinski, J Biol Chem, 1995. **270**(40): p. 23461-7.

145. Schumaker, K.S. and M.J. Gizinski, Proc Natl Acad Sci U S A, 1993. **90**(23): p. 10937-41.

146. Chaves, N., et al., J Chem Ecol, 2001. **27**(3): p. 611-21.

147. Chaves, N., T. Sosa, and J.C. Escudero, J Chem Ecol, 2001. **27**(3): p. 623-31.

148. Pedersen, M.B., C. Kjaer, and N. Elmegaard, Arch Environ Contam Toxicol, 2000. **39**(4): p. 431-9.

149. Fryer, M.J., et al., J Exp Bot, 2002. **53**(372): p. 1249-54.

150. Ruttledge, T.R., *The Involvement of a Redox Process in Development*, in *Chemistry*. 1992, University of Chicago: Chicago. p. 141.

151. Zeng, Z., *Cyclopropylquinone: A Probe of Redox Processes in Development and a Substrate for a Unique Photoannulation Reaction*, in *Chemistry*. 1994, University of Chicago: Chicago. p. 153.

152. Sanchez-Fernandez, R., et al., Proc Natl Acad Sci U S A, 1997. **94**(6): p. 2745-50.

153. Dauphin, A., et al., Protoplasma, 2007. **231**(1-2): p. 83-8.

154. Zhang, W.H. and Z. Rengel, Aust J Plant Phys, 1999. **26**(5): p. 401-409.

155. Tohma, H., et al., Tet Lett, 2001. **42**: p. 6899-6902.

156. Jorgenson, M.J. and A.W. Friend, J Am Chem Soc, 1965. **87**: p. 1815.